Transport phenomena through porous screens and openings: from theory to greenhouse practice

A. A. F. Miguel

Proefschrift

ter verkrijging van de graad van
doctor
op gezag van de rector magnificus,
Dr. C. M. Karssen,
in het openbaar te verdedigen
op woensdag 25 februari 1998
des namiddags te vier uur in de aula
van de Landbouwuniversiteit te Wageningen

ISN 9,52 ? 60

CIP-DATA KONINKLIJKE BIBLIOTHEEK, DEN HAAG

Miguel, A. A. F.

Transport phenomena through porous screens and openings: *from theory to greenhouse practice* / A.A.F. Miguel. [S.l.:s.n]

Thesis Wageningen. – With Ref. – With Summaries in English, Dutch, Portugese and Chinese

ISBN 90-5485-847-8

Subject headings: mass and heat exchange / porous materials / openings / screened greenhouses.

Cover: Fluid flow around a solid body

This thesis is also available as publication nr. 98-2 , ISBN 90-5485-843-5 of the DLO Institute of Agricultural and Environmental Engineering (IMAG-DLO), P.O.Box 43, NL-6700 AA Wageningen, The Netherlands

ABSTRACT

Miguel, A. A. F. 1998. ***Transport phenomena through porous screens and openings: from theory to greenhouse practice.*** **Ph.D. Dissertation, Landbouwuniversiteit, Wageningen. Also available as a publication of Instituut voor Milieu en Agritechniek (IMAG-DLO) Wageningen, Netherlands. 129 pp.; 44 figs.; 9 tables; 112 refs.; English, Dutch, Portuguese and Chinese summaries.**

Keywords: free and forced convective mass exchange, fluctuating flow, free convective heat transfer, porous screens, window openings, screened greenhouses.

The study of transport phenomena in multi-zone enclosures with permeable boundaries is fundamental for indoor climate control management. In this study, aspects concerning the air exchange through porous screens and openings, and heat transfer between the enclosure surface and inside air, were analysed. Basic physical laws were the starting point during the construction of the models. To illustrate the practical side of the research performed, the formulation developed was applied to the study of convective heat exchange within screened greenhouses, as well as to the study of airflow through greenhouse screens and window apertures.

Concerning the airflow through porous screens and window openings, the results obtained thoroughly demonstrate the importance of inertia and viscous effects, as well as window openings' geometry effects, on fluid flow. The airflow characteristics of porous screens and the structure of fluctuation of wind velocity, were quantified.

Regarding the study of free convection heat transfer within a screened greenhouse, the convective heat transfer coefficients between the air and the downward and the upward surfaces of the screen were obtained, among other

results.

The results obtained from this study can greatly contribute, in general, to a better climate control management of multi-zone enclosures, and specifically, to an improved application of porous screens and window apertures.

CONTENTS

Stellingen/Propositions

1. Darcy and Forchheimer already empirically described fluid flow through porous media in 1856 and 1901, respectively. However, the subject is still a ***modern topic***.
   In this dissertation.

2. A linear model as the Darcy law only describes flows at low Reynolds numbers. For screens this covers only part of the flow regimes occurring in practice. For a full description a non-linear model is need.
   In this dissertation.

3. Under commonly observed flow regimes, it is not appropriate to apply the Bernoulli's equation to porous screens.
   In this dissertation.

4. For a full exploitation of energy saving potentials of thermal screens, not only the temperature and wind-driven air exchange through fully closed screens have to be studied [1], but also the exchange through partially opened screens.
   [1] Balemans L. 1988. Assessment of criteria for energetic effectiveness of greenhouse screens. Ph.D. Dissertation, Ghent University, Belgium

5. In the study of airflow through openings, a constant discharge coefficient (0.61) does not account for the specific opening characteristics, thus contributing to inaccurate predictions.
   In this dissertation.

6. On-line estimation of ventilation of cavities can best be derived from a mass balance (e.g. CO_2 balance)

7. Science tells us what we can know, but what we can know is little, and if we forget how much we cannot know we become insensitive to many things of very great importance.
   B. Russell *(1946). History of western philosophy and its connection with political and social circumstances from the earliest times to present day. George Allen & Unwin. United Kingdom.*

8. The strict university educational programs force students to accept scientific ideas not by reasoning but by authority.

9. If the universe would be pre-determined, it does not make sense to define good or evil, nor to have despair or hope.

10. As a metronome, the coffee break marks the rhythm of a Dutch working day.

11. Asking *yes-no* questions blocks creative thinking.

12. We are our dreams of ourselves souls by gleams, and each to each other dreams of other's dreams.
F. Pessoa (1918) English Poems.

Propositions belonging to the Ph.D. thesis *"Transport phenomena through porous screens and openings: from theory to greenhouse practice"* of A. A. Ferreira Miguel (1998)

8. FINAL DISCUSSION AND CONCLUSION

PREFACE

This thesis results from my Ph.D. study at IMAG-DLO and at Wageningen Agricultural University (WAU), under a contract financed by Fundação C. Gulbenkian and JNICT (Portugal), and by Novem bv and Landbouwschap (the Netherlands). It finishes a very pleasant staying in the Netherlands, which I hope will stand for a close cooperation between these institutions and my University (Department of Physics of Évora University) in Portugal.

This thesis owes its existence to many people (within and outside the university community), whose guidance, encouragement and friendship were essential for the reaching of my goals. I would like to thank all of them.

First, I would like to express my gratitude and appreciation to Prof. Dr. Ir. G. P. A. Bot and to Prof. Dr. Ana Maria Silva, my promoters, for the guidance and advice they gave me during this study.

I am deeply indebted to Ir. N. J. van de Braak, for his assistance, inspiration and constructive criticism during all of the Ph.D. study.

My sincere gratitude to Dr. Ir. H. F. de Zwart for his assistance on making some computational programmes, mainly the programmes used to control the experimental set-up.

I thank Mr. H. Loeffen for his valuable help in some experimental measurements. I gratefully acknowledge the help of Ir. A. van't Ooster, Ir. J. J. G. Breuer and Mr. A. Ruisch for the setting of my experiments.

Grateful acknowledgements are due to my department colleagues in the Netherlands and in Portugal for many valuable discussions and thoughtful suggestions, in particular to Dr. Ir. J. C. Bakker (IMAG-DLO), Dr. Ir. W. K. P. van Loon (WAU), Dipl. Phys. J. A. Stoffers (IMAG-DLO), and to Prof. Dr. A. Heitor dos Reis (University of Évora).

On a personal note, I would like to express my thanks to all outside the university community, who contributed with their friendship for a pleasant

staying in the Netherlands, in particularly to the couple Barros. I am also indebted to Ir. Ana I. Costa, for her never-failing support and continuous friendship.

As in all of my life, I have been greatly supported by my mother and my sister. I dedicate this book to my father and my grand-parents, will live forever in my heart.

1. INTRODUCTION

1.1 PRELIMINARY REMARKS

The study of transport phenomena is an important topic in science and engineering. This is due to the essential (and sometimes decisive) role they play in distinct natural and industrial processes (geothermal operations, indoor climate control in buildings, flow over the earth's surface, drying and cooling processes, etc.).

In order to solve problems in transport phenomena, it is necessary to approach the specific problems from a general physical description. This leads to models which allow us to predict the phenomena described under a variety of conditions, with adequate accuracy. The physical principles applied in the building of these models are the conservation of mass, momentum and energy, and the relations between fluxes and driving forces. This results in non-linear differential equations, in space and time, from which analytical solutions can be obtained, although only in the simplest cases. Usually, these equations have to be solved with the help of numerical techniques like Euler and other integration technique for lumped parameter problem, or like the finite-difference and finite volume method for distributed parameter problem [1,2]. Unfortunately, numerical techniques are difficult to use and in most cases not very practical. Therefore, a very large number of the existing studies deals with mathematical simplifications, which neglect some physical aspects, while others deal with simple empirical correlations with an unknown range of validity and applicability [3,4].

This thesis describes a study of some transport phenomena in multi-zone enclosure, applied in a screened greenhouse: air infiltrations through screened greenhouses and free convective heat transfer between the various surfaces and the air within the greenhouse. Its main purpose is to develop a consistent formulation that is both

physically meaningful and useful in practice, and which helps to solve everyday problems, with higher accuracy and lower computational cost.

1.2 TRANSPORT PHENOMENA IN SCREENED GREENHOUSES - THE IMPORTANCE OF POROUS SCREENS

1.2.1 Reasons for studying screened greenhouses

Protected horticulture is an important contribution to economy of several countries around the world. In the Netherlands, it provides for about 6.6% of total export value and represents a value of about 10^{10} US dollar per year [5]. As a consequence, this topic is the subject of numerous research initiatives. At first thought, it might appear that the improvement of products quality and the reduction of production prices should be the main concerns. However, the related environmental aspects cannot be neglected, since protected horticulture is an important consumer of fossil fuel and chemical pesticides.

The potential benefits deriving from the use of screens in protected horticulture have been increasingly recognised in recent years. In the Netherlands about 75 % of total greenhouse area is equipped with screens. Thermal screens are a simple, cheap and effective means of reducing night-time heat loss. Shading screens control the solar radiation inside a greenhouse, while insect screens prevent the entrance of birds and insects. Therefore, screen strongly contribute to the reduction of greenhouse heating and refreshing costs, while being an effective alternative to chemical pesticides in the control of insect borne diseases.

1.2.2 Modelling the influence of porous screens in greenhouses: interest, previous research and needs

The use of screens in greenhouses has a considerable effect on growing conditions while they provide an extra resistance to mass, momentum and heat transport between

the interior and the ambient. The application of screens and thereby the exploitation of its potentials, has been restricted so far by an improper quantification of the effect on the growing conditions.

The physical modelling of behaviour of porous screens

- contributes to a better comprehension of physical phenomena around screens and it allow a correct interpretation of experimental data,
- allows diverse screening strategies to be compared (policy advice),
- improves design tools to optimise the application of screens,
- helps to decide about characteristics of a screening material (commodity forecasting) in order to support the manufacture of new screening materials,
- implemented in simulation programs helps the improvement of the climate control (the growing conditions) of a screened greenhouse.

Most literature reviews on greenhouse screens concern its influence on the radiative climate of greenhouses. The influence of screens on the incoming solar and thermal radiation have already been successfully modelled [6-9] and the optical or radiometric characteristics of different materials used for screens have been determined by several authors [6,10,11].

The influence of screens on convective heat exchange inside greenhouses and the study of fluid transport through screens have received little attention, and are poorly understood.

As to our knowledge, only one experimental study (unpublished communication presented by Stoffers [12] in Cambridge), is concern to the convective heat transfer in greenhouses divided by a horizontal screen. Fluid transport through screens was described by Balemans [11], Bailey [13], Sase and Christianson [14], and Kosmos et al. [15]. The first two, considered only the fluid flow under a Reynolds number smaller than 1 (Darcy flow regime). Sase and Christianson [14] and Kosmos et al. [15] considered the fluid transport through a screen to be described by Bernoulli's equation, and defined the airflow characteristics of a screen according to a "discharge

coefficient".

In all studies, the horizontal screen between the greenhouse ground and the roof was always considered closed between the greenhouse walls. The realistic situation of a screen opened only slightly [5] was never analysed.

1.3 Aim

Despite the existence of a lot of important studies on the transport phenomena in multi-zone enclosures with permeable walls, the subject is far from being fully understood. The study presented in this thesis seeks to clarify some aspects of transport phenomena occurring in multi-zone enclosures with permeable walls: air infiltration through enclosures containing openings and pores and heat transfer between the enclosure surfaces and the inside air. The theory developed is applied to the study of screened greenhouses and compared with experimental results. Thus, the study can be used as a tool to increase a more sustainable use of screens and window apertures.

1.4 Overview of the thesis

This thesis contains eight chapters. Chapters 2 to 6 are devoted to fluid transport through multi-zone enclosure with porous materials and openings. Chapter 7 concerns free (natural) convective heat exchange within the enclosure and Chapter 8 presents the general conclusions.

In Chapter 2, forced convection through pores and openings is discussed. An approach based on the momentum equation, developed in terms of the method of volume averaging is presented. The resulting approach is valid for porous material and non-porous material, and can be used in computational fluid dynamics to predict the velocity and pressure throughout the flow field. A simplified and accurate form is also developed, having a small number of parameters and simple mathematical operations.

In Chapter 3, the approach developed in Chapter 2 together with the mass conservation equation and the state equation of gases is used to study air exchange induced by fluctuating pressures. The network flow equations for air exchange in a multi-zone enclosure and equations for the pressure within each zone with compressible air are presented.

Fluid transport through permeable materials can also occur due to gradients of temperature and concentration, or as a result of combined effects (gradients of temperature, concentration and pressure generated by wind or mechanical means). A description of mixed convection through porous media supported by thermodynamics and fluid mechanics basic laws, is presented in Chapter 4. As a result the mass variation of the medium and the interaction between the matrix and the fluid within the medium can be studied.

Chapter 5 is devoted to measure the airflow characteristics of porous screens. Nine different thermal, shading and insect screens were tested by means of a DC-pressurisation method. Their permeability and porous inertia factor were determined according to Forchheimer equation (porosity measured with a microscope). Special attention is given to the airflow characteristics variation (permeability and porosity) due to screen damage by handling.

In Chapter 6 the approaches presented in Chapter 2 to 4 are applied to the study of air exchange in a screened greenhouse. This study is complemented with a power-spectrum analysis of wind velocity, in order to clarify and characterise the structure of pressure fluctuations (turbulence), and to identify the frequencies of the main eddies present in the wind field. The fluctuations in the wind velocity are related to the mean velocity, and the wind pressure is interpreted in terms of the mean wind velocity.

Chapter 7 is devoted to free convective heat transfer inside screened greenhouses. The heat transfer coefficient at various surfaces is expressed as a relation between dimensionless Nusselt's number and the Rayleigh's number. Subsequently, an experimental study is performed to determine free convection heat transfer

coefficients (between air and heating pipes, air and horizontal screen, and air and inner roof surface) in a greenhouse with characteristic lengths close to those of real greenhouses. The screen surfaces presented some roughness, as the screens used in greenhouses. Other practical aspects, such as the influence of the position of the heating pipes in relation to the screen, and the presence of a crop, on the convective heat transfer between the various surfaces and the air, is discussed.

Finally, Chapter 8 presents the most important conclusions of the present study and includes a recommendation on possible future research.

1.5 References

[1] **Patankar, S. V.** 1980. Numerical heat transfer and fluid flow, Hemisphere, New York, USA

[2] **Baker, A. J.** 1985. Finite element computational fluid mechanics, MacGraw-Hill, New York, USA

[3] **Combarnous, M. and Bernard D.** 1988. Modelling free convection in porous media: from academic cases to real configurations. Proceedings of 1988 National Heat Transfer Conference, Houston, USA

[4] International Energy Agency (IEA) 1992. Energy conservation in buildings and community systems programme. Annex 20: Airflow patterns within buildings - Airflow through large openings on buildings. Report edited by J. van der Maas.

[5] **Zwart, H. F. de** 1996. Analysing energy-saving options in greenhouse cultivation using a simulation model. Ph.D. Dissertation, Agricultural University of Wageningen, The Netherlands

[6] **Bailey, B. J.** 1981. The reduction of thermal radiation in glasshouse by thermal screens. Journal of Agricultural Engineering Research **26**, 215-224

[7] **Rosa, R.** 1988. Solar and thermal radiation inside a multispan greenhouse, Journal of Agricultural Engineering Research **40**, 285-295

[8] **Silva, A. M., Miguel, A. F. and Rosa, R.** 1991. Thermal radiation inside a single

span greenhouse with a thermal screen, Journal of Agricultural Engineering Research **49**, 285-298

[9] **Miguel, A. F., Silva, A. M. and Rosa, R.** 1994. Solar irradiation inside a single span greenhouse with shading screens. Journal of Agricultural Engineering Research **59**, 61-72

[10] **Nijskens J., Deltour J., Coutisse S. and Nisen A.** 1985. Radiation transfer through covering materials, solar and thermal screens of greenhouses. Agricultural and Forest Meteorology **35**: 229-242

[11] **Balemans, L.** 1989. Assessment of criteria for energetic effectiveness of greenhouse screens Ph.D. Dissertation. University of Gent, Belgium

[12] **Stoffers, J. A.** 1984. Energy fluxes in screened greenhouses. Communication presented in Agricultural Engineering Conference (AgEng 84), Cambridge, United Kingdom [unpublished]

[13] **Bailey, B. J.** 1978. Glasshouse thermal screens: air flow through permeable materials. Departmental Note DN/G/859/04013. NIAE, Wrest Park, Silsoe, Bedford, United Kingdom

[14] **Sase S. and Christianson L. L.** 1990. Screening greenhouses-some engineering considerations. ASAE Paper No. NABEC, 90-201

[15] **Kosmos S. R., Riskowski G. L. and Christianson L. L.** 1993. Force and static pressure resulting from airflow through screens. ASAE **36**: 1467-1472

2. Forced fluid motion through openings and pores [+]

Abstract: A theoretical and experimental study of forced flow through permeable media is presented. The mathematical model is based on the momentum equation and developed in terms of the method of volume averaging, which results in an approach that is valid for fluid motion through both porous and non-porous media. The approach can be used in computational fluid dynamics (CFD) to predict the velocity and pressure throughout the flow field. Solving this model numerically is difficult and in some practical applications the detail of CFD solutions is not required. To account for this, a simplified form of model is also developed which provides an alternative that can be used in one-dimensional analysis. Thus, the description presented has a wide application.

2.1 INTRODUCTION

Forced convection through pores and openings can occur through mechanical means (fans), the effect of gravity and the effect of wind. For a proper quantification of the phenomenon it is necessary to know how the fluid motion is related to the driving forces and to the characteristics of the transmitting medium.

When a fluid is forced through a permeable medium (containing pores or openings) energy is lost, which causes the pressure to drop over the slab of the medium. The pressure drop over openings is generally presented as being proportional to the fluid velocity squared [1]. A term, which is linearly dependent on fluid velocity, is added for extremely narrow openings [2]. For a porous medium, with Reynolds numbers less than 1, the pressure drop is generally considered to be proportional to the fluid velocity (Darcy's law). For Reynolds numbers greater than 1, the existence of a non-linear flow regime has been demonstrated experimentally. As a result, an extra squared fluid velocity term has been added to match the experimental results [3,4].

[+] ***Building and Environment*** **(in press)**

The aim of this paper is to establish a more detailed theoretical modelling of fluid flow through pores and openings. A mathematical model is presented based on the momentum conservation equation and developed in terms of a methodology called method of volume averaging. The resulting approach is a non-linear differential equation, valid to describe flows through media with pores up to large openings. Solving this equation even by numerical means is difficult and usually impractical. In order to account for this, a simplified form of the approach is also presented in order to quantify with good accuracy the magnitude of the phenomenon using a small number of parameters and ordinary mathematical operations. Thus, the description presented can be widely applied.

2.2 MATHEMATICAL FORMULATION

Conservation of momentum - the equation of motion

The equation of motion for a single-phase flow in a general flow field can be written as

$$\rho\partial\mathbf{u}/\partial t+(\rho\mathbf{u}.\nabla)\mathbf{u} =-\nabla P+\mu\nabla^2\mathbf{u} \qquad (1)$$

where u is the vector velocity, P the total pressure (with gravitational force per unit mass included) and μ the dynamic viscosity.

The drawback of applying equation (1) is the very local character of the state variables. This characteristic prevents a detailed description of porous media because it is only valid inside the pores. To overcome this, equation (1) will be developed with the help of a methodology called method of volume averaging, resulting in an equation valid over a small volumetric element which is representative for the medium under study. The validity of the resulting approach is based on the following assumptions:

- the medium is homogeneous at a macroscopic scale
- the solid matrix is rigid

- there are no chemical reactions between the solid matrix and the fluid
- the conditions are isothermal

The method used for the volume averaging is presented in the Appendix.

2.2.1. The equation of motion developed using the method of volume averaging

Averaging the terms of equation (1) in a control volume (Fig. 2-1) following the procedure indicated by equation (A.3) in the Appendix, the intrinsic phase average can be expressed as

$$\langle \rho \partial \mathbf{u}/\partial t \rangle_i + \langle (\rho \mathbf{u}.\nabla)\mathbf{u} \rangle_i = -\langle \nabla P \rangle_i + \langle \mu \nabla^2 \mathbf{u} \rangle_i \qquad (2)$$

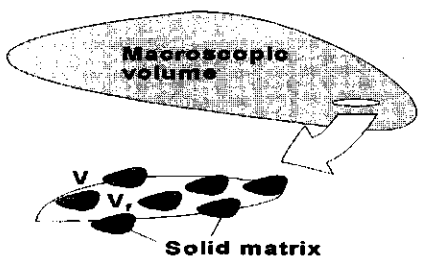

FIG. 2-1. Macroscopic region and averaging volume for a solid-fluid system.

The porosity, density and the fluid viscosity are considered constants in the averaging volume. According to equation (A.5) in the Appendix, the first left-hand side term of (2) can be written as

$$\rho \partial \langle \mathbf{u} \rangle_i / \partial t + \rho \partial (\tilde{\mathbf{u}}) / \partial t \qquad (3.1)$$

Following the procedure indicated by equation (A.7) in Appendix, the second left-hand side term of equation (3) becomes

$$\rho(\langle \mathbf{u} \rangle_i . \nabla \langle \mathbf{u} \rangle_i + \tilde{\mathbf{u}} . \nabla \langle \mathbf{u} \rangle_i + \langle \mathbf{u} \rangle_i . V_f^{-1} \int \mathbf{n}.\tilde{\mathbf{u}} dA + \tilde{\mathbf{u}} . V_f^{-1} \int \mathbf{n}.\tilde{\mathbf{u}} dA) \qquad (3.2)$$

and the right-hand side term

$$-\nabla\langle P\rangle_i - V_f^{-1}\int \tilde{P}\, dA + \mu\ \nabla^2\langle \mathbf{u}\rangle_i + \mu\, V_f^{-1}\int \mathbf{n}.\nabla\tilde{\mathbf{u}}\, dA \qquad (3.3)$$

At this point we need a representation for $\tilde{P}$ and $\tilde{u}$ as functions of the flow field in order to obtain the closed form. For this, we will express the spatial deviation as a linear function of some phase-averaged quantity, as used by Whitaker [10] in the derivation of Darcy's law, and as supported by Slattery in previous work [6]. The closure problem requires that the spatial deviation of the velocity and pressure be represented in terms of intrinsic averaging velocity, which can be given by

$$\tilde{\mathbf{u}} = \Gamma.\langle \mathbf{u}\rangle_i \qquad (4)$$

$$\tilde{P} = \mu\Phi.\langle \mathbf{u}\rangle_i \qquad (5)$$

where Γ and Φ are tensors which relate the intrinsic phase average velocity to the spatial deviation of velocity and pressure, respectively.

Substituting equations (4) and (5) in (3) yields

$$\rho\partial\langle \mathbf{u}\rangle_i/\partial t + \rho\partial(\Gamma.\langle \mathbf{u}\rangle_i)/\partial t + \rho[\langle \mathbf{u}\rangle_i.\nabla\langle \mathbf{u}\rangle_i + \Gamma.\langle \mathbf{u}\rangle_i.\nabla\langle \mathbf{u}\rangle_i +$$
$$\langle \mathbf{u}\rangle_i.\langle \mathbf{u}\rangle_i.(V_f^{-1}\int \mathbf{n}.\,\Gamma dA + V_f^{-1}\Gamma.\int \mathbf{n}.\Gamma dA)] = -\nabla\langle P\rangle_i + \mu\ \nabla^2\langle \mathbf{u}\rangle_i +$$
$$+\mu\langle \mathbf{u}\rangle_i(V_f^{-1}\int \mathbf{n}.\nabla\Gamma dA - V_f^{-1}\int \mathbf{I}.\Phi dA) + \mu\nabla\langle \mathbf{u}\rangle_i(V_f^{-1}\int \mathbf{n}.\Gamma\, dA) \qquad (6)$$

where I is the unit tensor.

While intrinsic average pressure is used exclusively because it corresponds more closely to the measured value, superficial average velocity is generally preferred in practical situations. The spatial deviation of the velocity and pressure is much smaller than the average value of the corresponding intrinsic phase. So Γ and Φ will be small parameters. As $\langle \mathbf{u}\rangle_i \gg \Gamma\langle \mathbf{u}\rangle_i$ and $\langle \mathbf{u}\rangle$ are related by $\langle \mathbf{u}\rangle_i$ through $\langle \mathbf{u}\rangle = \varepsilon\langle \mathbf{u}\rangle_i$ (see Appendix), equation (6) becomes

$$(\rho/\varepsilon)\partial\langle \mathbf{u}\rangle/\partial t + (\rho/\varepsilon^2)\langle \mathbf{u}\rangle.\nabla\langle \mathbf{u}\rangle = -\nabla\langle P\rangle_i + \mu\langle \mathbf{u}\rangle.[(1/\varepsilon)(V_f^{-1}\int \mathbf{n}.\nabla\Gamma dA - V_f^{-1}\int \mathbf{I}.\Phi dA)] -$$
$$\rho\langle \mathbf{u}\rangle.\langle \mathbf{u}\rangle.[(1/\varepsilon^2)(V_f^{-1}\int \mathbf{n}.\Gamma dA)] + \mu\nabla\langle \mathbf{u}\rangle.[(1/\varepsilon)V_f^{-1}\int \mathbf{n}.\Gamma\, dA] + (\mu/\varepsilon)\nabla^2\langle \mathbf{u}\rangle \qquad (7)$$

Equation (7) is the key relation in this exercise. Compared with equation (1), in addition to the terms accounting for the convective inertia effects $\{(\rho/\varepsilon^2)\langle \mathbf{u}\rangle.\nabla\langle \mathbf{u}\rangle\}$

and the viscous resistance of fluid flow $\{(\mu/\varepsilon)\nabla^2\langle\mathbf{u}\rangle\}$, new terms accounting for the effects of interaction between the fluid and the matrix appear: $\{\rho\langle\mathbf{u}\rangle.\langle\mathbf{u}\rangle.[(1/\varepsilon^2)(V_f^{-1}\int\mathbf{n}.\Gamma dA)]$, $\mu\nabla\langle\mathbf{u}\rangle.[(1/\varepsilon)V_f^{-1}\int\mathbf{n}.\Gamma dA]$, $\mu\langle\mathbf{u}\rangle.[(1/\varepsilon)(V_f^{-1}\int\mathbf{n}.\nabla\Gamma dA - V_f^{-1}\int\mathbf{I}.\Phi dA)]\}$.

In the next section, the terms accounting for the effects of interaction between the fluid and the matrix will be discussed, in order to clarify their physical meaning and to present them in a more convenient and traditional way.

2.2.2 The range of validity of the motion equation

In order to complete the formulation of the motion equation developed in Section 2.2.1, the range of validity must be analysed. Therefore in this section two types of medium will be analysed: a medium with poor fluid transmissivity and a medium with high fluid transmissivity.

2.2.2-1 Medium with poor fluid transmissivity (the flow is considered to be incompressible [4])

If the flow is incompressible ($\nabla\langle\mathbf{u}\rangle=0$) and the volume of the solid matrix is larger than the volume occupied by the fluid ($(\mu/\varepsilon)\nabla^2\langle\mathbf{u}\rangle\approx 0$ [11]), then the second left-hand side term and the last right-hand side term of equation (7) can be discarded. This allows us to write for a steady flow

$$\rho\langle\mathbf{u}\rangle.\langle\mathbf{u}\rangle.[(1/\varepsilon^2)(V_f^{-1}\int\mathbf{n}.\Gamma dA)] = -\nabla\langle P\rangle_i + \mu\langle\mathbf{u}\rangle.[(1/\varepsilon)(V_f^{-1}\int\mathbf{n}.\nabla\Gamma dA - V_f^{-1}\int\mathbf{I}.\Phi dA)] \quad (8)$$

Darcy domain

In the range of Darcy's law (Reynolds numbers not exceeding 1 [4]) the velocities are very small. So, the squared fluid velocity term is negligible compared to the linear fluid velocity term, and we obtain from equation (8)

$$\mu\langle\mathbf{u}\rangle.[(1/\varepsilon)(V_f^{-1}\int\mathbf{n}.\nabla\Gamma dA - V_f^{-1}\int\mathbf{I}.\Phi dA)] = \nabla\langle P\rangle_i \quad (9)$$

The term in brackets can be associated with the viscous resistance force due to

momentum transfer at the matrix-fluid interface and is traditionally identified as [10,11]

$$[(1/\varepsilon)(V_f^{-1} \int \mathbf{n}.\nabla\Gamma dA - V_f^{-1} \int \mathbf{I}.\Phi dA)] = -K^{-1} \quad (10)$$

where K is the permeability of the medium (m^2).

Permeability represents the ability of the medium to transmit the fluid through it. In accordance to kinetic gas theory [11], permeability is related to the reciprocal of the collision frequency of diffusing particles against the solid matrix and the kinematic fluid viscosity.

Forchheimer domain

In the Forchheimer domain [4] the pressure gradient is proportional to a linear term of fluid velocity plus a squared velocity term (equation (8)). The term in brackets that refers to the linear term is given by equation (10). The left-hand side term in brackets relating to the pores' inertia effects is traditionally identified as [3,12]

$$[(1/\varepsilon^2)(V_f^{-1} \int \mathbf{n}.\Gamma dA)] = YK^{-1/2} \quad (11)$$

where Y is a porous inertia factor.

2.2.2-2 Medium with high fluid transmissivity

A medium is very transmissive to fluid when its permeability is very high ($K \to \infty$ and $\varepsilon \approx 1$ [11]). According to equations (10) and (11), the terms concerning the viscous resistance force, brought about by the momentum transfer at the matrix-fluid interface and the porous inertia effects can be discarded. The motion equation (7) will be

$$\rho\partial\langle\mathbf{u}\rangle/\partial t + \rho\langle\mathbf{u}\rangle.\nabla\langle\mathbf{u}\rangle = -\nabla\langle P\rangle + \mu\nabla^2\langle\mathbf{u}\rangle + \mu\nabla\langle\mathbf{u}\rangle.[(1/\varepsilon)V_f^{-1} \int \mathbf{n}.\Gamma dA] \quad (12)$$

In accordance with equation (11) the last right side term in brackets of (12) can be identified as $YK^{-1/2}$. The permeability of a high fluid transmissivity medium is very high ($K \to \infty$) and $Y\varepsilon K^{-1/2} \to 0$, that is, we recover the motion equation (1) valid for a fluid volume element.

2.2.3. Motion equation for a permeable medium

According to section 2.2.1 and 2.2.2 the motion equation for a permeable medium (containing pores or openings) can be rewritten as

$$(\rho/\varepsilon)\partial\langle\mathbf{u}\rangle/\partial t+(\rho/\varepsilon^2)\langle\mathbf{u}\rangle.\nabla\langle\mathbf{u}\rangle=-\nabla\langle P\rangle_i-(\mu/K)\langle\mathbf{u}\rangle-\rho Y K^{-1/2}\langle\mathbf{u}\rangle.\langle\mathbf{u}\rangle+$$
$$\mu Y\varepsilon K^{-1/2}\nabla\langle\mathbf{u}\rangle+(\mu/\varepsilon)\nabla^2\langle\mathbf{u}\rangle \qquad (13)$$

The advantages of the approach described by equation (13) when compared with the existing literature [1-4] are

- one equation is sufficient to describe flows through media with pores up to large openings instead of several equations,
- the approach was deduced without using empirical information.

The inertial factor Y was shown to be dependent on the porosity and a coefficient c_Y, and can be obtained using the relationship [12,13]

$$Y=c_Y\varepsilon^n \qquad (14)$$

The values usually employed are c_Y equal to 14.29×10^{-2} or 4.36×10^{-2} and n equal to -1.5 or -2.12, for channels filled with packed beds [12] and for permeable screening media [13], respectively.

Equation (13) is a non-linear differential equation and can be solved together with mass and energy balance equations using numerical techniques within CFD. The velocity, pressure and temperature throughout the flow field can be predicted.

Solving the transport equations numerically is difficult and in some engineering applications the detail of CFD solutions is not required. For these applications it is important to have a model which quantifies the phenomenon accurately and simply. This will be the subject of the next section.

2.2.4. Simplified motion equation for pores and openings

In dealing with most of practical applications, an one-dimensional flow description provides a good approximation [1-3]. Under this assumption equation (13) can be written as

$$(\rho/\varepsilon)\partial\langle u_j\rangle/\partial t+(\mu/K)\langle u_j\rangle+\rho Y K^{-1/2}\langle u_j\rangle\langle u_j\rangle+\Omega\langle u_j\rangle=-\partial\langle P_j\rangle_i/\partial j \quad (15)$$

with

$$\Omega=[\rho\varepsilon^{-2}-Re^{-1}L(Y\varepsilon K^{-1/2}+\varepsilon^{-1}\partial/\partial j](\partial\langle u_j\rangle/\partial j)$$

where j represents the flow direction (perpendicular to the transmitting medium), Re the Reynolds number and L a length dimension.

For porous media, according to Bear [4], $\partial u/\partial j=0$ and consequently

$$\Omega=0 \quad (16)$$

In order to obtain Ω for openings, consider a medium which has very high fluid transmissivity ($K \to \infty$ and second, third left-hand side terms can be discarded). Assuming a steady flow, the resulting equation can be integrated along a streamline and for any two points on this trajectory at distance H

$$0.5\rho\Delta\langle u\rangle^2=\Delta\langle P\rangle+0.5\rho Re^{-1}(L/H)\Delta\langle u\rangle^2 \quad (17)$$

with

$$\Delta\langle u\rangle^2=\langle u_{H1}\rangle^2-\langle u_{H2}\rangle^2$$

where u_{H1} and u_{H2} are the velocity at two different points of the streamline.

To obtain a non-steady equation again, an integral ($\int\partial\langle u\rangle/\partial t dH=H\,\partial\langle u\rangle/\partial t$) must be added, becoming

$$\partial\langle u\rangle/\partial t+0.5\rho C_c^{-2}\langle u\rangle^2/H=\Delta\langle P\rangle/H \quad (18.1)$$

with

$$0.5\rho\Delta\langle u\rangle^2=0.5\rho c_{lo}\langle u\rangle^2 \quad (18.2)$$

$$C_c=\{c_{lo}[1-Re^{-1}(L/H)]\}^{-1/2} \quad (18.3)$$

where H is the characteristic depth of the medium and c_{lo} a parameter accounting for kinetic energy loss.

In accordance with equation (18.1), for openings, the parameter Ω can be now written as

$$\Omega=0.5\rho C_c^{-2}\langle u\rangle/H \quad (19)$$

The coefficient C_c is dependent on Re and on the characteristics of the opening. The

influence of Re on the coefficient C_c is shown in Fig. 2-2. Fig. 2-2 shows that C_c is strongly dependent on Re only where Re<25. That is, for Re>25 the flow can be considered non-viscous and C_c becomes equal to $c_{lo}^{-1/2}$.

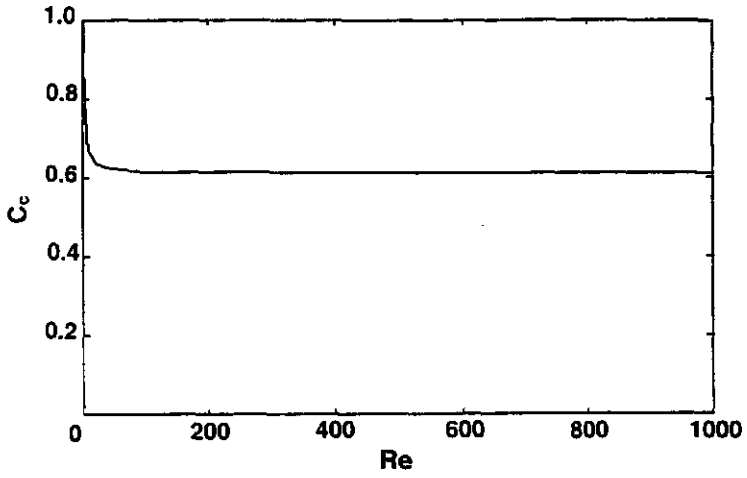

Fig. 2-2. Convective coefficient versus the Reynolds number (Re>1).

In order to use equation (15) for openings, we need to know c_{lo} for openings with various shapes and sizes. This will be determined in the next section.

2.3 EXPERIMENTAL STUDY

The purpose of this section is to determine the unknown parameters c_{lo} (for openings), Y and K (for porous materials). For porous materials the experiments were performed using porous screen samples with trade names "ECONET F" and "LS 10 PLUS". For openings the experiments were performed using openings of various

shapes and sizes. In both experiments, the samples were subjected to several air flows, causing a constant pressure drop between the sample sides (DC-pressurization method [13]).

2.3.1. Description of experiments

The experiments were conducted in a wind tunnel described in detail by Miguel et al. [13], as shown in Fig. 2-3.

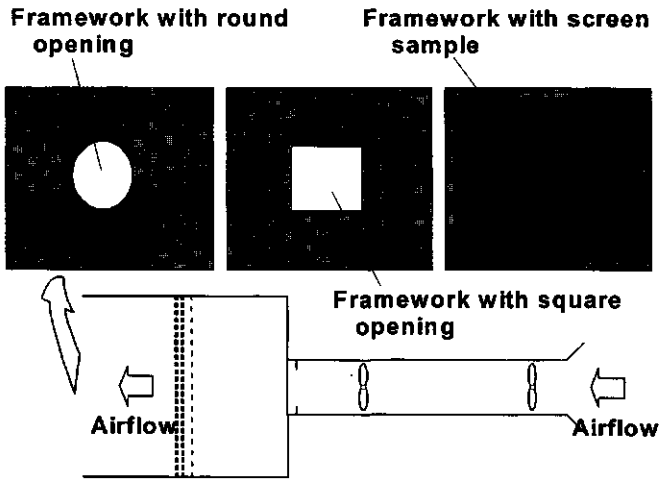

FIG. 2-3. Schematic representation of the test apparatus used to cause a pressure drop between the samples tested.

In order to determine the parameter c_{lo} a plane framework fixed to the outlet side of the test box was used, which allows an opening to be changed both in shape (square or round) and in area (the ratio between the area of the opening and the area of the framework can be varied between 0.01 and 0.95).

The experiments were performed satisfying a Reynolds range between 72 and $4x10^5$

(excluding the influence of viscous effects).

In order to determine the parameters Y and K, the test screens were fixed to the outlet side of the test box using a wooden frame, which prevents air leakage. The experiments were performed satisfying a Reynolds range between 0.7 and 97.

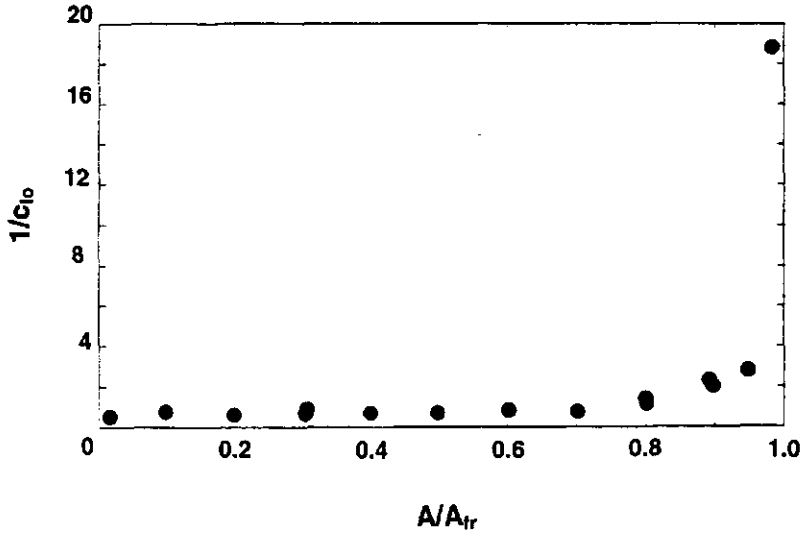

FIG. 2-4. The measured coefficient $1/c_{lo}$ for a round and square opening as a function of the ratio between the free area of the opening and the area of flow field.

2.3.2. Results and discussion

The data resulting from the experiments performed using openings were plotted as shown in Fig. 2-4.

The parameter c_{lo} seems to be independent of the shape of the opening (square or round) but depends on the ratio between the free opening area (A) and the flow field

area (A_{fr}). It is in full agreement with the equation

$$c_{lo}=\{2.7-0.04203\ \exp[3.7(A/A_{fr})^{1/2}]\}$$
$$\{1-[2.7-0.04203\ \exp[3.7(A/A_{fr})^{1/2}]]\ (A/A_{fr})^{2.5}\}^{1/2} \quad (20)$$

Substituting equation (20) in (18.3) provides

$$C_c^{-2}=[1-Re^{-1}(L/H)]\ \{2.7-0.04203\ \exp[3.7(A/A_{fr})^{1/2}]\}$$
$$\{1-[2.7-0.04203\ \exp[3.7(A/A_{fr})^{1/2}]](A/A_{fr})^{2.5}\}^{1/2} \quad (21)$$

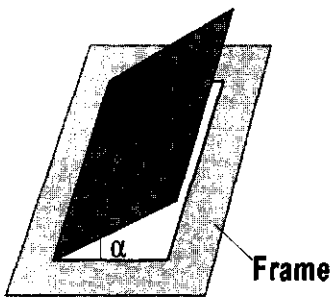

FIG. 2-5. Schematic representation of rectangular opening with a flap.

Similar experiments were conducted by Bot [14] using rectangular openings with flaps (Fig. 2-5) placed in a plane framework ($A \ll A_{fr}$). This study found practical application in apertures with doors and greenhouse windows. The data resulting from the experiments performed satisfying a Reynolds range between $2x10^2$ and $2.1x10^4$, and angles between the flap and the frame less than or equal to 90°, are represented in Fig. 2-6.

The parameter c_{lo} seems to be dependent on the dimensions (length and width ratio) of the opening and could be described by the following equation

$$c_{lo}=\{1.75+0.7\exp[-(L_l/L_s)\sin\alpha/32.5]\}$$
$$\{\sin\alpha[1+0.60(L_l/L_s)(\cos\alpha-2\pi((90-\alpha)/360)\sin\alpha)]\}^{-2} \quad (22)$$

and

$$C_c^{-2}=\{\{1.75+0.7\exp[-(L_l/L_s)\sin\alpha/32.5]\}\ \{\sin\alpha[1+0.60(L_l/L_s)$$
$$(\cos\alpha-2\pi((90-\alpha)/360)\sin\alpha)]\}^{-2}\ [1-Re^{-1}(L_s/H)]\} \quad (23)$$

where α is the opening angle between the flap and the frame, L_l the larger length of the opening and L_s the smaller length of the opening.

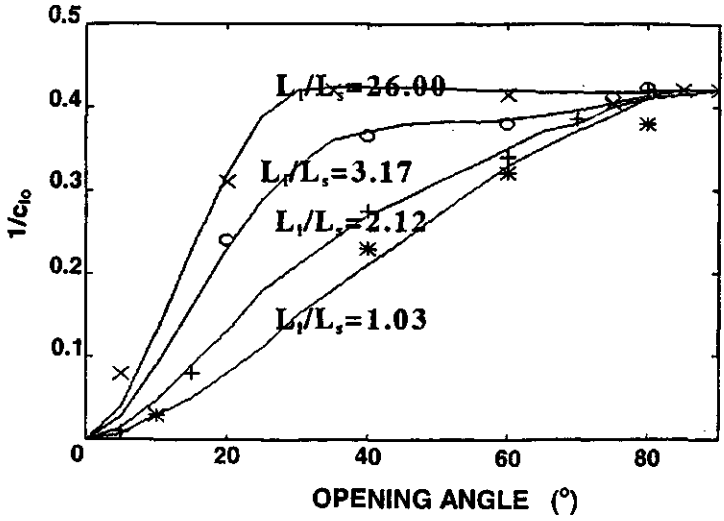

FIG. 2-6. The measured coefficient $1/c_{lo}$ for a rectangular opening as a function of opening angle between the flap and the frame.

According to equation (20), for $A=A_{fr}$ there are no flow obstructions and c_{lo} is zero ($C_c^{-2}=0$), i.e., pressure drop is equal to zero. Therefore, according to equations (20) and (22), for a non-viscous flow through a round or square opening in a large framework ($A/A_{fr}\approx 0$), and for an opening with opening angle of 90°, the coefficient C_c achieves values close to 0.60 and 0.63, respectively. These values are close to the value usually found for the so-called "discharge coefficient" in the literature (0.61).

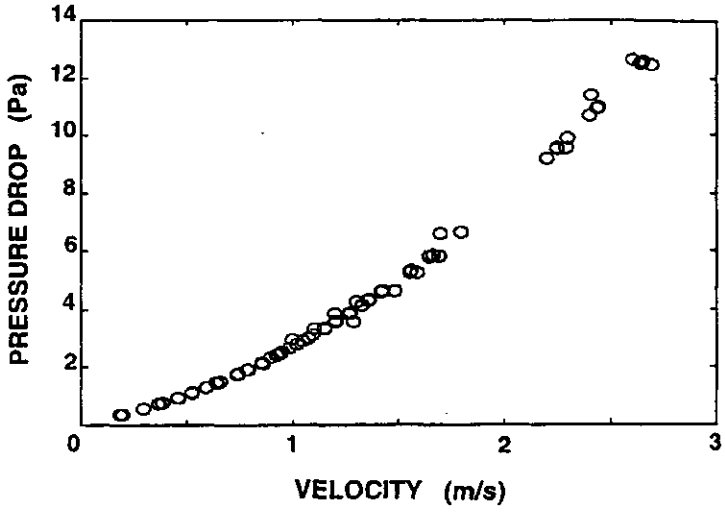

FIG. 2-7. Pressure drop as a function of the velocity for a porous screen trade name "ECONET F".

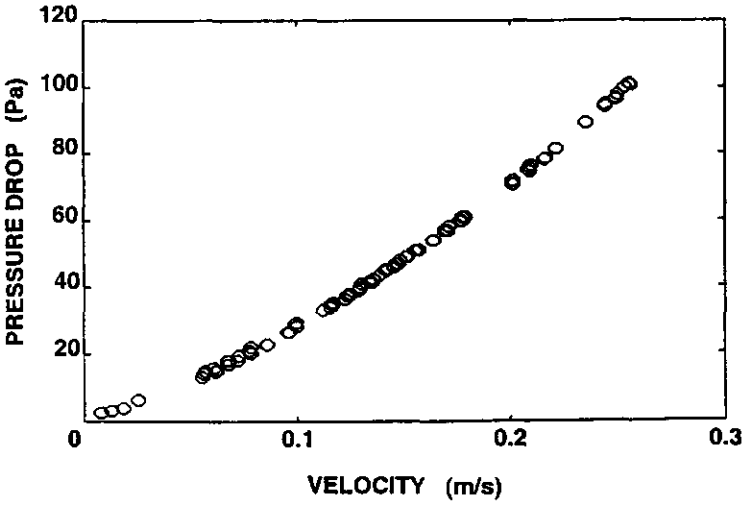

FIG. 2-8. Pressure drop as a function of the velocity for a porous screen trade name "LS 10 PLUS".

The data resulting from the experiments performed using porous screen samples were plotted as shown in Figs. 2-7 and 2-8.

The parameters Y and K are obtained fitting the experimental data with the Forchheimer equation. The permeabilities obtained for screen ECONET F and LS 10 PLUS were 6.51×10^{-09} m^2 and 6.79×10^{-11} m^2, and parameter Y equal to 0.457 and 7.18, respectively. The porosities can then be found using equation (14) and were 0.09 and 0.33, respectively.

Equation (15) together with equations (16), (21) and (23) form a simplified mathematical model to describe one-dimensional forced fluid motion through pores and openings.

2.4 CONCLUSIONS

This paper describes some physical aspects of forced convection through permeable media. The results described above show that, for forced convection, one theory seems to be sufficient to describe flow phenomena through porous media and through non-porous media (gaps, cracks, doors, windows).

The approach developed in this study enables the air infiltration in enclosed spaces to be analysed. We describe this application elsewhere [15].

2.5 REFERENCES

[1] **Allard F. and Utsumi Y.** 1992. Airflow through large openings, Energy and Buildings **26**, 133-145

[2] **Baker P. H., Sharples S. and Ward I. C.** 1987. Air flow through cracks, Build. and Environment **22**, 293-304

[3] **Forchheimer P.** 1901. Wasserbewegung durch boden, Z. Ver. Deutsch. **45**, 1782-1788 [in German]

[4] **Bear J.** 1972. Dynamics of fluids in porous media, American Elsevier Environmental Sciences Series, New York, USA

[5] **Gray W.** G. 1975. A derivation of the equations for multiphase transport, Chem. Engng. Sci. **30**, 229-233

[6] **Slattery J. C.** 1967. Flow of viscoelastic fluids through porous media, AIChE Journal **13**, 1066-1071

[7] **Howes F. A. and Whitaker S.** 1985. The spatial averaging theorem revisited, Chem. Engng. Sci. **40**, 1387-1392

[8] **Quintard M. and Whitaker S.** 1994. Transport in ordered and disordered porous media II: Generalized volume averaging, Transport in porous media **14**, 179-206

[9] **Quintard M. and Whitaker S.** 1987. Écoulement monophasique en milieu poreux: Effet des hétérogéneites locales, J. Méc. Théor. Appl. **6**, 691-726

[10] **Whitaker S.** 1986. Flow in porous media I: A theoretical deviation of Darcy's law, Transport in Porous media **1**, 3-25

[11] **Lebon G. and Cloot A.** 1986. A thermodynamical modelling of fluid flows through porous media: application to natural convection. Int. J. Heat Mass Transfer, **29**, 381-390

[12] **Ergun S.** 1952. Fluid flow through packed columns, Chemical Engineering Progress **48**, 89-94

[13] **Miguel A. F., van de Braak N. J., Silva A. M. and Bot G. P. A.** 1997. Analysis of the airflow characteristics of greenhouse screens, J. Agr. Eng. Research **67**, 105-112.

[14] **Bot G. P. A.** 1983. Greenhouse climate: from physical processes to a dynamic model, Ph.D. Dissertation, Agricultural University of Wageningen, The Netherlands

[15] **Miguel A. F., van de Braak N. J., Silva A. M. and Bot G. P. A.** 1998. Analysis of air exchange and internal pressures in enclosures induced by fluctuating outside pressures, Building and Environment (in press)

2.6 APPENDIX

Basic formulation of the method of volume averaging

Consider a homogeneous system whose averaging volume, represented in Fig. 2-1, is invariant with respect to time and space. For a two-phase system (solid matrix and fluid) the averaging volume is defined as

$$V=V_s+V_f \tag{A.1}$$

where V_s and V_f represent the volume of the solid and fluid contained within the averaging volume, respectively.

The fluid porosity ε is given by

$$\varepsilon=V_f/V \tag{A.2}$$

The porosity represents the volume fraction of fluid contained within the averaging volume of the medium and it is between 0 and 1 ($0<\varepsilon\leq 1$). Specifically for one opening it is 1 ($\varepsilon=1$, all open volume is filled with fluid).

The average of a local quantity Λ (fluid velocity, fluid pressure) in the averaging volume, can be formulated in terms of superficial (external) phase average or intrinsic (internal) phase average. The intrinsic (internal) phase average is defined as

$$\langle\Lambda\rangle_i=V_f^{-1}\int\Lambda\, dV \tag{A.3-1}$$

and the superficial (external) phase average as

$$\langle\Lambda\rangle=V^{-1}\int\Lambda\, dV \tag{A.3-2}$$

where $\langle\Lambda\rangle$ is the superficial phase average of local quantity Λ and $\langle\Lambda\rangle_i$ the intrinsic phase average of local quantity Λ.

These two averages are related by the porosity according to

$$\langle\Lambda\rangle=\varepsilon\langle\Lambda\rangle_i \tag{A.4}$$

The local values of the quantity Λ can also be related to the phase averages according to [5]

$$\Lambda=\langle\Lambda\rangle_i+\tilde{\Lambda} \tag{A.5}$$

where $\tilde{\Lambda}$ is the spatial deviation of Λ compared to $\langle\Lambda\rangle_i$.

In the analysis of equations governing transport phenomena in porous media it is usual to interchange differentiation and integration in order to express the quantity in terms of intrinsic phase average. This will be done by means of the spatial averaging theorem [6,7]. This theorem can be written in vector form as

$$\langle\nabla.\Lambda\rangle_i=\nabla.\langle\Lambda\rangle_i + V^{-1}\int\mathbf{n}.\Lambda dA \qquad (A.6)$$

where **n** is a unit vector and A the interfacial area contained within the averaging volume.

Substitution of equation (A.5) in equation (A.6) gives

$$\langle\nabla.\Lambda\rangle_i=\nabla.\langle\Lambda\rangle_i + V_f^{-1}\int\mathbf{n}.\langle\Lambda\rangle_i dA+V_f^{-1}\int\mathbf{n}.\tilde{\Lambda}dA \qquad (A.7)$$

As the system under consideration is homogeneous, $\langle\Lambda\rangle_i$ can be treated as a constant, and consequently the area integral becomes

$$V_f^{-1}\int\mathbf{n}.\langle\Lambda\rangle_i\, dA=(\varepsilon^{-1}V^{-1}\int\mathbf{n}dA).\langle\Lambda\rangle_i \qquad (A.8)$$

The integral in parenthesis is related to the structure of the volume studied and can be expressed by [8]

$$\varepsilon^{-1}V^{-1}\int\mathbf{n}dA=-\nabla\varepsilon/\varepsilon \qquad (A.9)$$

which can easily be proved to be zero for a homogeneous system.

If the system studied is heterogeneous, that is, it is characterised by more than one length scale, we will need to use a large-scale averaging [9]. Heterogeneous systems are beyond the scope of this study.

2.7 NOMENCLATURE

A	area [m^2]
C_c	coefficient accounting for convective inertia and viscous effects
c_{lo}	parameter accounting for kinetic energy loss
H	characteristic depth [m]
K	permeability [m^2]
L	length dimension [m]

P pressure [Pa]

Re Reynolds number

t time [s]

$\acute{u}$ velocity [ms^{-1}]

V volume [m^3]

Y inertial factor

Greek symbols

α opening angle between the flap and the frame [°]

ε porosity

Λ local general quantity likes velocity or pressure

$\langle\Lambda\rangle$ superficial (external) phase average of quantity Λ

$\langle\Lambda\rangle_i$ intrinsic (internal) phase average of quantity Λ

μ dynamic viscosity [Pa s]

ρ density [kg m^{-3}]

Subscripts

f fluid

fr flow field

i intrinsic

3. Analysis of air exchange induced by fluctuating external pressures in enclosures [+]

Abstract: A new approach using the equations of mass conservation and motion, and the state equation of gases, is proposed to characterise air infiltrations induced by fluctuating pressures. The approach is applied to a two-zone enclosure with openings and pores. Experimental data obtained for the purpose of testing the validity of the approach are found to agree well with the predicted values.

3.1 INTRODUCTION

Air infiltration in enclosures is the main process, which affects the mass and energy balance inside the enclosure and consequently the indoor climate [1]. The continuing interest in this topic is based on the lack of a comprehensive and satisfactory theory, despite much important work and a great number of studies that has been done [2,3].

Pressure due to wind is one of the main driving forces in the study of air infiltration in enclosures. Wind velocity fluctuates and therefore induces wind pressures (with a mean component and a fluctuating component) which influence pressure differences between the inside and outside of the enclosures.

The internal pressure in any enclosure is controlled by the wind pressure and by the characteristics of the enclosure envelope [4,5]. The nature of response of internal pressure due to the wind was first studied by Euteneuer [6]. However, he neglected the inertia effect of the airflow entering the opening. Inspired by the classical Helmholtz resonator model, Holmes [7] and Liu and Saathoff [8] studied the transient response of internal pressure fluctuations in a constant volume enclosure with one large opening using a second-order non-linear differential equation. Recently, Dewsbury [9] presented a model, which includes variation of the enclosure volume. Liu and Rhee [10] made an experimental study of the nature of the wind-induced Helmholtz oscillation of air pressure in buildings. They demonstrated that the tendency to

[+] ***Building and Environment*** **(in press)**

resonance increases concomitantly with a window area increasing relative to the volume of the building.

The differences in internal and external pressure induce air infiltrations in enclosures. The models available in literature describe the air infiltrations through narrow openings (pores, gaps, cracks) [11,12] and through large openings (windows, doors) [13,14]. For narrow openings the majority are based on empirical equations and for large openings on Bernoulli's equation. The empirical parameters in these equations are determined by performing experiments in which air is forced through the enclosure envelope, producing a constant pressure difference between inside and outside (DC-pressurization method [15]) or producing a sinusoidal pressure difference (AC-pressurization method [9,16,17]). The parameters are obtained by fitting the experimental data with appropriate equations.

The purpose of this paper is to present a coherent mathematical model, based on principles of physics, studying airflow in enclosures with openings and pores induced by fluctuating external pressures. The applicability of the model is illustrated through the study of air exchanges in a two-zone enclosure with openings and pores.

3.2 MATHEMATICAL FORMULATION

3.2.1. General description of the model

Consider an enclosure of volume V_e, exchanging air with the outside, through one opening with a large free area, or through a structure with narrow openings or pores of area A. Under the assumptions that

- the air within the enclosure is an ideal gas and compressible
- the air exchange with the exterior is unidimensional

we can write

The equation of mass conservation for air within the enclosure

$$dM/dt = A \rho u \qquad (1.1)$$

or

$$\rho dV/dt+Vd\rho/dt=A\ \rho\ u \quad (1.2)$$

with

$$V=V_e-\Sigma_n V_n$$

where u represents the air velocity through the infiltrations, M total mass of air in the enclosure, ρ the density of air in the enclosure, A the area of infiltrations, t the time, V the total volume of air in the enclosure, V_e the volume of enclosure and V_n the volume of objects within the enclosure.

Usually the enclosure envelope is considered to be rigid and not to deform ($dV_e/dt=0$). In reality, however, the roof and walls deform to an extent that depends on the magnitude of pressure exerted, influencing the airflow through the enclosure envelope. Bearing in mind the behaviour of elastic materials, the enclosure deformation can be simply calculated assuming

$$(V_e-V_{em})/V_{em}=\eta\ (p-p_m) \quad (2)$$

where V_{em} represents the mean volume of the enclosure, p the pressure, p_m the mean pressure and η the enclosure flexibility coefficient.

Substituting (2) in (1.2) yields

$$(V_{em}-\Sigma_n V_n)\rho^{-1}d\rho/dt=A\ u+\Sigma_n dV_n/dt-\eta V_{em}dp/dt \quad (3)$$

This equation indicates how the density of air within the enclosure is related to the airflow through the infiltrations, the enclosure flexibility and the volume change of objects within the enclosure.

The j-direction motion equation for air through openings and pores [18]

$$(\rho/\varepsilon)\partial u/\partial t+\mu K^{-1}u+\rho q|u|u=\partial p/\partial j \quad (4)$$

with

$$q=(4.36x10^{-2}\varepsilon^{-2.12}K^{-1/2}+0.5C_c^{-2}/H)$$

where ε is the porosity [18], K the permeability [18], μ the fluid dynamic viscosity, p the pressure, H the characteristic depth of the medium and C_c a coefficient accounting

for convective inertia and viscous effects.

For a porous medium [18]

$$C_c^{-2}=0 \tag{5.1}$$

for round and square openings [18]

$$C_c^{-2}=[1-Re^{-1}(L/H)]\ \{2.7-0.04203\ \exp[3.7(A/A_{fr})^{1/2}]\}$$
$$\{1-[2.7-0.04203\ \exp[3.7(A/A_{fr})^{1/2}]](A/A_{fr})^{2.5}\}^{1/2} \tag{5.2}$$

and for rectangular openings covered with movable flaps [18]

$$C_c^{-2}=\{\{1.75+0.7\exp[-(L_l/L_s)\sin\alpha/32.5]\}\ \{\sin\alpha[1+0.60(L_l/L_s)$$
$$(\cos\alpha-2\pi((90-\alpha)/360)\sin\alpha)]\}^{-2}\ [1-Re^{-1}(L_s/H)]\} \tag{5.3}$$

where α is the opening angle between the flap and the frame, Re the Reynolds number, A_{fr} the flow field area, L_l the larger length of the opening and L_s the smaller length of the opening.

The equation of state for air within the enclosure

$$p=\rho R_g T \tag{6}$$

where T represents the absolute temperature and R_g the specific gas constant.

For a polytropic expansion or compression of ideal gas with constant heat capacity, equation (6) can be rewritten as

$$p\rho^{-\beta}=\text{constant} \tag{7}$$

where β is 1.4 for isentropic air expansion/compression and 1.0 for isothermal air expansion/compression.

3.2.2. *Fluctuating pressure inside an enclosure where air is exchanged with the outside through one opening with a large free area or through a structure with narrow openings or pores*

Pressure within an enclosure with compressible air

When pressure is applied to the air inside the enclosure, this is compressed and its

density changes. Consider a polytropic compression/expansion of the air within the enclosure. Substituting equation (7) in (3) gives, after integration,

$$(V_{em}-\Sigma_n V_{nm})\beta^{-1}(\Delta p/p)+\eta V_{em}\,\Delta p=\int A\ u\ dt+\Sigma_n(V_n-V_{nm}) \quad (8)$$

with

$$\Delta p=p_i=p-p_m$$

where V_{nm} represents the mean volume of objects inside the enclosure and Δp or p_i the pressure change within the enclosure.

Considering a small pressure change ($p_i \ll p$), equation (8) can be conveniently rewritten as

$$[(V_{em}-\Sigma_n V_{nm})+\beta p_m \eta V_{em}]p_i=\beta p_m \int A\ u\ dt+\beta p_m \Sigma_n(V_n-V_{nm}) \quad (9)$$

Equations (8) and (9) describe the pressure change inside the enclosure which is the fluctuating component of internal pressure.

Transient response of internal air pressure

The internal pressure also changes in response to the fluctuations occurring in the external pressure. The transient response of internal pressure can be easily obtained by substituting equations (3) and (7) in (4). The resulting equation is quite long and may by summarised as

$$a_1 d^2p/dt^2+a_2|dp/dt|dp/dt+a_3 dp/dt-a_4 d(\Sigma_n V_n)/dt|dp/dt|-a_5 d^2(\Sigma_n V_n)/dt^2+$$
$$a_6 d(\Sigma_n V_n)/dt+p=p_{ext} \quad (10)$$

with

$$a=a(p,\beta\ ,p_m,\rho_m,\eta,H,A,\mu,K,q,V_{em},\Sigma_n V_n,\ \Sigma_n V_{nm})$$

where ρ_m represents the mean fluid density and p_{ext} the external pressure.

Since the volume of objects inside the enclosure does not deform, equation (10) can be simplified to

$$a_1 d^2p/dt^2+a_2|dp/dt|dp/dt+a_3 dp/dt+AH^{-1}p=AH^{-1}p_{ext} \quad (11)$$

with

$$a_1=\rho_m \varepsilon^{-1}[(V_{em}-\Sigma_n V_{nm})(\beta p_m)^{-1}+\eta V_{em}]$$

$a_2=\rho_m qA^{-2}[(V_{em}-\Sigma_n V_{nm})^2(\beta p_m)^{-2}+2\eta V_{em}(V_{em}-\Sigma_n V_{nm})(\beta p_m)^{-1}+(\eta V_{em})^2]$

$a_3=\mu K^{-1}[(V_{em}-\Sigma_n V_{nm})(\beta p_m)^{-1}+\eta V_{em}]-\rho_m(V_{em}-\Sigma_n V_{nm})(\varepsilon\beta p_m^2)^{-1}$

Equations (10) and (11) are second-order non-linear differential equations and the following situations can occur:

- for an enclosure with an opening with a relatively large free area ($K\rightarrow\infty \Rightarrow$ μK^{-1} and $4.36x10^{-2}\varepsilon^{-2.12}K^{-1/2}$ are negligible compared to $0.5C_c^{-2}/H$), equations (10) and (11) present two forms of solution:

a) for $A\ll(V_{em}-\Sigma_n V_{nm})$ or $A\ll\eta V_{em}$ the second order term is important and we have a damped resonance equation (gradual decay)

b) for $A\gg(V_{em}-\Sigma_n V_{nm})$ and $A\gg\eta V_{em}$ the second order term is very small and we have an oscillatory equation with very little damping

- for an enclosure with narrow openings and pores ($\mu K^{-1}\gg 0$, $q\gg 0$), equations (10) and (11) are always damped resonance equations.

Our finding that the larger the area of the opening in relation to the enclosure volume, the greater the tendency to resonance, is supported by the observations of Liu and Rhee [10].

As we mentioned earlier, Holmes [7], Liu and Saathoff [8] and Dewsbury [9], presented models to study the transient response of internal pressure in enclosures with compressible air. Although the models presented by these authors also contain second-order non-linear differential equations and describe internal pressures in enclosures with large openings, they fail to describe internal pressures in enclosures with narrow openings and pores. The model presented here also differs from the models of Holmes [7], and Liu and Saathoff [8] in the following aspects

- it accounts for the flexibility of the enclosure envelope
- it accounts for volume changes of objects within the enclosure.

Equations (10) and (11) can not only be used to describe the change in internal pressure due to sudden opening or breaking of an aperture (window, door, etc.) under external pressure but also to obtain parameters η, K, C_c, A and H. These parameters

can be obtained accurately using the experimental procedure described by Dewsbury [9], and will cause little impact on the indoor environment.

Oscillation of internal pressure in enclosures with openings and pores

The solution of equation (11) can be compared with the models presented by Liu and Saathoff [8] and Dewsbury [9], by means of a numerical study. This comparison considers the hypothetical case of an enclosure (rigid volume of 200 m^3, η=0 Pa^{-1}) with one window (area of 2x2 m^2). The example also uses the following values: a stagnation pressure of 500 Pa, the parameter β equal to 1.4 (isentropic expansion/compression), the leakage coefficient 0.6 and the leakage exponent 2, both in Dewsbury equation. We used the atmospheric pressure as the initial internal pressure, and the stagnation pressure as the external pressure at the opening. The result is presented as a dimensionless quantity r_p, which represents the ratio between the pressure in the enclosure and the stagnation pressure, as shown in Fig. 3-1.

From Fig. 3-1, it can be concluded that the profile of the solutions is oscillatory and exhibits damping. The maximum amplitude oscillation (first cycle) occurs in equation (11). A difference in amplitude of about 4% is obtained by using the Liu and Saathoff equation, and of 1.4% by using the Dewsbury equation.

It is of interest to know the effect of the flexibility of the enclosure envelope on the internal pressure profile. For this purpose, an enclosure with flexibility coefficient 0 and $5x10^{-3}$ Pa^{-1} (ηV_{em} equal to 0 and 1 m^3Pa^{-1}) was considered. The results obtained using equation (11) are plotted in Fig. 3-2.

Note that in the enclosure with a flexible envelope the maximum pressure in the first cycle of oscillation is about 6% less than the enclosure with no flexibility, and equilibrium is reached more quickly.

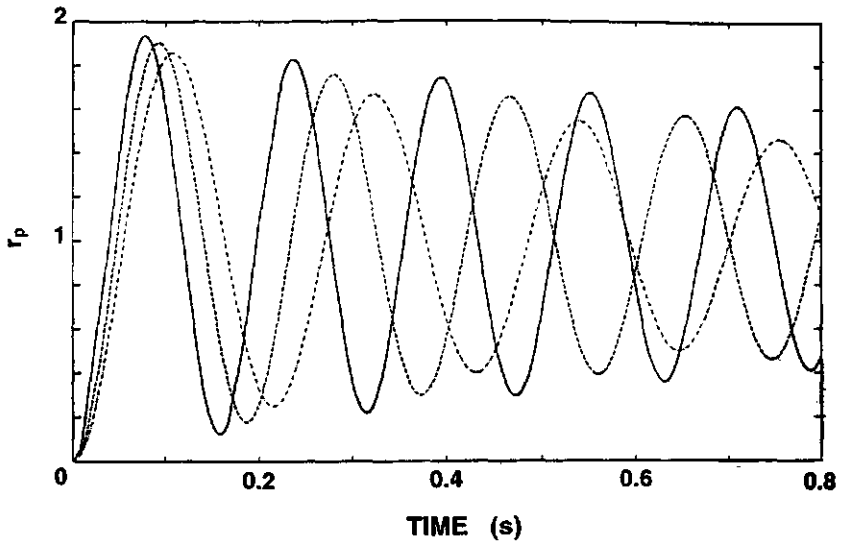

FIG. 3-1. Comparison of the solution presented by Liu and Saathoff [8] (-.-), by Dewsbury [9] (---) with the solution of equation (11) (—) for the internal pressure change due to sudden opening or breakage of an aperture.

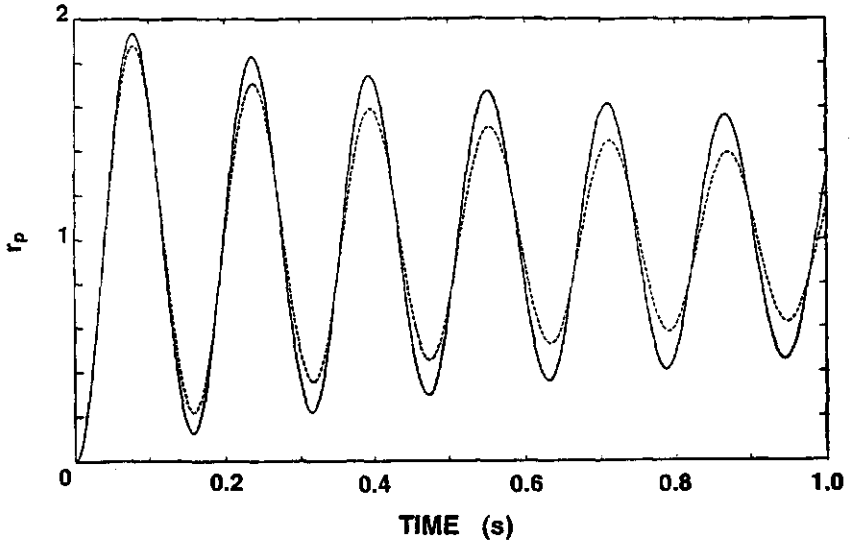

FIG. 3-2. Internal pressure change for an enclosure with flexible envelope (---) and with rigid envelope (—).

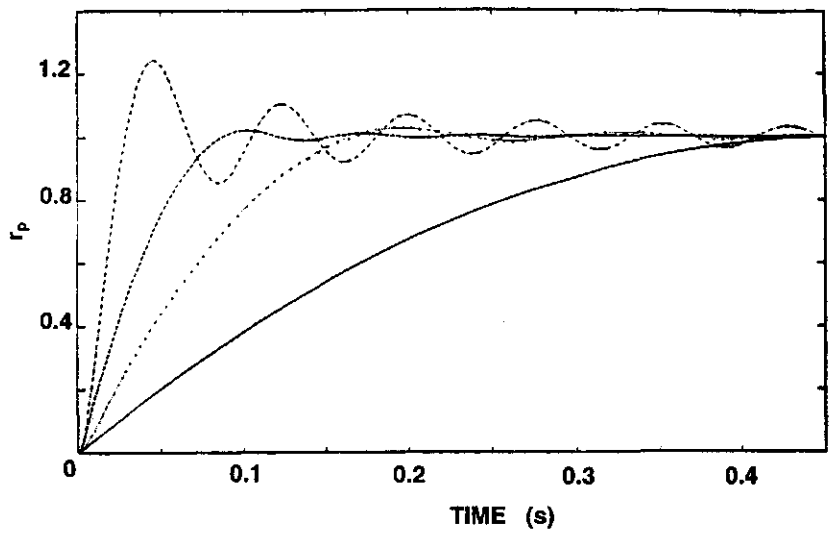

FIG. 3-3. Internal pressure change for enclosure with pores and narrow openings ($K=10^{-7}$ m^2: $\varepsilon=0.25$ (—) and $\varepsilon=0.75$ (...); $K=10^{-3}$ m^2: $\varepsilon=0.25$ (---) and $\varepsilon=0.75$ (-.-)).

To illustrate the nature of the solutions of equation (11) for narrow openings and for pores (beyond the range of the models available in the literature [7-9]), structures of permeability $K=10^{-3}m^2$ and $K=10^{-7}m^2$ (porosity $\varepsilon=0.25$ and $\varepsilon=0.75$) were considered. The values for the remaining quantities, and the assumptions made are the same as for the example included in Fig. 3-1, and the result is presented in Fig. 3-3.

Fig. 3-3 shows that, for the structure with permeability of $10^{-3}m^2$, the maximum value of the internal pressure coefficient (first cycle of oscillation) is about 1.242 for structure of porosity 0.75 (exceeding the internal pressure by about 24.2%) and 1.025 for structure of porosity 0.25 (exceeding the internal pressure by about 2.5%). For the structure with permeability of $10^{-7}m^2$, the internal pressure is exceeded by 1.6% and

0.2% for structures of porosity 0.75 and 0.25, respectively. In both situations the internal pressure is strongly damped and the equilibrium is reached almost immediately.

3.3 AIR EXCHANGE IN A MULTI-ZONE ENCLOSURE

In this section the formulation proposed in the previous sections is applied to the study of the air infiltration in

- an enclosure with one opening in an outside wall and a highly porous partition which divides the interior of the enclosure into two zones,
- the same as the above but using a partition with an opening.

3.3.1. Network equations

The airflow network which describes this two-zone enclosure (three nodes coupled by two non-linear resistances) is described in Fig. 3-4. According to equations (4) and (9), the motion and internal pressure change equations for zone 1 with openings or pores to zone 2 are

$$\rho_1\varepsilon_1^{-1}\partial u_1/\partial t+\mu K_1^{-1}u_1+\rho_1 q_1|u_1|u_1=(p_{i2}-p_{i1})/H_1 \quad (12)$$

$$[(V_{em}-\Sigma_n V_{nm})_1+\beta p_m\eta_1 V_{em1}]p_{i1}=\beta p_m\int(A_1u_1)\,dt \quad (13)$$

with

$$q_1=(4.36\text{x}10^{-2}\varepsilon_1^{-2.12}K_1^{-1/2}+0.5C_{c1}^{-2}/H_1)$$

For zone 2 with an opening to the exterior, the equations are

$$\rho_2\partial u_2/\partial t+\rho_2 q_2|u_2|u_2=(p_{ext}-p_{i2})/H_1 \quad (14)$$

$$[(V_{em}-\Sigma_n V_{nm})_2+\beta p_m\eta_2 V_{em2}]p_{i2}=\beta p_m\int(A_2u_2-A_1u_1)\,dt \quad (15)$$

with

$$q_2=0.5C_{c2}^{-2}/H_2$$

By solving this set of equations we obtain the air velocity through each opening or porous material as well as the internal pressure of each zone.

3.3.2 Experimental study

In an attempt to give experimental support to the model developed, an experimental study was carried out in a two-zone enclosure with a piston in the top, which pressurizes the air within the cube.

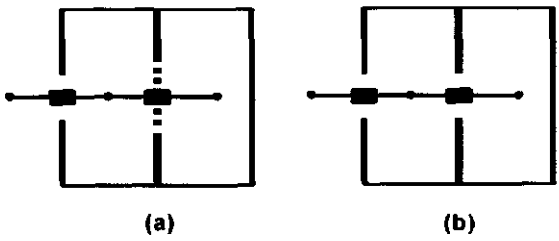

FIG. 3-4. Schematic representation of flow network for a two-zone enclosure with a highly porous material in the partition (a) and with an opening in the partition (b) (-■- resistance ● node)

Description of the experiments

The experiments were carried out in a cube-shaped enclosure (with dimensions of approximately 2.5x2.5x2.5 m^3), whose inside walls were hermetically sealed with aluminium foil. The walls of the cube are strengthened in order to avoid deformation. A round opening (diameter 0.59 m) was made in the ceiling of the enclosure. A horizontal partition divides the enclosure into two equal zones (Fig. 3-5). A square opening of 0.40x0.40 m^2 was made in the partition. The area of the opening could be adjusted and a permeable screen could be mounted in it. Two screens were used in this experiment: thermal screen type LS 10 PLUS and insect screen type ECONET F. The airflow characteristics (K,ε) were obtained by forcing air through these materials

(causing a constant pressure drop between the screen sides) and fitting the experimental data with the Forchheimer equation. Their respective permeabilities were 6.79×10^{-11} m^2 with porosity 0.09, and 6.51×10^{-09} m^2 with porosity 0.33 [18].

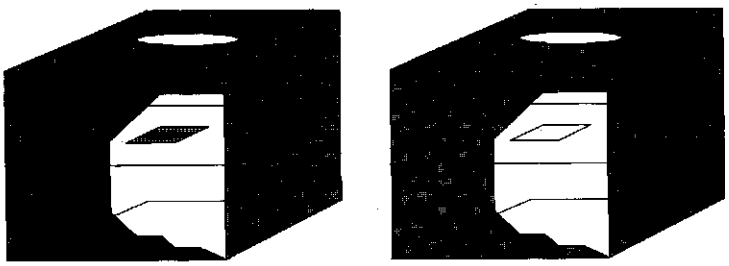

FIG. 3-5. Schematic representation of a two-zone enclosure with a highly porous material in the partition (a) and with an opening in the partition (b).

A cylinder (internal diameter 0.59 m) with a piston connected to a crankshaft was placed on top of the round opening (Fig. 3-6), in order to simulate the external pressure variations.

Fluctuating pressures of various magnitudes could be generated by changing the rotational speed of the crankshaft. This enabled the inflow and outflow of air through the round opening induced by the fluctuating wind pressure to be simulated. The frequency domain of the rotation of the crankshaft used in this study ranged from 0.02 Hz to 0.25 Hz.

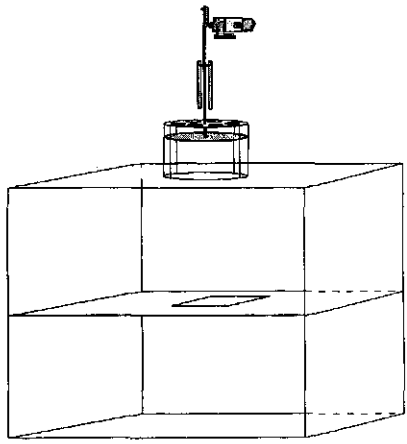

FIG. 3-6. Device used to simulate the wind induced fluctuating pressure.

A hot-wire anemometer (response time of 9.5 Hz) was placed 18 cm above the round opening in order to give readings of air (wind) velocity. The internal pressure was measured using membrane pressure transducers, in the inside openings and at six different points in the enclosure. A computer with a DAS1600 board (maximum sampling frequency 1000 Hz) controlled these measurements.

To obtain the effective mean air velocity through the openings and through the screens we applied the tracer gas (N_2O) constant flow and decay rate method. In the tracer gas constant flow method the gas is injected continuously with a constant flow into the cube and the concentration change in each zone is measured. In the decay rate method a quantity of tracer gas N_2O is supplied into the cube and the decline in concentration is measured. An IR gas analyser measures the gas concentration. Both methods are based on the principle of a perfect mixing of the inside air. To maintain a uniform gas concentration within zone 1 of the cube a small fan was placed near the ground. The air velocity resulting from the action of this fan was 1.1×10^{-5} m/s (accuracy within ±12%) for the screen, and 1.4×10^{-3} m/s (accuracy within ±8%) for the

opening. In zone 2 no fans were used.

Results and discussion

The values obtained from the solution of set of equations (12) to (15) were compared to experimental values of mean effective air velocity through the openings and the screens. The mean effective velocity and the mean effective pressure are the mean velocity and pressure during half of the period of time, respectively (on average, half of time is used for inflow and the other half for the outflow [13]).

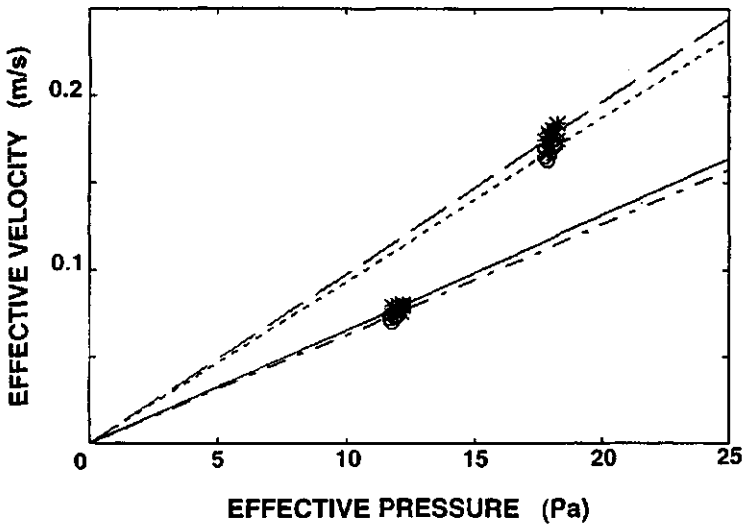

FIG. 3-7. Experimental (x, 0) and computed (__) effective air velocity through a round opening placed in the enclosure top, versus the effective pressure measured above the tope of the cube, for three rotational speeds of the crankshaft (corresponding to frequencies 0.08 Hz, 0.16 Hz and 0.24 Hz).

Fig. 3-7 shows the experimental and predicted mean effective air velocity through the round opening placed in the top, versus the mean effective pressure for a square opening, and a screen LS 10 PLUS mounted in the partition.

The mean effective air velocity through the top opening in the case of the square opening in the partition is larger than when the screen is in the partition. This is because the inside air volume available for pressurization or depressurization is larger in the case of the square opening than in the case of the screen.

Figs. 3-8 through 3-10 show the experimental and predicted mean effective velocities through the square opening, and through the ECONET F and LS 10 PLUS screens mounted in the partition.

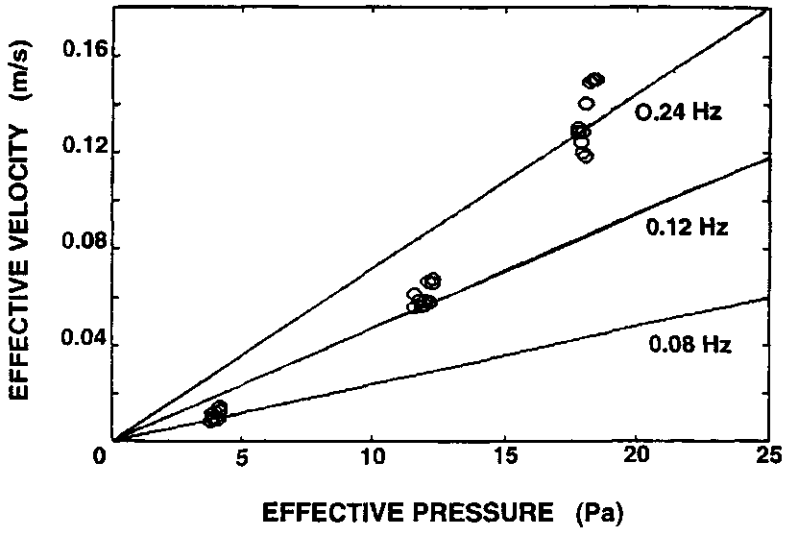

FIG. 3-8. Experimental (0) and computed (__) effective airflow through a square opening mounted in the enclosure partition, versus the wind velocity.

In Fig. 3-10, experimental data for frequency 0.24 Hz only are represented because for lower frequencies the air velocities were too low (less than $6x10^{-4}$ ms^{-1}) to obtain reliable results with the method used for the measurements.

Although a small fan was placed near the base of the cube, the mixing of the air

within the enclosure was not perfect and caused scattering in the results. Sudden changes of pressure in the experimental room due to opening of doors, etc., also seem to contribute to the scattering in the experimental data. As the data in Fig. 3-10 are in the order of $1x10^{-3}$ ms^{-1} (very small values), the sensitivity to the above mentioned factors is greater and consequently a larger scatter in experimental data is obtained.

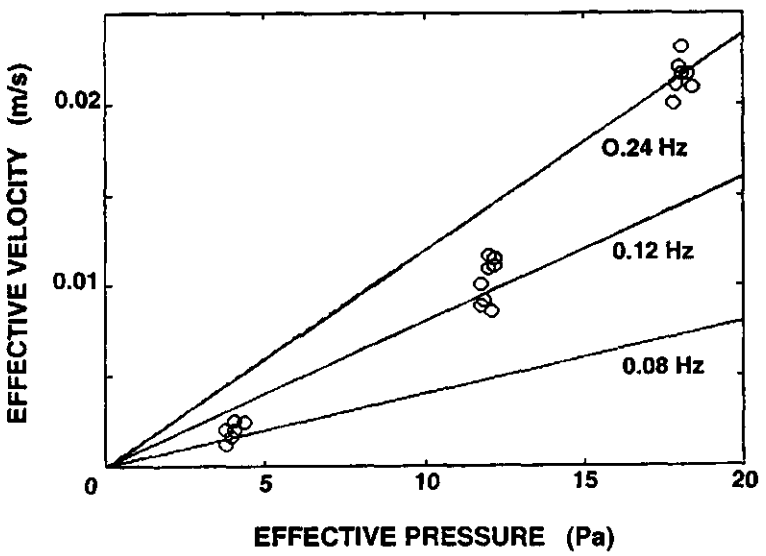

FIG. 3-9. *Experimental (0) and computed (__) effective airflow through a screening material* trade name "ECONET F" mounted in the enclosure partition, versus the wind velocity.

Note that, because of the limitations of the experimental apparatus used, the data collected do not fall within the same range of pressure for each frequency. Fortunately, this does not affect the results obtained, and the values measured for the values of pressure tested were found to agree fairly well with the values predicted by the proposed model.

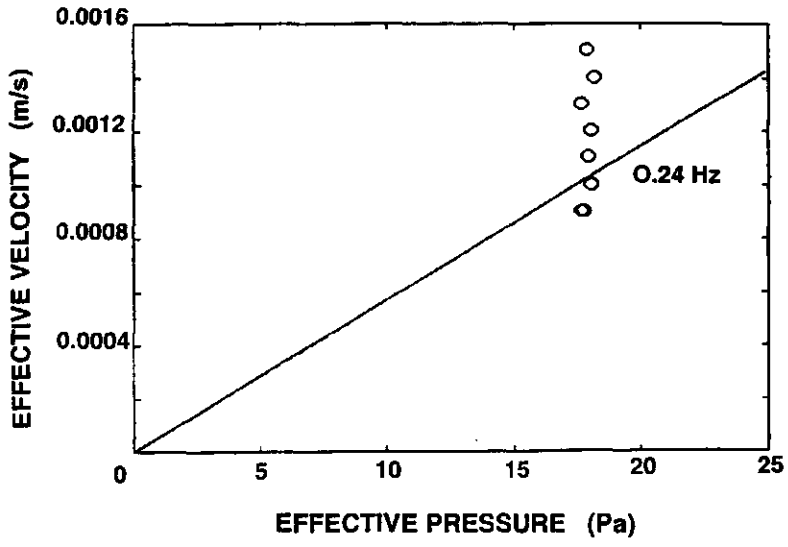

FIG. 3-10. Experimental (0) and computed (__) effective airflow through a screening material trade name "LS 10 PLUS" mounted in the enclosure partition, versus the wind velocity.

3.4 CONCLUSIONS

The models developed in this paper enable the computation of the pressure within enclosures and air velocity through structures ranging from pores to large openings.

The internal pressure model is based on the assumption that the air is an ideal gas and is compressible, and takes into account the flexibility of the enclosure envelope and the presence of objects within the enclosure.

Both the models available in the literature, and the model presented here to predict the transient response of internal pressure are second-order non-linear differential equations. However, the presented model has the advantage of being able to be used in enclosures containing apertures ranging in size from large openings to pores. Our approach can be used to describe the internal pressure change due to sudden opening

or breakage of an aperture under external pressure and also to obtain parameters η, K, C_c, A and H by fitting the approach with data obtained by the AC pressurization method.

The mathematical model presented for the air infiltrations through the enclosure envelope is simple in form and is valid for the description of fluctuating flows through openings and pores.

The approach proposed is not only a mathematical abstraction but is also supported experimentally. Experimental data obtained for the purpose of testing the validity of the approach are found to agree well with predicted values.

3.5 REFERENCES

[1] **Haghighat F., Fazio P. and Unny T. E.** 1988. A predictive stochastic model for indoor air quality. Building and Environment **23**, 195-201

[2] **Jones P. J. and Whittle G. E.** 1991. Computational fluid dynamics for building air flow prediction - current status and capabilities. Building and Environment **26**, 95-109

[3] **Cook N. J.** 1985. The designer's guide to wind loading of building structures *Part 2 Static structures*, Butterworths, London

[4] **Euteneuer G. A.** 1971. Einfluss des windeinfalls auf innendruck und zugluft-Erscheinung in teilweise offenen bauwerken, Der Bauingenieur **46**, 355-360 [in German]

[5] **Liu H.** 1975. Wind pressure inside buildings. Proceedings of the second U.S. National Conference on Wind Engineering Research, Fort Collins, Colorado, USA

[6] **Euteneuer G. A.** 1970. Druckanstieg im inneren von gebauden bei windeinfall, Der Bauingenieur **45**, 214-216 [in German]

[7] **Holmes J. D.** 1978. Mean and fluctuating internal pressures induced by wind, Wind Engineering Report 5/78, Department of Civil and Systems Engineering, James Cook University of North Queensland, Australia

[8] **Liu H. and Saathoff P. J.** 1981. Building internal pressure: sudden change, ASCE **107**, 309-321

[9] **Dewsbury J.** 1996. AC pressurization: Analysis by non-linear optimisation, Buildings Services Engineering Research and Technology **17**, 65-71

[10] **Liu H. and Rhee K. H.** 1986. Helmholtz oscillation in building models, J. Wind Engineering and Industrial Aerodynamics **24**, 95-115

[11] **Etheridge D. H.** 1977. Crack flow equations and scale effect, Build. and Environment **12**, 181-189

[12] **Baker P. H., Sharples S. and Ward I. C.** 1987. Air flow through cracks, Build. and Environment **22**, 293-304

[13] **Allard F. and Utsumi Y.** 1992. Airflow through large openings. Energy and Buildings **18**, 133-45

[14] **Haghighat F., Rao J. and Fazio P.** 1991. The influence of turbulent wind on air change rates - a modelling approach, Build. and Environment **26**, 95-109

[15] **Miguel A. F., van de Braak N. J., Silva A. M. and Bot G. P. A.** 1997. Analysis of the airflow characteristics of greenhouse screens, J. Agr. Eng. Research **67**, 105-112.

[16] **Card H. W., Sallman A., Graham R. W. and Drucker E.** 1978. Air leakage measurements of buildings by an infrasonic method, Technical Report TR-78-1, Department of Electrical and Computer Engineering, Syracusa University, USA

[17] **Utsumi Y., Kobayashi H., Kadoya T. and Yoshino H.** 1996. Measuring technique of leakage area of houses by AC-pressurization method. Fifth International Conference on Air Distribution in Rooms (ROOMVENT 96), 29-34

[18] **Miguel A. F., van de Braak N. J., Silva A. M. and Bot G. P. A.** 1998. Forced fluid motion through pores and openings, Building and Environment (in press)

3.6 NOMENCLATURE

A area of opening [m^2]

C_c coefficient accounting for convective and viscous effects

H characteristic depth [m]

L_l larger length of opening [m]

L_s smaller length of opening [m]

K permeability [m^2]

M mass [kg]

p pressure [Pa]

Re Reynolds number

R_g specific gas constant [$m^2s^{-2}K^{-1}$]

r_p pressure coefficient

T temperature [K]

t time [s]

u superficial velocity [$m^3m^{-2}s^{-1}$]

V volume of air [m^3]

V_e volume of enclosure [m^3]

V_n volume of objects within the enclosure [m^3]

Greek symbols

β ratio between specific heat capacity at constant pressure and at constant volume

ε porosity

η enclosure flexibility coefficient [Pa^{-1}]

μ dynamic viscosity [Pa s]

ρ density [kg m^{-3}]

Subscripts

ext external

i internal

m mean

4. Modelling mixed fluid motion through porous media: description of matrix-fluid interaction [+]

Abstract: Fluid flow through a porous medium is studied, applying thermodynamics and fluid mechanics. The porous medium is treated as a subsystem composed of a solid matrix saturated with fluid (bulk fluid and adsorbed fluid), surrounded by external fluid. Thermodynamic equilibrium is assumed between the matrix and fluid phases. Mathematical relations are provided to describe the interaction between the fluid and the matrix, as well as between the fluid flow and the driving potentials. The methodologies of measuring the thermal and flow characteristics of the porous media are briefly described. For natural convection the influence of the air adsorbed on the solid matrix is of special interest. It is quantified experimentally for different porous media.

4.1 INTRODUCTION

Transport phenomena inside permeable media is a topic of great importance due to a large number of technical applications, such as filtering, geothermal operations, oil extraction, indoor climate control, etc.. The driving force for transport can be either due to mechanical means, such as pumps, the effect of gravity and/or the effect of wind (forced fluid motion), or due to temperature and/or concentration gradients (free or natural fluid motion). If forced and free flows are combined we have mixed fluid motion.

A large number of papers have been published in the last two decades on mass and heat transfer in porous media. A comprehensive review of literature is presented by Combarnous and Bernard [1]. Despite the existence of a lot of important studies on this field, the subject is far from being fully understood. One of the main limitations is related to the description of the fluid behaviour within the solid matrix and the relation

[+] ***Transport in porous media*** **(to be submitted)**

with external driving potentials. It is clear that a correct understanding of this interaction will be essential to a better comprehension of transport phenomena.

This study leads to a better understanding of this interaction by using the thermodynamics to describe physically the behaviour of fluid within the solid matrix. This description is applied together with the fluid mechanics basic laws in order to incorporate this interaction on the motion equation. Finally, in order to complete this analysis, the magnitude of the interaction between the internal fluid and the matrix is quantified experimentally using the relations developed.

4.2 Fluid flow through a permeable medium: basic equations

A system composed of a solid matrix saturated with fluid (subsystem matrix-fluid) is submerged in an external fluid, having the total system a volume Ω. The mass of solid matrix is considered constant and deformation of matrix does not occur.

The ability of the subsystem matrix-fluid to transmit fluid through it is a generalised fluid conductivity. This quantity is related to the volume fraction of the fluid contained within the solid matrix, usually identified as effective porosity or only porosity. Porosity is given by

$$\varepsilon=V_f/V_{m\text{-}f} \tag{1}$$

where V_f represents the volume of internal fluid (bulk and adsorbate fluid) and $V_{m\text{-}f}$ the volume of solid matrix saturated with fluid.

The density $\rho_{m\text{-}f}$ of the subsystem matrix-fluid is

$$\rho_{m\text{-}f}= \varepsilon \rho_f+(1-\varepsilon)\rho_{sm} =\varepsilon(\rho_f-\rho_{sm})+\rho_{sm} \tag{2}$$

where ρ represents the density and subscripts sm and f solid matrix and fluid, respectively.

The equations of conservation of fluid mass, momentum and energy in a three-dimensional space are:

Mass conservation equation [2]

$$\partial(\varepsilon\rho_f)/\partial t+\nabla.\ \rho_f\mathbf{u}=0 \tag{3}$$

Momentum conservation equation [3]

$$(\rho_f/\varepsilon)\partial\mathbf{u}/\partial t+(\rho_f/\varepsilon^2)(\mathbf{u}.\nabla)\mathbf{u}=-\nabla P-\kappa^{-1}\mathbf{u}-\rho_f\sigma|\mathbf{u}|\mathbf{u}+(\mu_f/\varepsilon)\ \nabla^2\mathbf{u} \tag{4}$$

Energy conservation equation [2]

$$[\varepsilon\rho_f C_f+(1-\varepsilon)\rho_{sm}C_{sm}]\partial T/\partial t+\nabla.\ (\varepsilon\rho_f C_f\ \mathbf{u}T)=-\nabla.J_h \tag{5}$$

with

$$J_h=\lambda_{eff}\nabla T \tag{5.1}$$

and

$$\lambda_{eff}=[\varepsilon\lambda_f+(1-\varepsilon)\lambda_{sm}] \tag{5.2}$$

where κ is the fluid conductivity (the ability of the medium to transmit fluid through it), σ the porous inertial coefficient ($\sigma=c(\mu\kappa)^{-1/2}$ with c a coefficient related with porous inertia), $\mathbf{u}$ the fluid velocity, μ the dynamic viscosity, T the temperature, P the total external pressure, C the specific heat and λ the thermal conductivity. The subscript f means fluid, sm solid matrix and eff effective.

For porous media the flow is often considered steady and incompressible [2] hence the mass and momentum conservation equations can be simplified to

$$\nabla.\rho_f\mathbf{u}=0 \tag{6}$$

$$(1+c\ Re)\ \kappa^{-1}\ \mathbf{u}-(\mu_f/\varepsilon)\nabla^2\mathbf{u}=-\nabla P \tag{7}$$

with

$$Re=\rho_f|\mathbf{u}|(\kappa/\mu_f)^{1/2}$$

For lower Reynolds numbers ($Re\approx 0$) equation (7) can be rewritten as

$$\kappa^{-1}\mathbf{u}-(\mu_f/\varepsilon)\nabla^2\mathbf{u}=-\nabla P \tag{8}$$

This equation is the Brinkman's relation [4], which is consistent with no-slip condition. When the volume of the solid matrix is larger than the volume occupied by

the fluid, the last-left hand side term of equation (8) can be neglected. Then, the velocity becomes proportional to the pressure gradient (Darcy's relation).

4.3 FLUID ABSORPTION WITHIN A POROUS MEDIUM AND THE EFFECT ON FLUID FLOW

Inside a porous structure there is a film of adsorbed fluid on the matrix, which has practical consequences for the magnitude of fluid flow. The phenomenon is presented schematically in figure 4-1. This figure shows a cross section of a solid matrix saturated with fluid, with two main regions: solid matrix with fluid adsorbate on the solid matrix and bulk fluid.

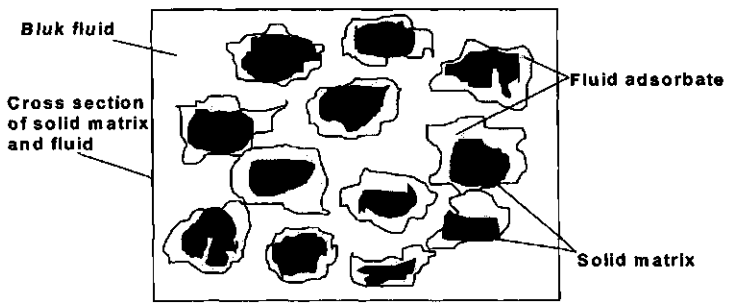

FIG. 4-1. Schematic cross section of a solid matrix saturated with fluid

The total mass M of subsystem matrix-fluid is

$$M_{m\text{-}f}=M_{sm}+M_f \tag{9}$$

with

$$M_f=M_{ad}+M_{bl}$$

where subscript sm stand for solid matrix, f for fluid, ad for adsorbate, m-f for matrix fluid and bl for bulk.

The change of fluid adsorbate and bulk fluid within the medium influences the amount of fluid flow through the medium. Those interactions can be described using thermodynamics concepts. In particular, the first law of thermodynamics is used. This law is a statement of the principle of conservation of energy, and relates the change of internal energy of a system with thermal, mechanical and diffusive interactions between the system and the surroundings.

4.3.1 Mass change in the subsystem matrix-fluid

Following the formalism developed by Heitor [5], and assuming that the superficial stress of fluid within the matrix and in the surroundings is equal, the equation (A-5) presented in the Appendix become

$$T(\delta S_t)=\delta \mathbf{F}.\delta \mathbf{r}_{m\text{-}f}-\delta P\ \delta V_{m\text{-}f}+\delta\omega\ \ \delta M_{m\text{-}f}+\delta T\ \delta S_{m\text{-}f} \qquad (10)$$

with

$$\delta \mathbf{F}=\Sigma_i(\delta \mathbf{F}_i)$$

and

$$T(\delta S_t)\geq 0$$

where V represents the volume, M the mass, ω the chemical potential, δS_t the creation of entropy in the process, S the entropy, **r** the vector position and **F** the vector force ($\Sigma_i \mathbf{F}_i$ the total of F due to the effects of mechanical means, gravity, wind, etc.).

The mass change in the subsystem matrix-fluid is given by

$$\delta M_{sm}+\delta M_{ad}+\delta M_{bl}=\delta M_{m\text{-}f}=\varsigma_V\,(\delta P+\delta p)+\varsigma_S \delta T+T(\delta S_t/\delta\omega) \qquad (11)$$

with

$$\varsigma_V=(\delta V_{m\text{-}f}/\delta\omega)$$

$$\varsigma_S=-(\delta S_{m\text{-}f}/\delta\omega)$$

$$\delta p=(\mathbf{I}.\delta \mathbf{F})/\delta A_{m\text{-}f}$$

where the coefficient ς_V define the rate between the variation of volume of subsystem

composed by the solid matrix saturated with fluid and the variation in chemical potential of the whole system, the coefficient ς_S defines the rate between the variation of entropy of subsystem matrix-fluid and the variation in chemical potential of the whole system, and **I** represents the unit vector.

Equation (11) relates the change of mass in a subsystem matrix-fluid with intensive quantities (P,p,T) and generalises the relation obtained by Heitor et al. [6]. This equation is useful for the study of porous media. Especially on the optimisation of strategies related to the injection, maintenance and extraction of fluid in porous media, as well as to provide additional information to be used in the motion equation.

Near the equilibrium, the last right-hand side term of equation (11) is small enough to approximate the equation by

$$\delta M_{m\text{-}f} = \varsigma_V (\delta P + \delta p) + \varsigma_S \delta T \tag{12}$$

For isobaric conditions

$$\delta M_{m\text{-}f} = \varsigma_S \delta T \tag{13.1}$$

and for isothermal conditions

$$\delta M_{m\text{-}f} = \varsigma_V (\delta P + \delta p) \tag{13.2}$$

Although the parameters ς_V and ς_S are physically defined here, theoretical values are rather difficult to find. Consequently, those parameters should be evaluated based on experiments [6].

4.3.2 Effects on fluid flow

As the mass of solid matrix is constant and the variation of $\delta M_{m\text{-}f}$, δp, δF and δT are in spatial coordinates (δx,δy,δz), equation (12) yields

$$\nabla M_{m\text{-}f} = \varsigma_V (\nabla P + \nabla p) + \varsigma_S \nabla T \tag{14}$$

So

$$\nabla P = -\nabla p + (V_{m\text{-}f}/\varsigma_V)\nabla p - (\varsigma_S/\varsigma_V)\nabla T \tag{15}$$

From the analysis of equation (15), it can be concluded that in absence of density

and temperature gradients $\nabla P=-\nabla p$. That is, the pressure gradient (∇p) due to the action of external force is independent of parameters ς_V and ς_S. If $\nabla p=0$

$$\nabla P=(V_{m\text{-}f}/\varsigma_V)\,\nabla\rho-(\varsigma_S/\varsigma_V)\nabla T \quad (16)$$

that is, the pressure gradient (∇P) depends on ς_V and ς_S. The following situations can occur:

- $\varsigma_S=0$: ∇P is only due to gradient of ρ,
- $\varsigma_V\gg 0$ and $\varsigma_S\ll 0$: ∇P is only due to gradient of the temperature,
- $\varsigma_V>0$ and $\varsigma_S<0$: ∇P can occur due to gradient of concentration and the gradient of the temperature.

These results are in agreement with the work of Heitor et al. [6].

Insertion of equation (16) into the momentum equation gives new insight of the driving potential on the fluid flow. Substitution of equation (16) in (4) yields

$$(\rho_f/\varepsilon)\,\partial\mathbf{u}/\partial t+(\rho_f/\varepsilon^2)(\mathbf{u}.\nabla)\mathbf{u}=-[-(V_{m\text{-}f}/\varsigma_V)\nabla\rho+(\varsigma_S/\varsigma_V)\nabla T]-\kappa^{-1}\mathbf{u}$$
$$-\rho_f\sigma|\mathbf{u}|\mathbf{u}+(\mu_f/\varepsilon)\,\nabla^2\mathbf{u} \quad (17)$$

Equation (17) shows how the gradients of ρ and T are related to the fluid velocity. The interaction between fluid and matrix defined by parameters ς_S and ς_V is also clearly included.

4.4 Methodologies for measuring parameters ς_V, ς_S, κ, σ, ε and λ_{eff}

In order to use the previous mass, momentum and energy conservation equations, the parameters ς_V, ς_S, κ, σ, λ_{eff} and ε must be known. These are obtained by fitting experimental data with appropriate equations (equations (1), (5.1), (7) and (13)). Then, the following set of experiments must be performed

- the parameters κ and σ can be obtained from forcing the air through the porous medium producing a constant pressure drop over the sample (DC-pressurisation method) and fitting experimental data with the help of

equation (7) [8]. This method of measuring is the subject of the study performed by Miguel et al. [9] using porous screens,

- measuring the fluid volume within porous media and the volume of solid matrix with fluid, the porosity ε is obtained from the ratio between them (equation (1)),
- λ_{eff} can be measured, for example, with the nonsteady state probe method based on the measurement of the temperature response [10] or with a steady state method based on the well known Fourier law of heat conduction,
- parameters ς_V and ς_S can be obtained from isothermal and isobaric conditions and fitting experimental data with equations (13.1) and (13.2). This will be the subject of the next section.

4.5 EXPERIMENTAL DETERMINATION OF PARAMETERS ς_V AND ς_S FOR DIFFERENT POROUS MEDIA

In order to evaluate parameters ς_V and ς_S, a set of experiments was performed using different porous media. The media used were samples of a sponge (ρ=3.23x10^{-2} g/cm^3), a brick (ρ=1.92 g/cm^3), and two thin greenhouse porous screens trade mark "ECONET SF" (ρ=0.352 g/cm^3) and "PH 20" (ρ=0.304 g/cm^3).

First, to have the samples understudy matrix free from fluid, they were placed in an evacuated oven at a temperature of 102°C during six days. Then, the samples were placed in an exsiccator and exposed to air with various constant water vapour pressures and at various constant temperatures during fifteen to twenty five days, to obtain an equilibrium between the atmosphere of the exsiccator and the samples. The samples were exposed to temperature levels between 10 °C and 30 °C and water vapour pressures between 201 Pa and 1760 Pa. The various water vapour pressures were achieved using several saturated solutions (NaOH, LiCl, $CaCl_2$, etc.). The variation of saturated water vapour pressure with temperature was taken into account. The possible effect of hysteresis on the measurements was studied by performing

experiments changing from high to low temperature level and reverse.

The mass of the samples under isothermal and isobaric conditions was determined using an analytical balance with an accuracy of the 0.01×10^{-6}kg.

Figure 4-2 through 4-4 show the mass concentration difference from the initial conditions (solid matrix free from fluid (bulk or absorbed)) referring to the samples mentioned above.

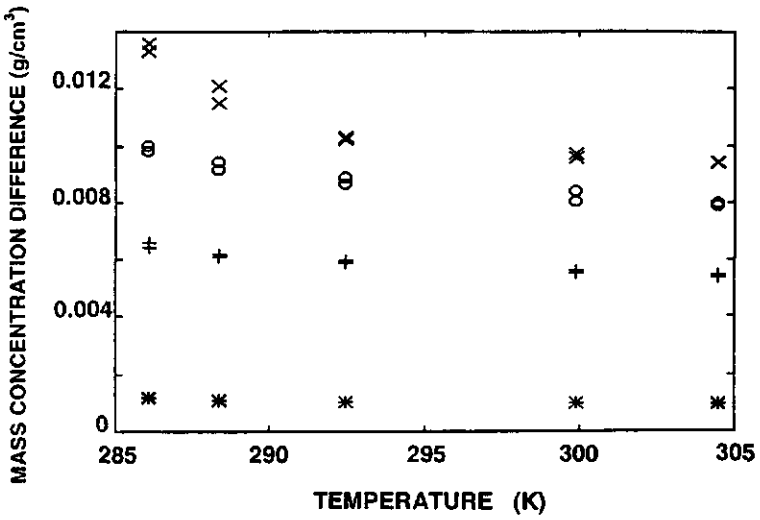

FIG. 4-2. Mass concentration difference from the initial conditions as a function of temperature for a sample of brick and for various water vapour pressures (✳ 201 Pa, + 808 Pa, O 1570 Pa and x 1760 Pa).

Parameters ς_V and ς_S were obtained fitting experimental mass concentration difference with equations (13.1) and (13.2). From figure 4-2 through 4-4 it is possible

to conclude that:

- for samples studied the effect of hysteresis on the measurements is present,
- as it is expected the influence of air and vapour adsorption by the solid matrix is high at low temperatures and high water vapour pressures for samples represented in figures 4-2 and 4-3,
- for the brick ς_V/V ranges between 0.006 and 0.01 kg/(Pa m^3), and ς_s/V between –0.015 and -0.2 kg/(m^3 K),
- for the greenhouse screens ς_S is close to zero for both screens and, ς_V/V is $9.9x10^{-4}$ kg/(Pa m^3) (ECONET SF) and $1.1x10^{-3}$ kg/(Pa m^3)) (PH 20).

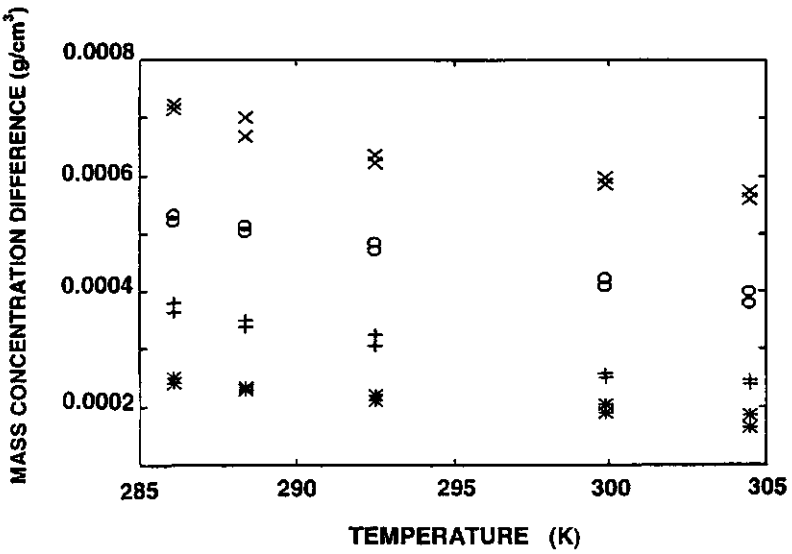

FIG. 4-3. Mass concentration difference from the initial conditions as a function of temperature for sample of sponge and for various water vapour pressures (✳ 201 Pa, + 808 Pa, O 1570 Pa and x 1760 Pa).

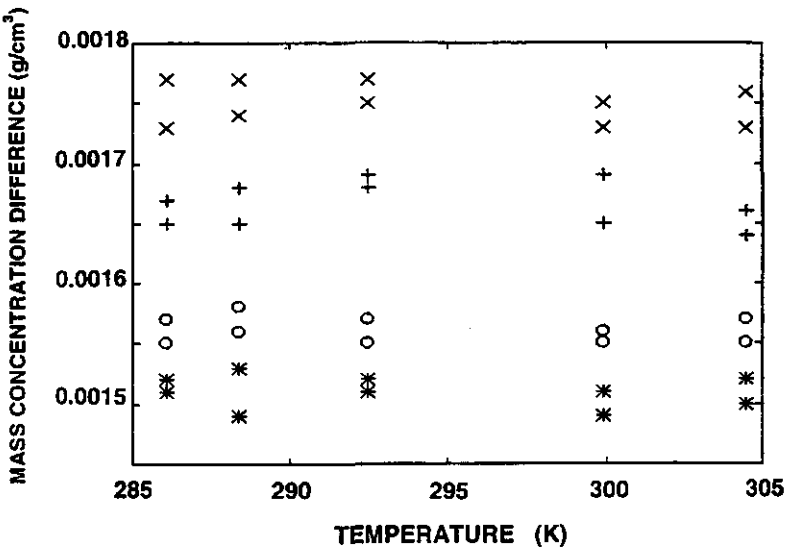

FIG. 4-4. Mass concentration difference from the initial conditions as a function of temperature for sample of greenhouse porous screen "ECONET SF" (✳,+) and "PH 20" (O,x), for various water vapour pressures (✳ and O 1570 Pa, + and x 1760 Pa).

4.6 FINAL COMMENTS

This study presents a description of transport phenomena in porous media within the framework of thermodynamics and general fluid dynamics. It is shown that thermodynamics is well suited for describing interaction between solid matrix and fluid. Insertion of this description into momentum equation (derived from fluid dynamics) gives new insight of fluid transport through porous media.

In order to be more realistic, parameters which account for adsorption isotherms and

adsorption isobars were determinated based on experiments for different porous media. Based upon the results obtained it is clear that adsorption isobars and isotherms (ς_V and ς_S) has significant importance on sponge and brick samples. For greenhouse porous screens ς_S was close to zero , that is, the temperature doesn't have significant effect on air absorption by the solid matrix.

4.7 REFERENCES

[1] **Combarnous, M. and Bernard, D.** 1988. Modelling free convection in porous media: from academic cases to real configurations. Proceedings of the 1988 National Heat Transfer Conference, Houston, USA

[2] **Bear, J.** 1972. Dynamics of fluids in porous media, American Elsevier Environmental Sciences Series, New York, USA

[3] **Miguel, A. F., van de Braak, N. J., Silva, A. M. and Bot, G. P. A.** 1998. Forced fluid motion through permeable materials, Building and Environment (in press)

[4] **Brinkman, M.C.** 1947. A calculation of the viscous force exerted by a flowing fluid on a dense swarm of the particles, Appl. Sci. Res., **A1**, 27-34

[5] **Heitor, A.** 1992. Formalismo termodinâmico com base nos parâmetros críticos com aplicações ao estudo das capacidades térmicas e dos processos reversiveis. Ph.D. Dissertation, University of Évora, Portugal [in Portuguese]

[6] **Heitor, A., Silva, O. and Rosa, R.** 1994. Heat and mass transfer in porous materials, Characterization of Porous Solids III, **87**, 207-209

[7] **Chapman, S. and Cowling, T. C.** 1970. The mathematical theory of non-uniform gases. Cambridge University Press, Cambridge, United Kingdom

[8] **Forchheimer, P.** 1901. Wasserbewegung durch boden, Z. Ver. Deustsch., **45**, 1782-1788 [in German]

[9] **Miguel, A. F., van de Braak, N. J., Silva, A. M. and Bot, G. P. A.** 1997. Analysis of the airflow characteristics of greenhouse screening materials, J. Agric.

Engng. Research **67**, 105-112.

[10] **Loon, W. K. P. van** 1991. Heat and mass transfer in frozen porous media. Ph.D. Dissertation, Agricultural Wageningen University. The Netherlands

4.8 APPENDIX

Thermodynamics analysis: budget equation of properties of a system

The following formulation is based on a formalism presented by Heitor (1993) for the interaction between two thermodynamic subsystems.

Consider a thermodynamic system consisting of n subsystems. The principle of conservation requires that, for each subsystem, the change in internal energy is a consequence of thermal, mechanical and diffusive interactions between the subsystem and its surroundings. This constitutes the first law of thermodynamic and from a mathematical point of view we can write for the total system

$$\delta U=\Sigma_n(\delta U_n)=\Sigma_n(\mathbf{F}_n\delta\mathbf{r}_n+\zeta_n\delta\mathbf{A}_n-P_n\delta V_n+T_n\delta S_n+\omega_n\delta M_n) \quad \text{(A-1)}$$

where U_n is the internal energy, T_n the temperature, P_n the pressure, V_n the volume, M_n the mass, ω_n the chemical potential, S_n the entropy, and ζ_n, $\mathbf{F}_n$ and $\mathbf{r}_n$ are the vectors for superficial stress, force and position of the subsystem n, respectively.

The subsystems can exchange quantities like energy, entropy, volume and mass. The budget equation for a quantity Λ is then

$$\Sigma_n(\delta\Lambda_n)=\delta\Lambda_t \quad \text{(A-2)}$$

where $\delta\Lambda_n$ is the variation of the quantity Λ in the subsystem n and $\delta\Lambda_t$ represent the creation or destruction of quantity Λ in the transfer process.

For the case of conservatives quantities like energy, volume and mass we only have to write

$$\Sigma_n(\delta\Lambda_n)=0 \quad \text{(A-3.1)}$$

but for the entropy the second law of thermodynamics imposes

$$\Sigma_n(\delta S_n)=\delta S_t \qquad \text{(A-3.2)}$$

where S_n is the entropy in subsystem n.

Specifically the exchange of Λ between a subsystem s and the remaining thermodynamic system ($n\neq s$) can be written as

$$\delta\Lambda_t=\Sigma_{n\neq s}(\delta\Lambda_n-\delta\Lambda_s) \qquad \text{(A-4)}$$

Taking into account equations (A-1) through (A-4) we can write

$$T_s\delta S_t=\Sigma_{n\neq s}(\mathbf{F}_n-\mathbf{F}_s)\delta\mathbf{r}_n+\Sigma_{n\neq s}(\zeta_n-\zeta_s)\delta\mathbf{A}_n-\Sigma_{n\neq s}(P_n-P_s)\delta V_n+\Sigma_{n\neq s}(T_n-T_s)\delta S_n+$$
$$\Sigma_{n\neq s}(\omega_n-\omega_s)\delta M_n\geq 0 \qquad \text{(A-5)}$$

were $T_s\delta S_t$ is the so-called availability function.

Equation (A-5) describes the thermal, mechanical and diffusive interactions between the subsystem s and the remains thermodynamic system composed by the subsystems $n\neq s$.

4.9 NOMENCLATURE

A	area [m^2]
c	coefficient related with porous inertia
C	specific heat [$J\ kg^{-1}K^{-1}$]
F	force [N]
M	mass [kg]
P,p	pressure [Pa]
S	entropy [$J\ K^{-1}$]
T	temperature [K]
U	internal energy [J]
u	velocity [$m\ s^{-1}$]
V	volume [m^3].

Greek symbols

ε	porosity
Λ	quantity like volume, entropy or mass

μ	dynamic viscosity [Pa s]
ρ	density [kg m^{-3}]
σ	inertial coefficient [m^{-1}]
κ	fluid conductivity [$m^3 s\ kg^{-1}$]
λ	thermal conductivity [W $m^{-1}K^{-1}$]
ω	chemical potential [J kg^{-1}].

Subscripts

ad	adsorbate
bl	bulk
eff	effective
f	fluid
m-f	solid matrix - fluid
sm	solid.

5. Analysis of the airflow characteristics of greenhouse screening materials [+]

Abstract: Experiments and analyses were conducted to examine the airflow characteristics of some currently employed greenhouse screens and the ability to predict airflow through them. Nine different thermal, shading and insect screens were tested and their airflow characteristics were defined, based on the Forchheimer equation, in terms of permeability and porosity. Further, an analysis was made of the effect on these characteristics of damage caused by handling of the screen materials. Experiments demonstrated that thermal screens have permeabilities of close to $10^{-11}m^2$ and some thermal screens, mainly woven sheet screens, can be damaged by handling, whereby the permeability is increased up to 3.5 times.

5.1 INTRODUCTION

The potential benefits resulting from the use of screens in protected horticulture have been increasingly recognised in recent years. Screens are a simple and successful means for avoiding night-time heat loss and controlling the solar radiation inside a greenhouse, as well as for preventing the entrance of birds and insects. In order to optimise the use of screens in agriculture, an extensive knowledge of their characteristics is required. A number of authors have worked on the measurement of the optical or radiometric characteristics of different materials used for screens [1,2], while others have worked on the measurement of the airflow characteristics (characteristics related to fluid transport through a screen). These characteristics have been evaluated in empirical terms of "permeability" based on the Darcy's law [3,4], or "coefficient of discharge" based on Bernoulli's flow theory [5,6].

The purpose of the present study is to discuss the more general physics of transport phenomena through permeable materials in order to provide a simple and accurate

[+] ***J. Ag. Engng. Research* 67, 105-112**

methodology for identifying the airflow characteristics of materials currently used as screens. Through experiments conducted in two different experimental arrangements these characteristics were determined in the range of Reynolds number commonly observed for porous thermal screens and porous insect screens. An analysis is also included of the effect of overall damage caused by opening and closing the screen.

5.2 PRESSURE DROP AND FLOW RELATIONSHIP

For one-dimensional mass transfer through a permeable material the motion equation can be expressed as [7]

$$(\rho/\varepsilon)\partial u/\partial t+(\rho/\varepsilon^2)u(\partial u/\partial x)=-\partial p/\partial x-(\mu/K)u-\rho(Y/K^{1/2})\,|u|u+(\mu/\varepsilon)(\partial^2 u/\partial x^2) \quad (1)$$

with

$$u=\varepsilon\, u_i$$

where u is the superficial fluid velocity, u_i the velocity through the material, ρ the density, p the pressure, μ the dynamic viscosity, Y the inertia factor and x the direction of flow. The parameter ε is the porosity and represents the volume fraction of fluid contained within the total volume of the medium, while parameter K is the permeability of the medium and represents the ability of the medium to transmit the fluid through it.

The dimensionless factor Y is often obtained from Ergun [8] using the relationship obtained in packed columns of spheres

$$Y=1.75/(150\varepsilon^3)^{1/2}\ (=0.143/\varepsilon^{1.5}) \quad (2)$$

5.3 MOTION EQUATION AND AIR FLOW CHARACTERISTICS OF A POROUS SCREEN

To illustrate the magnitude of the permeability of a permeable material and subsequently evaluate its effects on the airflow, consider the definition of permeability presented by Lebon and Cloot [9] based on kinetic gas theory. According to this theory, the permeability is related to the reciprocal of the collision frequency of

diffusing particles and the kinematic fluid viscosity. For a porous material the collision frequency is greater than 10^3 Hz [10] and as the kinematic fluid viscosity of air is the order of magnitude of 10^{-5} m^2s^{-1}, the permeability will be of a magnitude less than 10^{-7} m^2 (the second and third right-hand side terms of Eqn (1) are of great importance). For openings (windows, doors) the collision frequency will be close to zero and consequently the permeability $K \rightarrow \infty$. That means, the second and third right-hand side terms of Eqn (1) become zero and for openings we obtain the standard Navier-Stokes equation. For a steady, non-viscous flow, the Navier-Stokes equation can be integrated along a streamline and we obtain the Bernoulli equation.

Consider forced flow through a porous material (the study of openings is beyond the scope of this paper). According to Bear and Bachmat [11], for Reynolds numbers (Re) smaller than 150 the flow is incompressible ($\partial u/\partial x=0$). Then the second left-hand side term and the fourth right-hand side term of Eqn (1) can be discarded. For a steady flow, Eqn (1) becomes

$$(\mu/K)u+\rho(Y/K^{1/2})\,|u|u=\partial p/\partial x \qquad (3)$$

Eqn (3) is the well known Forchheimer equation for highly porous materials. For very small velocities [11] (Re<1) the quadratic term in velocity can be neglected and we obtain the Darcy law.

$$u=(K/\mu)\partial p/\partial x \qquad (4)$$

Darcy's law is the equation which defines permeability of a porous material.

Instead of permeability some authors [5,6] use the discharge coefficient, resorting to Bernoulli's equation, to characterise a screen. According to the above we can therefore conclude that the discharge coefficient will be appropriate only when convective inertia effects are present (Re>150). Under commonly observed situations this will be very unlikely for porous screens. Notice that, for wind velocities of 5 m/s (wind pressure approximately 15 Pa) the Reynolds number ($Re=\rho u_i d/\mu$) for a typical thermal screen is 5 (mesh size d=0.03 mm) and for an insect screen is 89 (mesh size d=0.11 mm).

As the subject of this study is porous screens, these will be characterised in terms of permeability and porosity, using Eqns (3) and (4).

5.4 EXPERIMENTAL STUDY

In order to obtain the airflow characteristics of porous screens as well as the inertial factor Y (Eqns (1) and (2)), experiments were carried out using two different test arrangements. Although both apparatus have the same principle, in that air is forced through the test samples in order to create a pressure drop, their ranges of applicability are different: one is used for Re less than 1 (in accordance with the range of Eqn (4)) and the other for Re greater than 1 and less than 100 (in accordance with the range of Eqn (3)).

Description of test apparatus

For Re<1, the screen samples (diameter 6 cm) were mounted in a tube (internal diameter 6 cm and length 20 cm) separated by fibre rings of 0.5 cm thickness (Fig. 5-1a) containing 20 pieces of each screen sample (in order to ensure a larger pressure drop). The tube was connected to the upper side of a cylindrical reservoir (radius 15 cm and length 120 cm) connected by a stiff tube (diameter 6 cm) (Fig. 5-1b). The measurements are based on the pressure drop caused by natural suction of air through the samples as a result of water flow induced by gravity.

The volumetric flow rate was controlled using a valve in the outlet duct, and was measured using a glass and a stopwatch. The pressure drop was measured using an inclined tube manometer Lambrecht KG type 655 (accuracy 1 mm of alcohol), with one part connected to the test apparatus and the other connected to the air in the experimental room.

For 1<Re<100, the experiments were carried out in a test apparatus as shown in Fig. 5-2a. It comprises a test box (2.5 m x 2.5 m x 2.5 m) with two screens (installed at 1.60 m from the inlet side and separated by 10 cm) in order to ensure that a uniform

air velocity distribution approaches the test screen. The test screens (2.48 m x 2.48m) were fixed to the outlet side of the test box using a wooden frame (Fig. 5- 2b) which prevents air leakage.

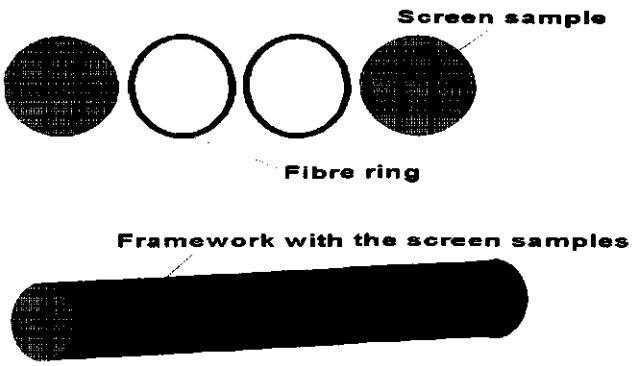

FIG. 5-1a. Diagram of the frame containing the test screens (Re<1).

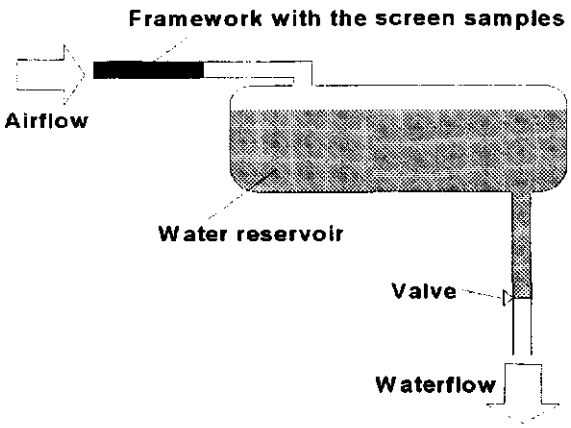

FIG. 5-1b. Diagram of the apparatus for testing screens with Reynolds number less than 1.

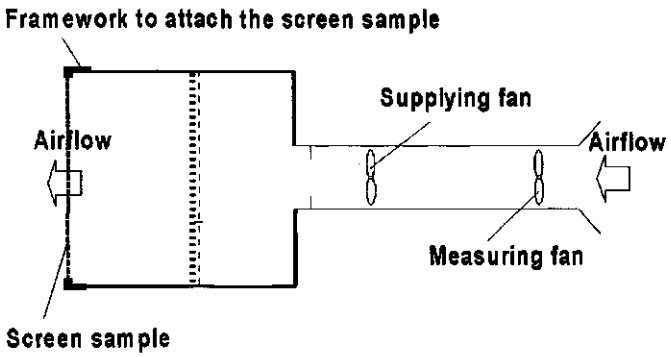

FIG. 5-2a. Diagram of the apparatus for testing screens with Reynolds number greater than 1.

The airflow supplied by the fan was regulated by controlling the rotational speed of the fan. The pressure drop through the test screen was measured using a membrane pressure transducer (accuracy 0.01 Pa), with one part connected to the test section of the apparatus (at 0.80 m upstream from the test screen) and the other connected to the air in the experimental room. The volumetric flow rate was measured from the frequency of rotation of a calibrated measuring fan.

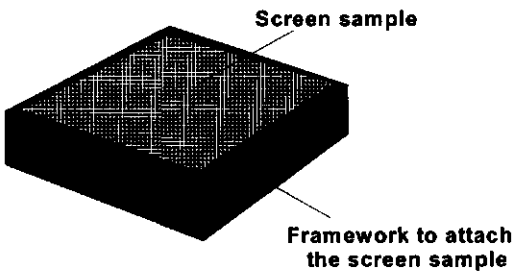

FIG. 5-2b. Diagram of the frame used to fix test screens to the test box (Re>1).

Description of screens tested

Measurements were performed on nine different screens including thermal and insect screens provided by two firms. The specifications for each screen are summarised in Table 5-1.

The porosity of each screen was measured with the help of a microscope. As screens are made of thin materials, porosity was computed as the ratio between the area occupied by the fluid (air) and the total mesh area (solid matrix and air).

TABLE 5-1. Screen specifications

SAMPLE	DESCRIPTION	TRADE NAME	POROSITY [m^2/m^2]
1	Insect screen, polyester rectangular mesh	Econet FL	0.34±0.030
2	Insect screen, polyester rectangular mesh	Econet SF	0.26±0.040
3	Thermal screen, polyester woven sheet	EH/P	0.09±0.011
4	Thermal screen, parallel polyethylene strips held together by thread	LS 10	0.09±0.017
5	Thermal screen, parallel polyethylene strips held together by thread	LS 10 Plus	0.06±0.019
6	Thermal screen, parallel polyethylene strips held together by thread	SLS 10	0.06±0.014
7	Thermal screen, polyester woven sheet	Phormilux	0.05±0.013
8	Thermal screen, parallel polyethylene strips held together by thread	SLS 10 Ultra	0.05±0.017
9	Thermal screen, polyester woven sheet reinforced with thread	PH 20	0.05±0.016

Description of the experiments

For each screen sample, measurements were taken using the test apparatus shown in Figs. 5-1 and 5-2 in order to obtain the volumetric flow rate and the pressure drop through the sample.

Variation in screen porosity and even tearing can occur due to tension created by the airflow. In order to prevent this, in accordance with the explanation in appendix, experiments were carried out with pressures lower than 150 Pa.

In order to take asymmetry in the screen structure into account, the tests were carried out with the air flowing in both directions through the screen. The possible effect of hysteresis on the measurements was accounted for by performing experiments between low and high airflow rates, and the reverse.

First, individual new screen samples were tested. As handling (opening/closing) easily damages some screens, tests were also made on screens which had been folded ten times.

During the tests, the data were collected every 15 s for periods of 10-20 min to be sure that conditions were at steady state.

5.5 RESULTS AND DISCUSSION

For each material tested, the data resulting from the experiments performed were plotted as pressure drop versus the superficial velocity, as shown in Figs. 5-3 to 5-5. In all the samples tested, the equation that best seemed to fit the curves obtained was a second order polynomial $\Delta p=au^2+bu+c$ (i.e. the data presented fit Eqn (3) the Forchheimer equation). The coefficients are presented in Table 5-2.

Therefore, provided the best fit coefficients are found (zero order term can be neglected compared with the other terms), the permeability and factor Y can be calculated from Eqn (3) (fluid properties included in Eqn (3) were obtained for the mean air temperature of experimental room). The results are listed in Table 5-3.

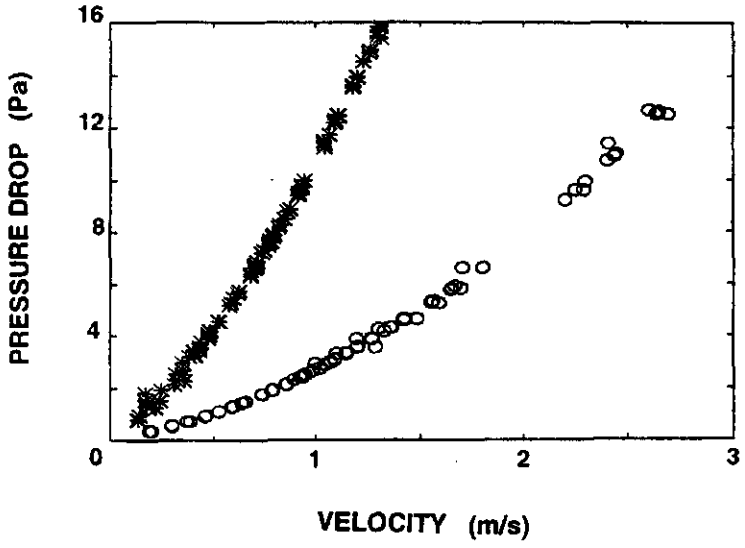

FIG. 5-3. Pressure drop as a function of the superficial velocity for insect screens (sample 1 (o) and sample 2 (✳)).

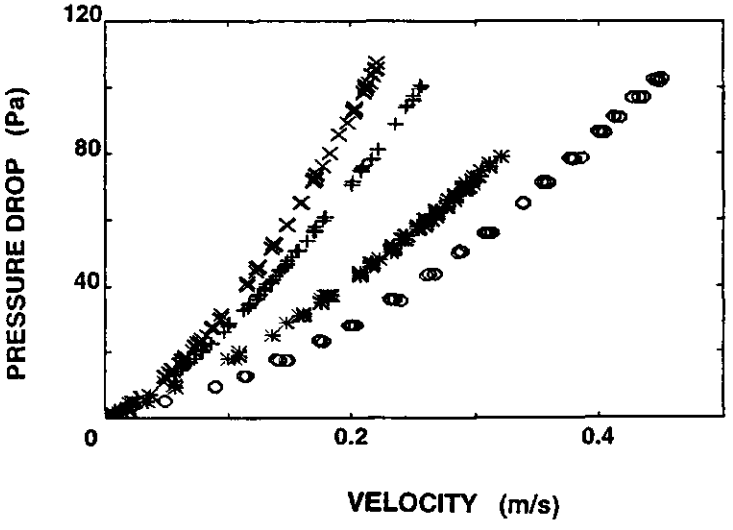

FIG. 5-4. Pressure drop as a function of the superficial velocity for thermal screens (sample 3 (o), sample 4 (✳), sample 5 (+) and sample 6 (x)).

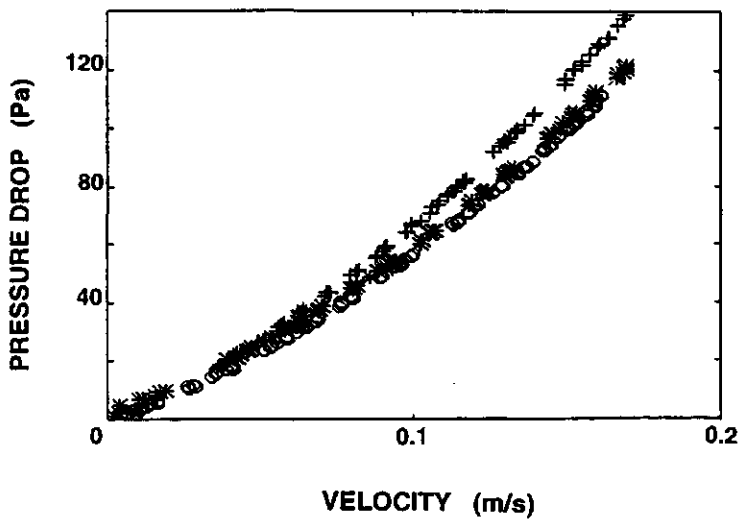

FIG. 5-5. Pressure drop as a function of the superficial velocity for thermal screens (sample 7 (o), sample 8 (*) and sample 9 (+)).

TABLE 5-2. Coefficients for the best fit equation ($\Delta p=au^2+bu+c$)

SAMPLE	a	b	c	r^2	ND(*)
1	1.255	1.414	0.102	0.98	106
2	4.119	6.625	-0.330	0.97	104
3	303.17	101.43	-11.91	0.99	105
4	348.53	134.06	10.45	0.98	109
5	729.03	205.12	-11.95	0.99	103
6	1130.2	241.73	-16.10	0.99	118
7	1957.8	371.37	-12.10	0.99	115
8	1953.9	369.87	17.30	0.99	117
9	2174.7	458.21	-16.23	0.99	104

(*) Number of fitted data

TABLE 5-3. Permeability K and inertial factor Y of new screens

SAMPLE	K [m^2]	Y
1	$6.51x10^{-09}$	0.457
2	$1.39x10^{-09}$	0.758
3	$9.08x10^{-11}$	12.03
4	$6.87x10^{-11}$	12.29
5	$4.49x10^{-11}$	22.11
6	$3.81x10^{-11}$	29.01
7	$2.48x10^{-11}$	40.62
8	$2.48x10^{-11}$	40.54
9	$2.01x10^{-11}$	40.86

Data on porosity and inertial factor Y obtained in the present study and some additional data obtained from Lee [12], covering materials with porosities between 0.78 and 0.86, are included in Fig. 5-6. These data fit an equation similar to the one used by Ergun [8], which expresses the relationship between the factor Y and porosity as follows

$$Y=c_Y\varepsilon^n \tag{5}$$

The best fit gives c_Y equal to $4.36x10^{-2}$ and n equal to -2.12. These coefficients are approximately 30% smaller and 29% larger than the coefficients c_Y and n respectively obtained by Ergun [8] for packed columns of spheres.

The factor Y obtained from Fig. 5-6 cover materials with permeabilities between 0.05 and 0.86. Thus, we can now use Y and Eqn (3) to derive the permeability and the porosity of screens damaged by handling, provided the pressure drop and the superficial velocity are known. Experiments were performed in the test apparatus shown in Fig. 5-2 and the results are listed in Table 5-4. According to the results presented in Table 5-4, damage caused by handling (10 times folded) does not occur

in the insect screen samples but occurs in the thermal screen samples. Excluding screen sample 3, damage is mainly found in woven sheet screens. The permeability becomes about 3.5 times higher (porosity about two times higher) for woven sheet screens and about 1.9 times higher (porosity about 1.5 times higher) for screens with parallel strips held together by thread.

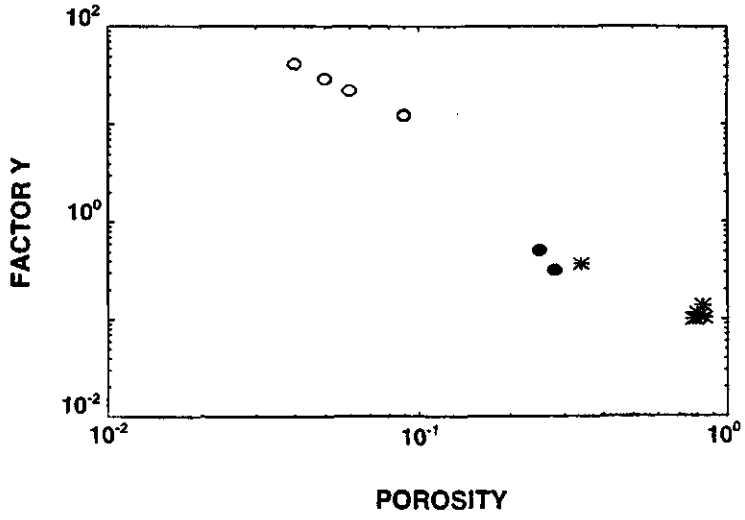

FIG. 5-6. Inertial factor Y versus porosity for different types of screens (insect screen data •, thermal screen data 0, data from Lee [12] ✳)

The tests carried out with the air flowing in both directions gave the same results, so no influence of airflow direction through the screen or hysteresis was detected in any of the materials tested.

TABLE 5-4. Permeability K and porosity ε of screens folded ten times

SAMPLE	K [m^2]	ε	$r^{2(**)}$	ND(***)
1	$6.50x10^{-09}$	0.33	0.99	102
2	$1.39x10^{-09}$	0.26	0.98	106
3	$9.97x10^{-11}$	0.10	0.99	112
4	$7.33x10^{-11}$	0.10	0.99	101
5	$6.79x10^{-11}$	0.09	0.98	104
6	$7.22x10^{-11}$	0.10	0.99	109
7	$8.63x10^{-11}$	0.10	0.99	108
8	$4.04x10^{-11}$	0.09	0.99	109
9	$4.22x10^{-11}$	0.09	0.99	104

(**) For regression $\Delta p=au^2+bu+c$
(***) Number of fitted data for regression $\Delta p=au^2+bu+c$

5.6 CONCLUSIONS

1. For commonly observed situations (Re<100), the pressure drop through a porous screen is described by the Forchheimer equation. According to this equation, the permeability and porosity describe the airflow characteristics of a porous screen.

2. The inertial factor Y in porous screens differs from that for packed columns of spheres and is described by $Y=4.36x10^{-2}\varepsilon^{-2.12}$

3. Undamaged porous screens usually used as thermal screens have permeabilities close to $10^{-11}m^2$ and insect screens have permeabilities less than $10^{-8}m^2$.

4. Damage caused by handling was found only in thermal screens, mainly woven sheet screens, and can cause an increase in permeability of up to 3.5 times.

5.7 REFERENCES

[1] **Bailey B. J.** 1981. The reduction of thermal radiation in glasshouses by thermal screen. Journal of Agricultural Engineering Research, **26**: 215-222

[2] **Nijskens J., Deltour J., Coutisse S. and Nisen A.** 1985. Radiation transfer

through covering materials, solar and thermal screens of greenhouses. Agricultural and Forest Meteorology, **35**: 229-242

[3] **Bailey B. J.** 1978. Glasshouse thermal screens: air flow through permeable materials. Departmental Note no. DN/G/859/04013. National Institute of Agricultural Engineering, Silsoe, United Kingdom

[4] **Balemans L.** 1988. Assessment of criteria for energetic effectiveness of greenhouse screens. Ph.D. Dissertation, Ghent University, Belgium

[5] **Sase S. and Christianson L. L.** 1990. Screening greenhouses-some engineering considerations. ASAE Paper No. NABEC, 90-201

[6] **Kosmos S. R., Riskowski G. L. and Christianson L. L.** 1993. Force and static pressure resulting from airflow through screens. ASAE, **36**: 1467-1472

[7] **Miguel A. F., van de Braak N. J., Silva A. M. and Bot G. P. A.** 1998. Forced fluid motion through permeable materials, Building and Environment (in press)

[8] **Ergun S.** 1952. Fluid flow through packed columns, Chemical Engineering Progress, **48**: 89-94

[9] **Lebon G. and Cloot A.** 1986. A thermodynamical modelling of fluid flows through porous media: application to natural convection. International Journal of Heat and Mass Transfer, **29**: 381-390

[10] **Chapman S. and Cowling T. C.** 1970. The mathematical theory of non-uniform gases. Cambridge University Press, Cambridge, United Kingdom

[11] **Bear J. and Bachmat Y.** 1990. Theory and applications of transport phenomena in porous media, Kluwer Academic Publishers

[12] **Lee K. B.** 1986. Heat and mass transfer in highly porous media, Ph.D. Dissertation, University of Texas at Austin, U.S.A.

5.8 APPENDIX

Porosity and consequently permeability are not always constant parameters, as a

screen may be deformed under pressure. The solid matrix preserves its density but the open area increases.

According to Bear and Bachmat [11], the mass conservation for the solid matrix can be written as

$$\partial/\partial t[\rho_s(1-\varepsilon)]+\nabla[(1-\varepsilon)(\rho_s u_s)]=0 \quad (A.1)$$

where u_s and ρ_s are the velocity and the density of solid matrix, respectively.

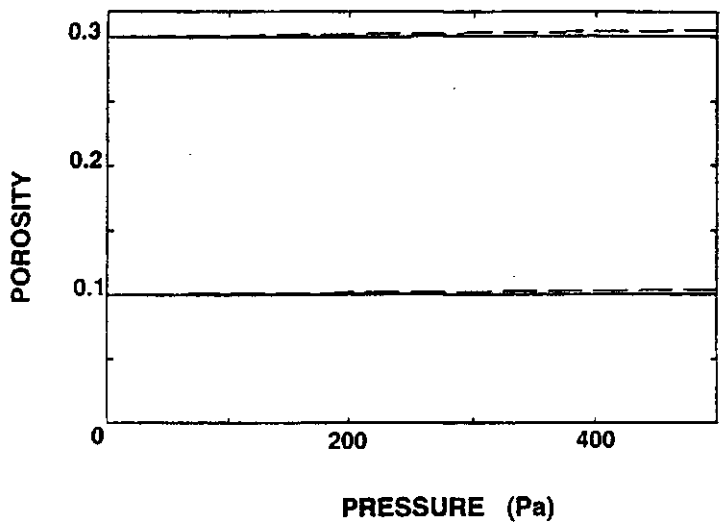

FIG. 5-A1. Pressure-induced porosity variation for porous screens with initial porosities 0.10 and 0.30 and compressibility coefficient of 10^{-5} Pa (represented by --) and 10^{-9} Pa (represented by –).

Where the density of the solid matrix is constant, and considering the medium to be homogeneous ($\nabla\varepsilon\approx 0$) , Eqn (A.1) becomes

$$\partial\varepsilon/\partial t=(1-\varepsilon)\,\nabla u_s \quad (A.2)$$

Eqn (A.2) is a first-order differential equation and its integration yields

$$\varepsilon=1-(1-\varepsilon_0)/\exp(\int\nabla u_s dt) \quad (A.3)$$

with

$\int \nabla u_s dt = \upsilon$

where ε_o is the initial porosity (measured at standard atmospheric pressure) and υ the volumetric strain [11].

For an elastic matrix, the volumetric strain is proportional to the pressure, and Eqn (A.3) becomes

$$\varepsilon = 1-(1-\varepsilon_o)/\exp(\eta^{-1}\Delta p) \qquad (A.4)$$

where η is the compressibility coefficient of the matrix.

Eqns (A.3) and (A.4) show how the porosity changes with the increase of pressure.

In order to prevent variation in screen porosity during the experiments, a simulation study is performed based on equation (A.4). Fig. 5-A.1 shows the porosity variation due to pressure for the test screens used (initial porosity 0.10 and 0.30 and compressibility coefficient of the matrix 10^{-5} Pa and 10^{-9} Pa). According to Fig. 5-A.1, for a pressure drop of less than 150 Pa, the porosity variation from initial conditions (zero pressure drop) is always less than 0.05%. This pressure is the maximum value used in the experiments.

5.9 NOMENCLATURE

d	mesh size [m]
i,j,l	unit vectors in direction x, y and z
K	permeability of the screen [m^2]
p	pressure [Pa]
u	superficial fluid velocity [ms^{-1}]
u_i	fluid velocity through a permeable material [ms^{-1}]
u_s	velocity of solid matrix [ms^{-1}]
Re	Reynolds number ($Re= \rho u_i d/ \mu$)
t	time [s]

Υ	inertial factor
ε	porosity
μ	dynamic viscosity [Pa s]
ρ	density [kg m^{-3}]
∇	(i $\partial/\partial x$+j $\partial/\partial y$+l $\partial/\partial z$)

Subscripts

o	initial
s	solid

6. PHYSICAL MODELLING OF NATURAL VENTILATION THROUGH SCREENS AND WINDOWS IN GREENHOUSES [+]

Abstract: In the previous chapters the physical basis of air exchange through porous materials and openings were presented. In this chapter, formulation presented in chapters 2, 3 and 5 is applied to study natural ventilation through screens and window openings in greenhouses. The wind velocities and air temperature differences which drive the airflow were characterised. Fluctuations in wind velocity were related to the mean wind velocity through a parameter which is evaluated based on a power spectrum analysis. In turn, wind pressure was related to this mean wind velocity such that turbulence was taken into account. An experimental study was conducted in twin-span glasshouses in order to validate the approach presented. The predictions made of airflow versus wind pressure and temperature differences agree reasonably well with experimental data, differences between them being less than 20%, in general.

6.1 INTRODUCTION

Natural ventilation of a greenhouse is a complex process which depends on the greenhouse characteristics (number, location and geometry of windows, area of leaks, etc.) as well as on the external ambient conditions. Although its important impact on the mass and energy balance which affects the indoor climate conditions, the subject is far from being fully understood.

As far as is known natural ventilation through greenhouse window openings were first studied experimentally by Morris and Neale [1] in 1954. Since them much progress has been made in understanding the phenomena and new challenges appear. The rather high oil prices reached in the end of the 70's, followed by the wide public concern about the ecological aspects related to the high quantities of fossil fuel consumption in the North-western Europe, contributed to the development of new

[+] ***J. Ag. Engng. Research*** **(in press in a modified form)**

energy saving strategies. The potential energy saving benefits resulting of the use of screens between the crop and the roof was demonstrated by Bailey [2], Bailey and Cotton [3] and Silva et al [4]. Recently [5], the use of screens in window openings was adopted in order to prevent the entrance of insects and so decrease the need for use of chemical pesticides. Consequently, the study of airflow through screens is also an important topic.

The existing analytical models on the subject can be divided into two categories as follow:

- Empirical and semi-empirical approaches for the study of airflow through window openings [6-13] and airflow through screens [2,5,14].
- Governing fluid mechanics equations solved numerically [15-17].

All models in the first category are based on the idea that there is a simple non-linear relationship between the airflow and the potentials which drive this flow. Such analyses consider the air inside the greenhouse as incompressible and they are commonly based on purely empirical correlations or on Bernoulli's equation, resulting in dimensionless numbers (such as the Euler number) with empirical correction factors. However, the simplifying assumptions used together with the correction factors, which are obtained for specific experimental conditions, considerably restrict the range of validity of this approach.

In the second category of models, a numerical simulation procedure is applied to solve the continuity equation, the momentum equation and the energy equation, to determine the velocity, temperature and pressure fields and consequently the flow patterns inside the greenhouse.

The study presented in this paper has two objects in view:

- to improve understanding of the physics of the air exchange process through porous screens (thermal, shading or insect) and through window openings. More specifically, to establish the flow network of a greenhouse with a window opening and a screen partially or totally open, and to describe the characteristics of

the driving potentials;

- to present a simple and accurate formulation which describes airflow through porous screens and window openings caused by wind and stack effect.

6.2 THEORY

6.2.1 Motion equation

The physics of free and forced fluid motion through porous materials and openings reveals that this phenomenon depends upon the characteristics of the opening or porous material under study and the characteristics of the potentials which drive the flows. A model , which accounts these dependencies, is presented in by Miguel et al. [18]. According to these authors, the airflow through each opening or porous screen is related to the driving potential as

$$\varepsilon^{-1}\partial Q/\partial t+[\mu(\rho K)^{-1}+4.36x10^{-2}\varepsilon^{-2.12}A^{-1}K^{-1/2}|Q|]Q+0.5(A\,\varepsilon^{2}Hc_c^{2})^{-1}|Q|Q=$$

$$-\rho^{-1}A\Delta p_w/H-\rho^{-1}A\Delta p_{st}/H \qquad (1)$$

where Q is the airflow (m^3/s), ρ the air density, A the exchange area, μ the dynamic viscosity of the air, ε the porosity of the material (the volume fraction of fluid contained within the total volume of the medium), K the permeability of the material (for openings $K\rightarrow\infty$), c_c the coefficient accounting for the convective effect (for porous screens $1/c_c^2\approx 0$), H the characteristic depth, Δp_w the wind induced pressure difference and Δp_{st} the pressure difference due to thermal differences.

In order to evaluate the airflow through a multi-zone enclosure or through an enclosure with several openings, a flow network must be established. A screened greenhouse can be considered as a two-zone enclosure and the airflow network, which represents this, is illustrated in Fig. 6-1.

In the case of a greenhouse with one window opening and one screen, the flow network is composed of three nodes coupled by two resistances (Fig. 6-1a). When one

aperture is made in the screen the network is composed of three nodes coupled by three resistances (Fig. 6-1b).

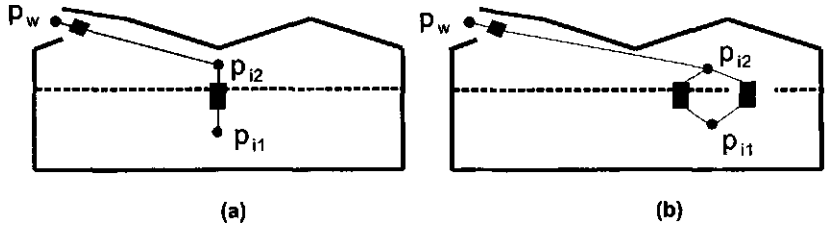

Fig. 6-1. Schematic representation of a screened greenhouse (-■- flow resistance ● node).

6.2.2 Driving potential

The driving potentials which induce the airflow can be due to the difference in temperature (stack effect) or due to the wind velocity (which induces a wind pressure) or both. In both cases a steady flow caused by the mean value of the potential gradient is induced. In the case of the wind velocity an extra flow caused by fluctuations in the potential (turbulence) appears.

Fluctuating airflow through openings in enclosures driven by wind-induced pressures can be divided into pulsating flow and the penetration of eddies. The pulsating flow results from the wind fluctuation and the compressibility of air within the enclosure (the inside air is pressurized or depressurized). The eddy flow is due to the turbulence in the air stream, which creates a rotational effect on the air within the enclosure.

6.2.2.1 Airflow driven by temperature difference

When the air temperature on each side of the porous screen or opening is different, a stack pressure occurs, which drives an airflow. If it is assumed that the temperature is

different on each side, the pressure difference between the two sides is given by

$$\Delta p_{st}=\Delta\rho\ g\ \Delta h \qquad (2)$$

with

$$\Delta\rho=\rho\ \beta\ \Delta T$$

where ΔT is the absolute temperature difference measured in the bulk fluid, g the gravitational acceleration, Δh the vertical height difference through the screen or opening and β the coefficient of thermal expansion.

6.2.2.2 Airflow driven by wind velocity (wind pressure)

Wind velocity is not a steady quantity when measured over time. The instantaneous value at time t can be written as the sum of a mean component and a fluctuating component, that is, $\bar{u}$ and u', respectively. The average wind pressure over a time interval can be related to the wind velocity (in Appendix) by

$$\bar{p}_w=0.5\rho\ (\ \bar{u}_w^2+\overline{u'_w u'_w}\ ) \qquad (3)$$

where $\bar{u}_w$ is the mean wind velocity and u'_w the fluctuations in wind velocity.

Some anemometers give direct readings of the mean velocity and of the root mean square of the velocity. Assuming u'_w to have a Gaussian probability distribution, it is sometimes convenient to use the following equation instead of (3)

$$\bar{p}_w=0.5\rho\,\bar{u}_w^2+\rho\pi^{-1}u_{mrsw}^2 \qquad (4)$$

where u_{mrsw} is the root mean square wind velocity.

The more usual situation is to have anemometers which only give readings of mean velocity. Therefore, an approach which presents wind pressure as a function of mean velocity only, but does not neglect the effect of the fluctuating component, would be very useful. For this we need to relate the mean square fluctuating (turbulent) component of the wind velocity to the mean (static) component of wind velocity.

The dissipation rate of turbulent kinetic energy (r_μ) can be related directly to the mean velocity through the inertial subrange spectral density. According to

Kolmogorov's rule [21]

$$r_{\mu}^{2/3}=(3/4)c_{kl}^{-1}F_{(n)}(\bar{u}_w/2\pi)^{2/3}n^{5/3} \quad (5)$$

where $F_{(n)}$ is the inertial subrange spectral density, n the frequency and c_{kl} Kolmogorov's constant (≈0.5).

Then, using the relation between the turbulent kinetic energy at a distance z from a surface and the dissipation rate of turbulent kinetic energy [21],

$$0.5\,\overline{u'_w u'_w}=c_{\mu}^{-0.5}[r_{\mu}\kappa(z+z_o)]^{2/3} \quad (6)$$

the mean square fluctuating component of wind velocity and the mean component are thus related as

$$\overline{u'_w u'_w}=3F_{(n)}(\bar{u}_w/2\pi)^{2/3}n^{5/3}c_{\mu}^{-0.5}[r_{\mu}\kappa(z+z_o)]^{2/3} \quad (7)$$

where κ represents the von Karman's constant (≈0.4), c_{μ} a constant (≈0.09), z the height at which the velocity is measured and z_o the surface roughness length (values for z_o can be found in Eurocode [22]).

Substitution of Eqn (7) in (3) yields

$$\bar{p}_w=\Upsilon(0.5\rho\bar{u}_w^2) \quad (8)$$

with

$$\Upsilon=1+3F_{(n)}(\bar{u}_w)^{-4/3}(2\pi)^{-2/3}n^{5/3}c_{\mu}^{-0.5}[\kappa(z+z_o)]^{2/3} \quad (9)$$

In Eqn (9), the value unity (right-hand side of the equation) represents the mean contribution of wind velocity, and the remaining the fluctuating contribution of wind velocity.

To obtain Υ it is necessary to know $F_{(n)}$ and n, and a power-spectrum analysis should be performed. The power-spectrum analysis [23] is a measure of the contribution of oscillations with continuously varying frequencies to the variance of a variable. This analysis not only enables Υ to determine but also yields extra information which can be used to clarify and characterise the structure of fluctuations (turbulence), and to identify the frequencies of the main eddies present in the wind

field.

Wind velocity is usually measured at a reference height, and a dimensionless coefficient, which relates the wind field at the reference height to the local wind field, should be introduced. This coefficient is determined by the velocity profile of the atmospheric boundary layer and by the orientation of the enclosure (greenhouse) with respect to the wind direction. These values have been obtained from measurements in boundary layer wind tunnels [24].

6.3 EXPERIMENTAL STUDY

In order to characterise the potentials which drive the flows, and to verify the applicability of the model (Eqn 1), experiments were conducted in two twin-span glasshouse oriented E-W, each one with the following dimensions (Fig. 6-2): eaves height 4.5 m, roof angle 22°, width 4.1 m and length 6.6 m. Inside each glasshouse a thermal screen trade name LS 11 (permeability $7x10^{-10}$ m^2 and porosity 0.09 obtained by Miguel et al. [20]), was assembled horizontally at a height of 2.90 m above the ground. In the first part of the experiments the screen was kept closed in each glasshouse. In the second part a narrow opening (0.02x3.80 m^2) was made in the centre of the screen, in order to simulate a horizontal slit.

The inside of each glasshouse was hermetically sealed, with insulating panels in the walls and polystyrene foam insulating layers on the soil surface, except the roof, where windows with flaps were located (two windows per span), each with an area of 2.05x0.90 m^2. The window opening angles could be set up to 30°.

Horizontal cylindrical electrical heaters with aluminised surfaces (eight cylinders 3.80 m long and 0.05 m in diameter, in pairs, separated by 0.35 m, each pair 1.15 m apart) were placed parallel to greenhouse width at a height of 0.20 m above the ground. In this way the geometry was equal to a standard greenhouse heating system. The heaters were controlled in such a way that a constant temperature difference was obtained between the air above and below the screen during the experiments.

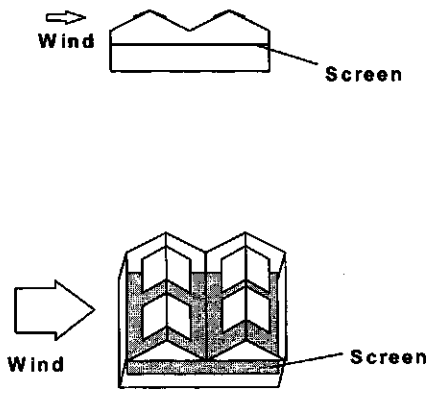

Fig. 6-2. Schematic cross section and top view of screened greenhouse

In each glasshouse, 25 copper-constantan thermocouples were installed to measure the temperature of the air above and below the screen, and the temperature of the outside air. They were distributed uniformly as follow: 10 thermocouples distributed in the air space below the screen, 10 in the air space above the screen and five in the outside air. The thermocouples were made of very thin wires ($2.5x10^{-5}$ m wire diameter) in order to ensure a rapid response [8] (response frequency approximately 12 Hz).

The pressure was measured using membrane pressure transducers. The inside pressure was measured above and below the screen (three probes in each part). The instantaneous wind pressure was measured outside at a distance of 0.20 m from the window opening. The wind velocity was measured using a fast response hot wire

anemometer (response frequency of 9.5 Hz) placed 0.20 m from the window opening. The wind direction was also determined.

The airflow was determined by means of a tracer gas technique. In the experiments, both the constant flow and decay rate method [9,25] were used. The airflow through the screen opening was obtained by subtracting the flow through the screen from the total flow.

The tracer gas (N_2O) was distributed in each glasshouse using two small fans and a system of perforated tubes at ground level. The air within the greenhouse during the experiments was sampled at 18 different locations in each glasshouse (distributed nine above and nine below the screen) and measured by means of an infra-red gas analyser.

The measurements were performed on 32 selected days between February and May of 1996 and consisted of two types:

- Airflow through the glasshouse windows and through the screen caused by wind velocity. These experiments were performed at temperature differences between inside and outside of less than 2.0±0.5°C and the wind velocity higher than 1.5 ms^{-1}).
- Airflow through the porous screen and through a narrow rectangular opening (0.02x3.80 m^2) in the screen caused only by a constant temperature difference between the air above and below the screen (steady state conditions). To prevent the influence of wind pressure, the measurements were performed with almost closed windows (leeside window openings open 2°).

In the first part of the experiment (airflow caused by wind effect), the data on the wind velocity, and temperature difference between inside and outside, were collected at sample frequencies of 8 Hz, over periods of 10 minute.

In the second part of the experiment (airflow caused by stack effect), data on constant temperature difference ($\Delta T \pm 1°C$) between the air above and below the screen were collected at sample frequencies of $1.66x10^{-2}$ Hz (each 60 s) during periods of 8 h, to obtain steady state conditions.

6.4 RESULTS AND DISCUSSION

6.4.1 Wind velocity and wind pressure

Spectrum analysis was performed using wind velocity data obtained over periods of 10 minute at sample frequencies of 8 Hz. The sampling frequency of the quantity measured determines the highest frequency detectable by the analysis, i.e., half the sampling frequency (Nyquist frequency) which in this study is 4 Hz.

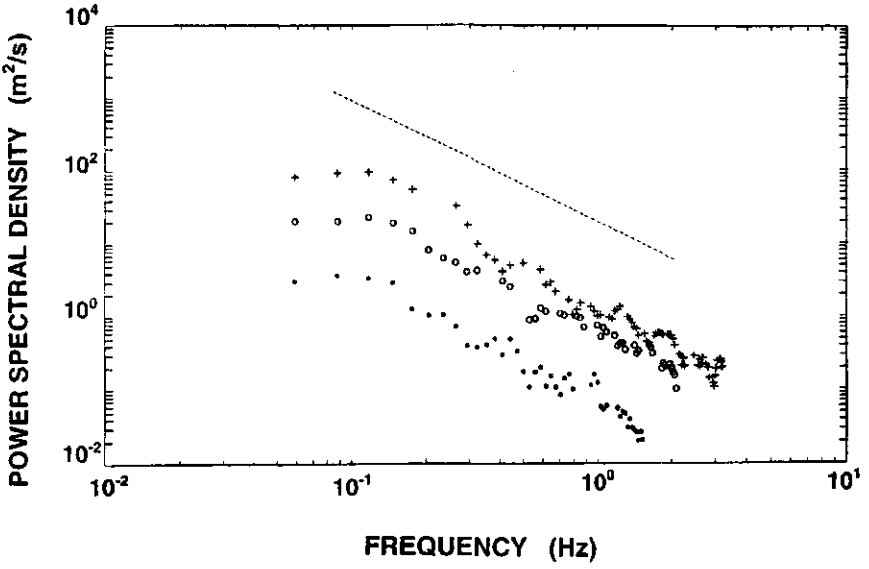

Fig. 6-3. Power spectral density of wind velocity, for mean wind velocities of 1.27 ms-1 (*), 3.49 ms-1 (o) and 5.50 ms-1 (+) measured at 0.20 m above the roof at windward side with closed windows(--- line with slope of -5/3).

As the wind characteristic on the leeside and windward side can be different [9], spectrum analysis were performed for both sides. The results obtained for a greenhouse with closed windows are plotted in Figs. 6-3 and 6-4.

Fig. 6-3 shows the power spectral density of wind velocity for three different mean wind velocities: 1.27 ms^{-1}, 3.49 ms^{-1} and 5.50 ms^{-1} m measured at 0.20 m above the

roof on the windward side.

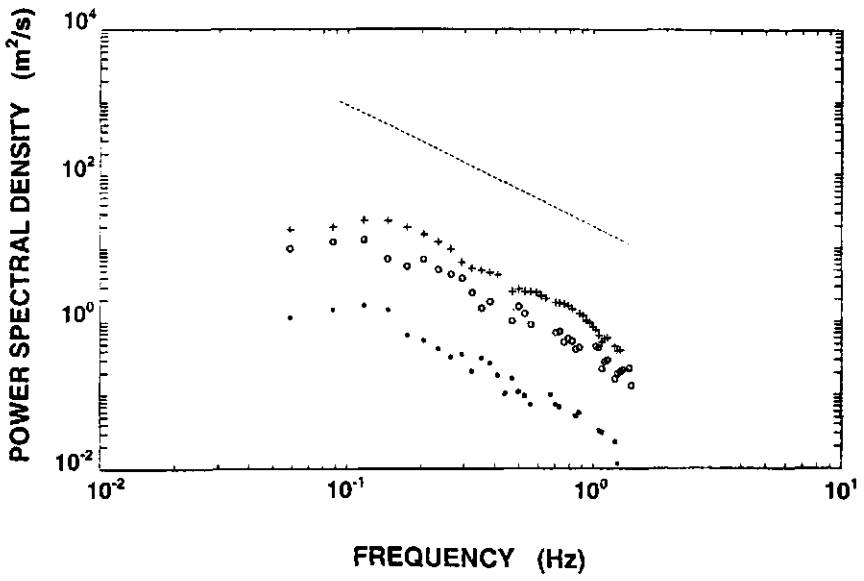

Fig. 6-4. Power spectral density of wind velocity for mean wind velocities of 0.52 ms^{-1} (✳), 2.44 ms^{-1} (o) and 3.49 ms^{-1} (+) measured at 0.20 m above the roof at leeside with closed windows (--- line with slope of -5/3).

The corresponding power spectral density of wind velocity measured on the leeside (mean wind velocities 0.52 ms^{-1}, 2.24 ms^{-1} and 3.37 ms^{-1} measured at 0.20 m above the roof on the leeside) are shown in Fig. 6-4.

The situations represented in Fig. 6-3 and 6-4 both exhibit a region in which the power spectral density is proportional to the frequency to the power -5/3 which is in accordance with Kolmogorov's rule. A similarity can also be observed between the power spectrum of wind velocity measured on the windward side and on the leeside. In both, the main peak of power spectral density of the fluctuations occurs at frequencies below 0.1-0.2 Hz, and for frequencies higher than 1 Hz there is no

significant contribution, i.e. low frequencies are dominant in the wind field. The fact that main energetic eddies of wind velocity occur in this range of lower frequencies, is supported by the studies of Kaimal et al. [26] and Bot [8].

Parameter Υ can be calculated from Eqn (9) together with values of power spectral density and frequency taken from Figs. 6-3 and 6-4. The surface roughness length z_o used in the calculations was 0.04 m [22] and the results are shown in Table 6-1. These results show the importance of wind fluctuations (turbulence) on the total wind pressure and that the turbulence contribution can reach 55% of the total.

TABLE 6-1. Mean wind velocity and parameter Υ [Eqn (9)]

$\bar{u}_w$ [ms^{-1}]	$\Upsilon=1+f(F_{(n)}, \bar{u}_w, n)$
0.52	1.13
1.27	1.13
2.24	1.39
3.37	1.48
3.49	1.48
5.50	1.52

6.4.2 Airflow through porous screens and openings

For airflow caused only by constant temperature differences (i.e., for quasi-steady conditions ($\partial Q/\partial t \approx 0$) and $p_w \approx 0$) values are presented in Figs. 6-5 and 6-6.

Fig. 6-5 shows the experimental values of airflow through the screen and the values predicted by Eqns (1) and (2) ($1/c_c^2 \approx 0$ [18]) versus temperature difference across the screen.

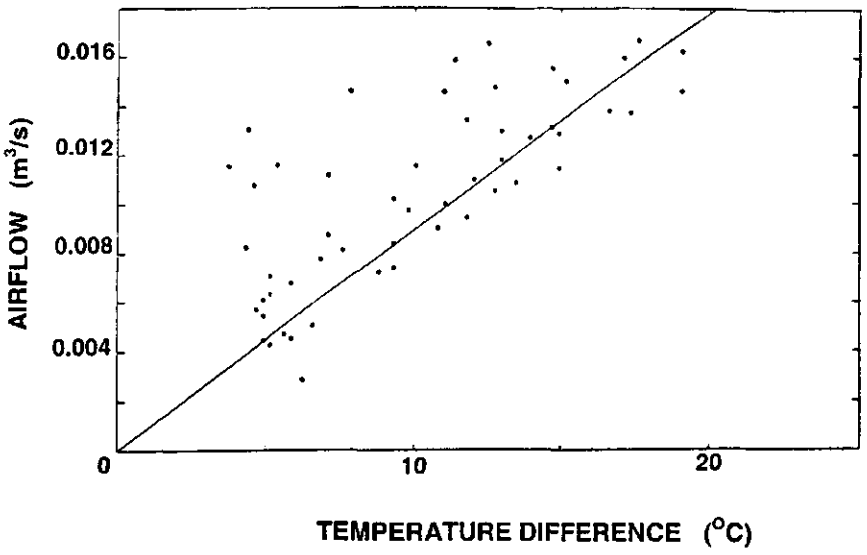

Fig. 6-5. Airflow through the screen versus the temperature differences across the screen (measured data ✳ and predicted –).

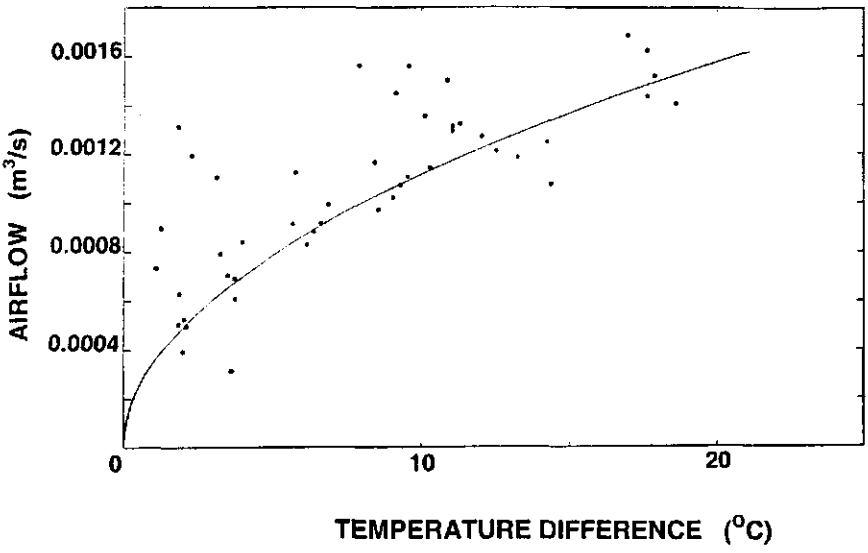

Fig. 6-6. Airflow through the rectangular opening made in the centre of screen versus the temperature differences across the screen (measured data ✳ and predicted –).

Fig. 6-6 shows the experimental values of airflow through the rectangular opening made in the centre of screen and the values predicted by Eqns (2) and (1) ($1/K \approx 0$ [18]), versus temperature difference.

For airflow induced by wind velocity only ($\Delta\rho \approx 0$), values are presented in Figs. 6-7 to 6-10. In these figures, airflow through a window opening or through the screen were compared with values obtained from Eqn (1) with $1/c_c^2 \approx 0$ [18] (for the porous screen) and Eqn (1) with $1/K \approx 0$ [18] (for a window opening).

Fig. 6-7 shows the experimental and the predicted airflow (flow network of Fig. 6-1a) through the windward side window and leeside window (opening angles 4°) versus the windward side pressure.

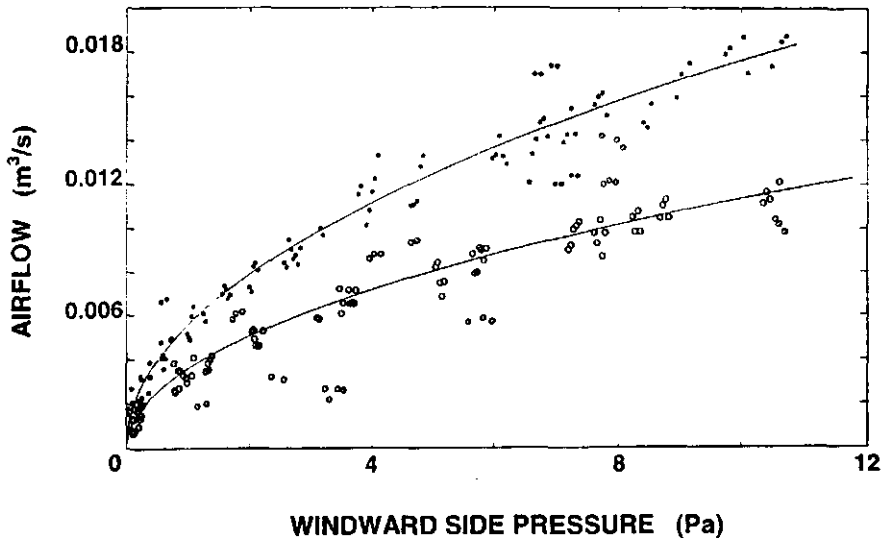

Fig. 6-7. Airflow through the windward side window (✳) and leeside windows (0) versus the windward side pressure, for an opening angle of 4° (predicted —).

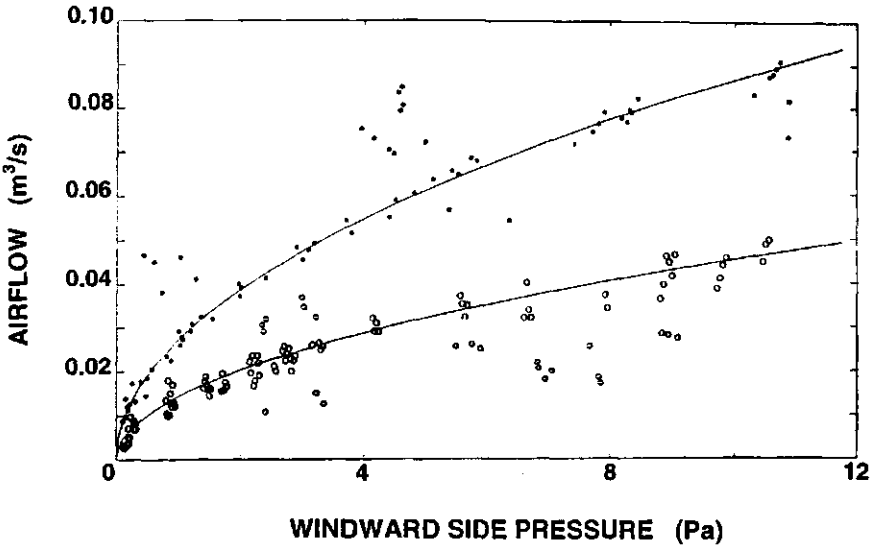

Fig. 6-8. Airflow through the windward side window (✳) and leeside windows (0) versus the windward side pressure, for an opening angle of 20° (predicted —).

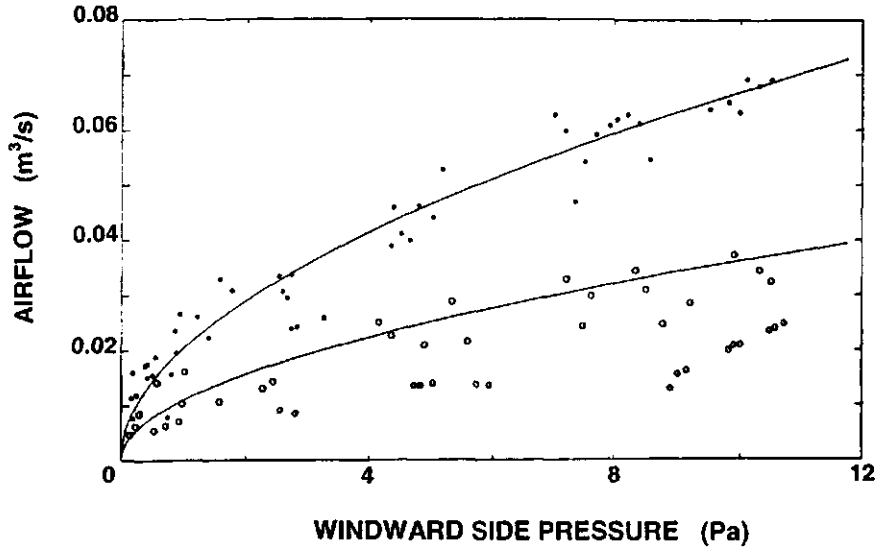

Fig. 6-9. Airflow through the screen versus the windward side pressure in a greenhouse with windward side window open (✳) or leeside window open (o), for an opening angle of 20° (predicted —).

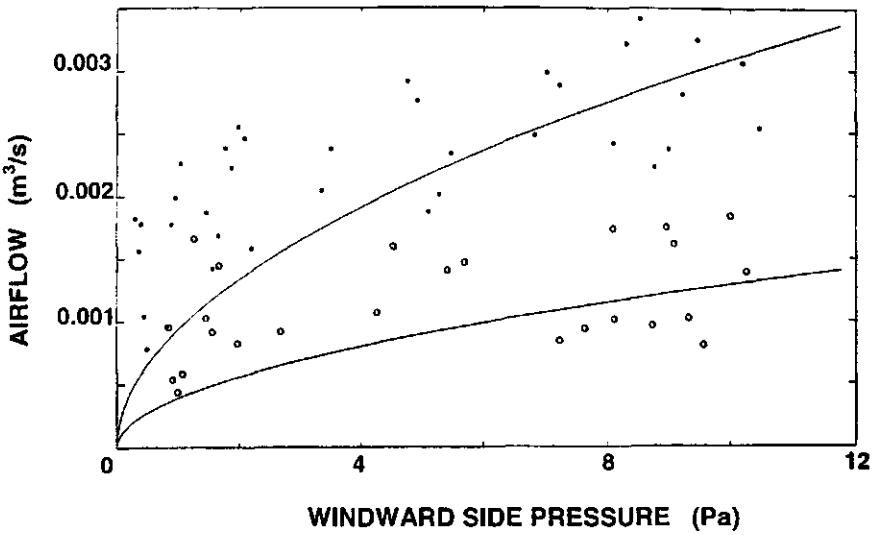

Fig. 6-10. Airflow through the rectangular opening made in the screen versus the windward side pressure in a greenhouse with windward side window open (✳) or leeside window open (o), for an opening angle of 20° (predicted –).

Fig. 6-8 shows the experimental and the predicted airflow (flow network of Fig. 6-1a) through the windward side window and leeside window versus the windward side pressure, for an opening angles of 20°.

Fig. 6-9 shows the experimental and the predicted airflow (flow network of Fig. 6-1a) through the screen versus the windward side pressure in a greenhouse with a windward side window open or a leeside window open (opening angle 20°).

Fig. 6-10 shows the experimental and the predicted airflow (flow network of Fig. 6-1b) through the narrow opening made in the screen versus the windward side pressure in a greenhouse with a windward side window open or a leeside window open (opening angle 20°).

Figs. 6-5 and 6-9 show the airflow through the porous screen driven by temperature

difference and by the wind field respectively and they exhibit two different flow regimes: the Darcy flow regime (Fig. 6-5) and the Forchheimer flow regime (Fig. 6-9). These findings are supported by the work of Bear and Bachmat [27] and Bailey [2]. For Reynolds numbers ($Re=\rho uK^{1/2}/\mu$) smaller than unity the airflow is proportional to the driving potential, which is the case for airflow induced by the usual range of temperature differences between greenhouses and the ambient air ($\Delta T<25°C$). For Reynolds numbers greater than unity a quadratic term of airflow must be added (Forchheimer flow regime) which is the case for flows induced by wind velocities above 0.25 ms^{-1}.

The experimental airflow values were compared with the equivalent values predicted with the model. The differences obtained are always less than 20%, except for Fig. 6-10. The larger scatter presented in this figure is due to the fact the airflow through the slit was obtained by subtracting the flow through the screen from the total flow. As the difference is small the error become relatively large.

6.5 Conclusions

1. The main energetic eddies responsible for the air exchange caused by turbulent wind velocity were found in the frequency range below 0.1-0.2 Hz.

2. The turbulent wind velocity was estimated to be between 13% and 52% of mean wind velocity, which means that it plays an important role in the total wind pressure.

3. The airflow through a porous screen (highly porous media) is described by the Forchheimer's equation. However, for an airflow driven by the usual range of temperature differences between greenhouses and the ambient air, the quadratic term of airflow can be neglected, such that the equation can be reduced to the Darcy law.

4. The airflow through screens and openings predicted by the theoretical approach agree reasonable well with the experimental values, difference between them being less than 20%, in general.

6.6 REFERENCES

[1] **Morris L. G. and Neale F. E** 1954. The infra-red carbondioxide gasanalyzer and its use in greenhouse research. National Institute of Agricultural Engineering report, Silsoe, United Kingdom

[2] **Bailey B. J.** 1978. Glasshouse thermal screens: air flow through permeable materials. Departmental Note no. DN/G/859/04013. National Institute of Agricultural Engineering, Silsoe, United Kingdom

[3] **Bailey B. J. and Cotton R. F.** 1980. Glasshouse thermal screens: influence of single and double screens on heat loss and crop environment. Departmental Note no. DN/G/982/04013. National Institute of Agricultural Engineering, Silsoe, United Kingdom

[4] **Silva A. M., Miguel A. F. and Rosa R.** 1991. Thermal radiation inside a single span greenhouse with a thermal screen. Journal of Agricultural Engineering Research, **49**, 285-298

[5] **Kosmos S .R., Riskowski G. L. and Christianson L. L.** 1993. Force and static pressure resulting from airflow through screens. Transactions of ASAE, **36**, 1467-1472

[6] **Okada M. and Takakura T.** 1973. Guide and data for greenhouse air conditioning. 3: Heat loss due to air infiltration of heated greenhouses. Journal of Agricultural Meteorology (Tokyo), **28**, 223-230

[7] **Kozai T. and Sase S.** 1978. A simulation of natural ventilation for a multi-span greenhouse. Acta Horticulturae, **87**, 39-49

[8] **Bot G. P. A.** 1983. Greenhouse climate: from physical processes to a dynamic model, Ph.D. Dissertation, Agricultural University of Wageningen, The Netherlands

[9] **De Jong T.** 1990. Natural ventilation of large multi-span greenhouses, Ph.D. Dissertation, Agricultural University of Wageningen, The Netherlands

[10] **Montero J. I., Antón A., Arnijas A. and Biel C.** 1990. Natural ventilation in polyethylene greenhouses with and without shading screens. Proceedings of the

international seminar and British-Israel workshop on greenhouse technology, Bet Dagan Israel, 65-71.

[11] **Fernandez J. E. and Bailey B. J.** 1992. Measurements and prediction of greenhouse ventilation rates. Agricultural and Forest Meteorology , **58**, 229-245

[12] **van't Ooster A.** 1994. Using natural ventilation theory and dynamic heat balance modelling for real time prediction of ventilation rates in naturally ventilated livestock houses. Ag. Eng. 94 Milano, Report N.94-C-012

[13] **Boulard T., Meneses J. F., Mermier M. and Papadakis G.** 1996. The mechanisms involved in the natural ventilation of greenhouses. Agricultural and Forest Meteorology, **79**, 61-77

[14] **Balemans L.** 1989. Assessment of criteria for energetic effectiveness of greenhouse screens Ph.D. Dissertation. University of Ghent, Belgium

[15] **Okushima L., Sase S. and Nara M.** 1989. A support system for natural ventilation design of computational aerodynamics. Acta Horticulturae, **248**, 129-134

[16] **Ouwerkerk E. N. J., Voskamp J. P. and Aliskan Y.** 1994. Climate simulation and validation for an aviary system for laying hens, Ag.Eng. 94 Milano, Report N.94-C-063

[17] **Mistriotis A., Bot G. P. A., Picuno P. and Scarascia-Mugnozza G.** 1997. Analysis of the efficiency of greenhouse ventilation using computational fluid dynamics, Agricultural and Forest Meteorology , **85**, 217-228

[18] **Miguel A. F., Van de Braak N. J., Silva A. and Bot G. P. A.** 1998. Forced fluid motion through openings and pores, Building and Environment (in press).

[19] **Miguel A. F., Van de Braak N. J., Silva A. and Bot G. P. A.** 1998. Analysis of air exchange induced by fluctuating external pressures in enclosures, Building and Environment (in press).

[20] **Miguel A. F., Van de Braak N. J., Silva A. and Bot G. P. A.** 1997. Analysis of the airflow characteristics of greenhouse screening materials, Journal of Agriculture Engineering Research **67**, 105-112

[21] **Tennekes H. and Lumley J. L.** 1972. A first course in turbulence. MIT Press, USA

[22] Eurocode ENV 1991-2-4. 1995. Basis of design and action on structures: Wind action.

[23] **Turkey J. W.** 1950. The sampling theory of power spectrum estimates. Symposium on Application of Autocorrelation Analysis to Physical Problems, Washington, Office Naval Research, 47-67

[24] **Clarke R. M.** 1970. Observational studies in the atmospheric boundary layer. Quarterly Journal Royal Meteorology Society, **96**, 91-114

[25] **Sherman M. H.** 1990. Tracer-gas techniques for measuring ventilation in a single zone. Building and Environment, **25**, 365-373

[26] **Kaimal J. C., Wyngaard J. C., Izumi Y. and Coté O. R.** 1972. Spectral Characteristics of surface-layer turbulence. Quarterly Journal Royal Meteorology Society, **98**, 563-589

[27] **Bear J. and Bachmat Y.** 1990. Theory and applications of transport phenomena in porous media, Kluwer Academic Publishers, USA

[28] **Peixoto J. P. and Oort A.** 1992. Physics of climate, American Institute of Physics, New York, USA

6.7 APPENDIX

Wind-induced external pressure

For a quasi-steady flow, we can write the j-direction momentum equation (Navier-Stokes equation) as

$$\rho u(\partial u/\partial j)=-\partial p/\partial j+\mu(\partial^2 u/\partial j^2) \qquad (A.1)$$

The wind is a turbulent airflow characterised by fluctuations of the physical quantities such as velocity and pressure. The turbulent fluctuations of these variables can be described by resorting to statistical methods. Using the Reynolds

decomposition method, the instantaneous quantity at time t can be written as the sum of a mean component (¯) and a fluctuating component (′). For velocity

$$u_w = \bar{u}_w + u'_w \tag{A.2}$$

with

$$\bar{u}_w = \tau^{-1} \int u_w \, dt$$

where τ is longer than the period of any significant fluctuation but is much shorter than any mean flow time scale and u_w is the wind velocity.

Substitution of Eqn (A.2) into (A.1) provides

$$\rho \bar{u}_w (\partial \bar{u}_w / \partial j) = -\partial \bar{p}_w / \partial j + \mu(\partial^2 \bar{u}_w / \partial j^2) - \rho \partial(\overline{u'_w u'_w}) / \partial j \tag{A.3}$$

where the third term on the right hand side represents the extra shear stress brought about by turbulent momentum transport.

Integrating the previous equation over j-direction, we obtain

$$\bar{p}_w = 0.5\rho \bar{u}_w^2 - (\mu \, \partial \bar{u}_w / \partial j - 0.5\rho \overline{u'_w u'_w}) + \varpi \tag{A.4}$$

where ϖ is the constant of integration.

If a situation without wind is considered ($\bar{u}_w = u'_w = 0$) and $\bar{p}_w = 0$. Thus, ϖ must be zero and

$$\bar{p}_w = 0.5\rho \bar{u}_w^2 - (\mu \, \partial \bar{u}_w / \partial j - 0.5\rho \overline{u'_w u'_w}) \tag{A.5}$$

In the lower boundary layer of the atmosphere [28]

$$\partial \bar{u}_w / \partial j = u^* / (\kappa h) \tag{A.6}$$

then, Eqn (A.5) becomes

$$\bar{p}_w = 0.5\rho(\bar{u}_w^2 + \overline{u'_w u'_w}) - \mu[c_{wf}^{1/2} \bar{u}_w / (\kappa h)] \tag{A.7}$$

with

$$c_{wf} = (u^* / \bar{u}_w)^2$$

where c_{wf} is the friction coefficient, h the height above the ground, u^* the friction velocity and κ the von Karman constant.

If the viscosity effect is neglected ($\mu c_{wf}^{1/2} / (\kappa h) \approx 0$), Eqn (A.7) can be reduced to a

relationship postulated and supported by experiments carried out by Bot [8] and de Jong [9].

6.8 NOMENCLATURE

A	area [m^2]
c_c	coefficient accounting for convective effect
c_{kl}	Kolmogorov's constant (≈ 0.5)
c_{wf}	friction coefficient
c_μ	turbulent kinetic energy constant (≈ 0.09)
$F_{(n)}$	power spectral density [$m^2 s^{-1}$]
g	gravitational acceleration [ms^{-2}]
h	height [m]
H	characteristic depth [m]
K	permeability [m^2]
L	characteristic length [m]
n	frequency [Hz]
p	pressure of air [Pa]
p_0	mean absolute pressure of air in enclosure [Pa]
p_{st}	stack pressure [Pa]
p_w	wind pressure [Pa]
Q	airflow [$m^3 s^{-1}$]
r_μ	turbulent kinetic energy dissipation rate [$m^2 s^{-3}$]
T	absolute temperature [K]
u	fluid velocity [$m^3 m^{-2} s^{-1}$]
u^*	friction velocity [ms^{-1}]
V	volume [m^3]

Y inertial factor

z height [m]

z_0 surface roughness length [m]

Greek symbols

β coefficient of thermal expansion [K^{-1}]

ε porosity

τ time [s]

κ von Karman's constant (≈ 0.4)

μ dynamic viscosity [Nsm^{-2}]

π constant (≈ 3.1416)

ρ density [$kg\ m^{-3}$]

Υ wind pressure coefficient

Subscripts

fr flow field

i inside

l larger length

rmsw root mean square wind velocity

s smaller length

st stack

w wind

7. Free convection heat transfer in screened greenhouses [+]

Abstract: Free convection heat transfer between heating pipes and air, horizontal screen and air and inner roof surface and air was studied experimentally in twin-span glasshouses, under constant heat flux conditions. Among others results, equation coefficients between Nusselt and Rayleigh numbers are presented for the inner surface of the greenhouse roof, screen surfaces and heating pipes. Special attention is given to the influence of the location of the heating pipes relative to the screen, as well as the presence of a crop, upon the convective heat transfer between different surfaces and air. The equation coefficients obtained in this work are between 2% and 75% greater than the equivalent equation coefficients found for smooth plates and cylinders by other authors.

7.1 INTRODUCTION

Free convection heat transfer is an important mechanism of energy transport between the surfaces of a greenhouse and the enclosed air [1-5]. However, little information and data on this subject are currently available in the literature and what there is, is almost exclusively devoted to unscreened greenhouses.

Despite the fact that the use of screens in greenhouses provides a simple and successful way of avoiding night-time heat loss and controlling solar radiation entering the greenhouse, studies on convective heat transfer have been performed almost exclusively in greenhouses without screens. As far as is known only one study was made by Stoffers [6] in 1984 for the purpose of determining convective heat transfer in greenhouses divided by a horizontal screen. It is believed that a better knowledge of the heat-transport processes will bring important improvements in greenhouse modelling.

[+] *J. Ag. Engng. Research* (in press)

The main object of this research was to produce information about free convective heat transfer inside screened greenhouses. To achieve this, experiments were performed in three twin-span glasshouse compartments having an airtight screen placed horizontally between the ground and the roof, in each of these compartments. The situations studied included the presence and the absence of an artificial crop, and the heating pipes positioned at two different heights. Thus, the influence of the crop and the location of the heating pipes on convective heat transfer was investigated. Equation coefficients are presented for convective heat-transfer coefficients between the inner surface of the greenhouse roof and air, screen surfaces and air, and heating pipes and air.

7.2 THEORETICAL BACKGROUND

Consider a multi-span greenhouse with a screen (partition) between the ground and the roof (two-zone enclosure), with adiabatic (highly insulated) ground and side walls. The enclosure is heated by pipes placed just above the ground. The mode whereby energy is transferred from the heating pipes to the outside of the greenhouse involves three different processes: conduction, convection and radiation. The energy from the heating pipes arrives by convection and radiation at the lower screen surface. The energy is conducted through the screen, arrives both by convection and radiation at the roof surface, where it is conducted through the glass and dissipated in the outside of the greenhouse cover by convection and radiation.

Convective and radiative heat flux density are related to the heat flux generated by the heating pipes Q_e by

$$Q_e=Q_{c\alpha}+Q_m \quad (1)$$

where Q_m represents the radiation heat flux density from the hot surface of the pipes to the environment and $Q_{c\alpha}$ the convective heat flux density from the surface of the pipes to the fluid.

7.2.1 Heat transfer by convection

The convective heat transfer is defined according to [7]

$$Q_{c\alpha}=\alpha(T-T_{\infty}) \quad (2)$$

where α represents the convective heat transfer coefficient, T the surface temperature and T_{∞} the temperature of the free stream fluid.

It was soon established that α is not a constant but a function of many parameters describing the heat transfer process. Since the work of Fishenden and Saunders [8] convective heat-transfer coefficient is expressed as a relation between the dimensionless Nusselt number (Nu) and the Rayleigh number (Ra) as

$$Nu=c_0 Ra^n \quad (3)$$

In Eqn (3)

$$Nu=\alpha l/\lambda \quad (4)$$

$$Ra=Gr\ Pr \quad (5)$$

$$Gr=\beta(T-T_{\infty})gl^3/\nu^2 \quad (6)$$

and

$$Pr=\nu/\Lambda \quad (7)$$

where β represents the volumetric coefficient of expansion of the air, g gravitational acceleration, l a characteristic dimension, ν kinematic viscosity, λ thermal conductivity, Λ thermal diffusivity, and Gr and Pr the Grashof and Prandtl numbers, respectively.

For experiments performed under constant heat flux conditions, results can also be presented in terms of a modified Grashof number [9]

$$Nu=c^*(Gr^*Pr)^b \quad (8)$$

with

$$Gr^*=Gr\ Nu=\beta\ Q_{c\alpha}\ g\ l^4/(\lambda\ \nu^2) \quad (9)$$

$$c^*=c_0^{1/(1+n)} \quad (10)$$

$$b=n/(1+n) \quad (11)$$

For experiments performed under constant heat flux conditions Eqn (8) can be advantageous because it is dependent on convective heat flux instead of temperature difference.

From Eqn (3) together with Eqns (4)-(7) it can be deduced that

$$\alpha=c_{\alpha}(T-T_{\infty})^{n} \tag{12}$$

and Eqn (2) rewritten as

$$Q_{c\alpha}=c_{\alpha}(T-T_{\infty})^{n+1} \tag{13}$$

with

$$c_{\alpha}=\{c_0/[]^{(1/n)-3}\nu\Lambda/(\beta g\lambda^{1/n})]^{n}\} \tag{14}$$

It should be noted that the fluid properties included in Eqns (3) to (14) should be measured for the mean temperature between the surface and the free stream fluid. The characteristic dimension l depends on the geometry of the system considered. For enclosures, Holman [7] suggests that the distance between surfaces in the direction of the air flow perpendicular to horizontal plates (ground, partitions) under study should be chosen as the characteristic dimension. For a horizontal cylinder (heating pipes), l should be taken as the diameter. For a greenhouse roof, Stoffers [6] suggests that the length of the roof under study should be chosen as the characteristic dimension.

7.2.2 Flow characteristics criterion

The coefficients c_0 and n can be calculated by experiment or theoretically [7]. Generally, the constant c_0 is presented as dependent on the geometry and orientation of the surface under consideration, and the exponent n dependent only on the convection regime.

There are three flow regimes, which can be considered: initial, laminar and turbulent regime. The initial regime is characterised by purely conductive heat transfer. In the laminar regime a circulation flow starts. This regime is characterised by convective currents parallel to the surface. Transport of momentum depends on the transport by

diffusion between the fluid layers. A turbulent regime appears when the flow becomes unstable and vortices arise. This regime is characterised by fluctuations in velocity, temperature and pressure.

The criterion for identifying the flow regime is the Rayleigh number. For plates in enclosed spaces Hollands et al. [10] suggest: $1700 < Ra < 3500$ (initial); $3500 < Ra < 10^6$ (laminar); and $Ra > 10^6$ (turbulent). For horizontal cylinders Holman [7] suggests: $10^3 < Ra < 10^9$ (laminar) and $Ra > 10^9$ (turbulent).

In this study, coefficients c_0, c^*, n and b were determined experimentally, on the basis of the relations given by Eqns (3), (8) and (12), for the case of free convective heat transfer between heating pipes and air, between the upper and lower surfaces of the screen and air, and between the inner surface of the roof and air.

7.3 EXPERIMENTAL ARRANGEMENT

Experiments were conducted in three twin-span glasshouse compartments (Fig. 7-1), each one with the following dimensions: eaves height 4.5 m, roof angle 22°, width 4.1 m and length 6.6 m.

The walls were made of 0.10 m thick insulating panels and the soil surface was covered with 0.05 m thick polystyrene foam insulating layers. Polyethylene film was used between the soil surface and the polystyrene foam in order to prevent the evaporation of soil water. Both walls and soil surfaces in contact with air within the greenhouse were covered with aluminium. The compartments roof was made of single glass with characteristics similar to commercial greenhouses (thickness 4 mm and thermal conductivity 0.88 $Wm^{-1}K^{-1}$).

Inside each compartment an air-tight aluminised screen (reflectivity to thermal radiation 85%) was assembled horizontally between the ground and the roof at a height of 2.90 m above the ground. This screen possessed roughness, as do the screens used in greenhouses.

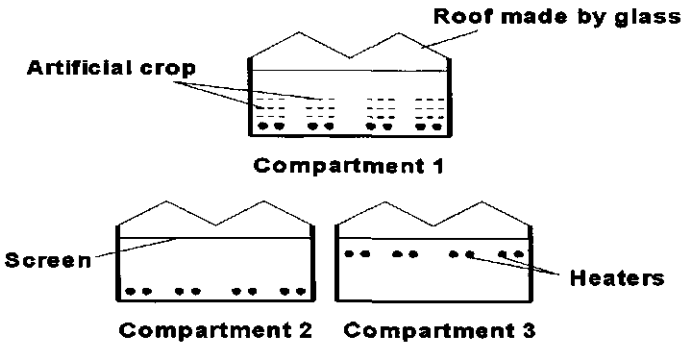

FIG. 7-1. Schematic cross section of compartments for determination of free convective heat transfer.

In order to generate temperature differences between the air and the screen (ground-zone enclosure), and between the air and the roof (roof-zone enclosure), horizontal electrical heaters with aluminised surfaces were placed between the ground and the screen. In each compartment (Fig. 7-1) were placed eight cylindrical electrical heaters (3.80 m long and 0.050 m in diameter), in pairs, separated by 0.35 m, each pair 1.15 m apart and generating an adjustable power of up to 820 W/m^2. The distance between the electrical heaters and the ground in compartments 1 and 2 was 0.20 m and in compartment 3 was 2.10 m. The different distances between the heating system and the screen, in compartments 2 and 3, allowed the influence of the position of the heating pipes with respect to the screen to be studied.

A combination of several aluminised strips (reflectivity to thermal radiation 85%) was placed in compartment 1 in order to simulate a crop (LAI≈1.9). The distance between the first layer of strips and the heating pipes was 2 cm and the last layer of strips was placed 42 cm from the pipes. Compartments 2 and 3 were kept empty. This allowed the influence of the crop on the convective heat transfer to be studied by comparing data obtained from compartments 1 and 2.

In each compartment, 46 copper-constantan thermocouples were installed to

measure the temperature of the air, heating pipes, screen and inner surface of the roof. They were distributed as follows: six distributed on the roof, ten in the air space above the screen, twelve distributed on the screen, ten in the air space below the screen and eight on the heating pipes. In order to make sure that the thermocouples sensed the correct temperature of the heating pipes, the screen surface and the inner surface of the roof, they were bonded to the surface and covered with a thin layer of material with the same optical properties as the surface. To reduce conductive heat flux, the thermocouples were made of thin wires (each wire 0.025 mm in diameter). They were connected to the surface along their length (≈20 cm) to ensure that the sensing point was at the surface temperature.

Net radiometers (spectral range 0 to 60 μm) were placed above and below the screen to measure the radiative heat losses. The radiometers were positioned in such a way that all radiation fluxes incident to or leaving both the screen surfaces and the inner side of the roof could be detected. The net thermal radiation at the heating pipes was estimated using the model developed by Silva et al. [11].

7.4 DESCRIPTION OF EXPERIMENTS

Measurements were made at night between 27 October 1995 and 4 December 1995, in order to exclude the effects of short wave radiation on the measurements. The three compartments were kept "dry", i.e. without vapour condensation on the screen surface, inner surface of the walls or inner surface of the roof.

The thermocouples and net radiometers were scanned by a data-logging system at intervals of 30 s and for periods of time of 12-13 h to record data during the steady state periods. As the temperature inside the greenhouse changes as a result of changes in the outside temperature, the criterion used to evaluate steady state conditions was a quasi-constant temperature difference ($\Delta T \pm 1$°C) between the surfaces and the air.

In each compartment the heat flux supplied by the electrical heaters was the only

parameter that was controlled. Experiments were performed for twelve different constant values of heat flux during 39 nights.

7.5 RESULTS

The data obtained in this study cover a range of Rayleigh numbers of $7.5x10^8 < Ra < 1.6x10^{10}$, $5.6x10^8 < Ra < 8.4x10^{10}$ and $9.0x10^4 < Ra < 9.9x10^5$, for the inner surface of the roof, the screen surfaces and heating pipes, respectively. These values were obtained assuming the characteristic lengths l in Eqns (4), (6), (9) and (14) to be: (a) the length of the roof (for the heat transfer coefficient between the inner surface of the roof and the air); (b) the diameter of the heating pipes (for the convective coefficient between the heating pipes and the air); and (c) the distance between the downward facing surface of the screen and the ground, and the distance between the upward facing surface of the screen and the roof eaves, for the convective coefficients between the screen surfaces and the air, respectively.

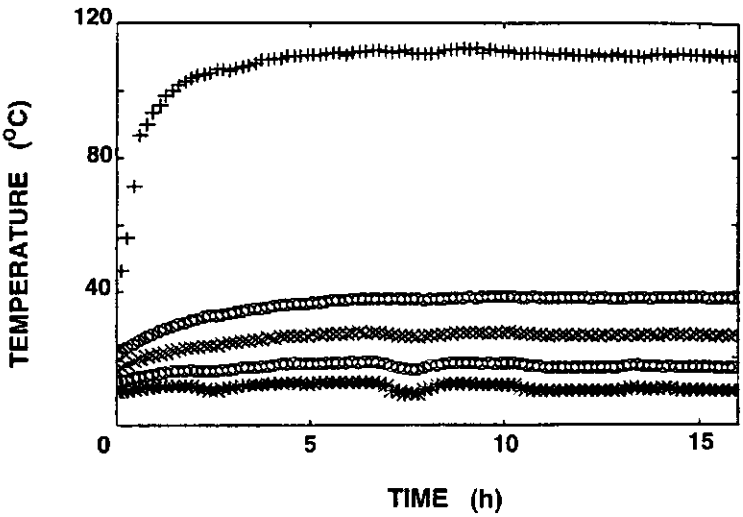

FIG. 7-2. Time variation of the average temperature of the air above and below the screen (○), heating pipes (+), screen surface (x) and inner roof surface (✳), during the night of 19 November 1995 in compartment 2.

The conductive heat losses through the insulated ground and walls were determined by calculations from the thermal properties of the materials given by the manufacturers together with the measurement of the temperature distribution. The radiative flux inside the compartments was measured experimentally using radiometers. These fluxes represent a maximum of 1.6% (conductive heat loss) and 10.3% (radiative flux) of the heat generated by the heating pipes. That is, the minimum convective heat flux was always greater than 88% of the supplied heat flux. Therefore, inaccuracies in the corrections for conductive and radiative terms only cause a small error in the convective term.

As mentioned previously, the experiments were performed over a period of several hours to ensure that a steady state was reached. Figure 7-2 shows the variation over time of the average temperature of the air (above and below the screen), screen surface temperature and inner roof surface temperature for the night of 19 November 1995 in compartment 2. It will be noted that the temperature difference between the surfaces and the air remained constant after approximately 8 h, which means that a steady state condition had been reached. Similar results were obtained for the other test nights, and the steady state was always reached within 10 h of the beginning of the experiment.

Figures 7-3 to 7-5 present the convective heat flux ($Q_{c\alpha}$) versus the temperature difference ($T-T_{\alpha}$), between the inner surface of the roof and the air, between upper and lower facing surfaces of the screen and the air, and between the heating pipes and the air, respectively.

According to Figs. 7-4 and 7-5, the distance of heating pipes from the downward facing screen surface do not influence the convective heat transfer between lower surface of the screen and air, and between heating pipes and air. The presence of the crop increases the convective heat flux and hence the convective heat-transfer coefficient by approximately 16% between the heating pipes and the air.

The data, presented in Figs. 7-3 to 7-5, can be fitted with Eqn (13) and coefficients c_{α} and n found by logarithmic regression analysis. These coefficients are presented in

Table 7-1.

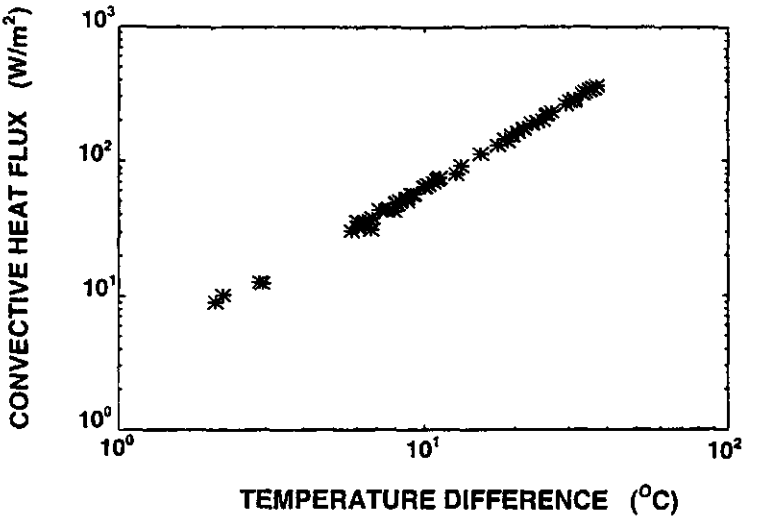

FIG. 7-3. Convective heat flux versus the temperature difference between inner surface of roof and the air (all compartments).

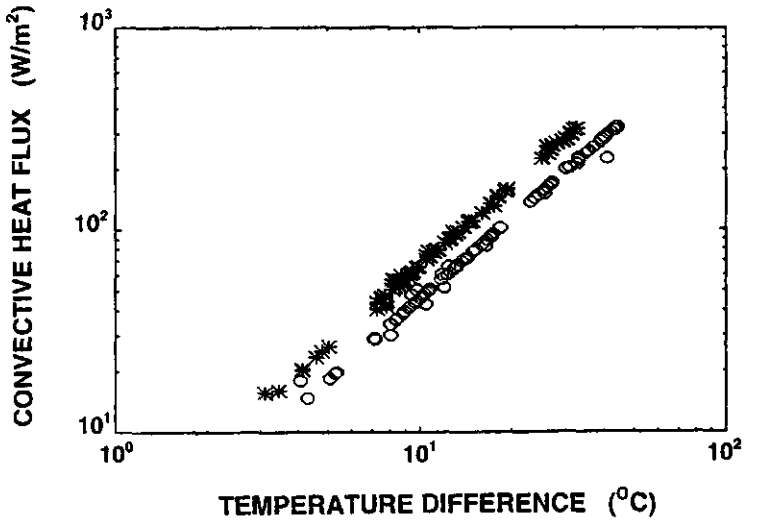

FIG. 7-4. Convective heat flux versus the temperature difference between the screen [upward facing surface (✳) and downward facing surface (○)] and the air (all compartments).

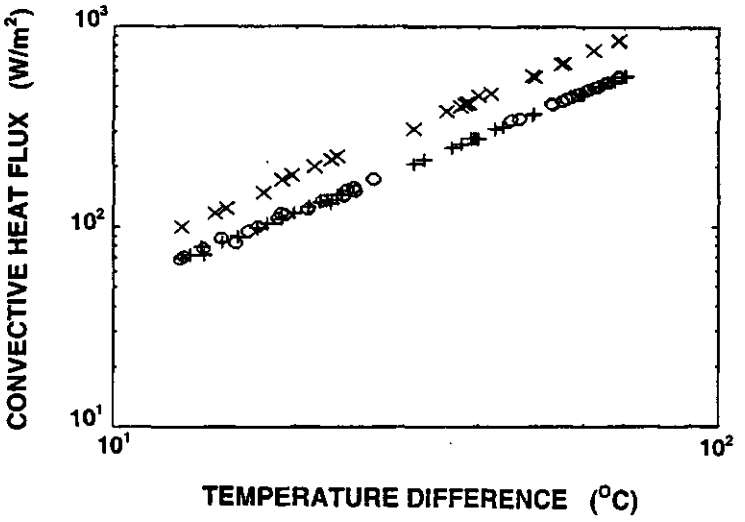

FIG. 7-5. Convective heat flux versus the temperature difference between the heating pipes in the compartment 1 (x), 2 (+) and 3 (O) and the air.

TABLE 7-1. Coefficients c_α and n for the best fit of Eqn (13)

	c_α	n	r^2	ND(*)
Inner surface of roof	3.02	0.32	0.97	98
Upper surface of screen	3.24	0.30	0.96	82
Lower surface of screen	2.17	0.31	0.97	69
Heating pipes 1	3.37	0.26	0.98	35
Heating pipes 2	2.99	0.24	0.98	38
Heating pipes 3	3.03	0.24	0.99	39

(*) Number of fitted data

According to Table 7-1, the exponent n obtained for the screen surfaces and inner surface of the roof is close to 1/3 (turbulent flow regime) and for the heating pipes close to 1/4 (laminar flow regime) . If it is assumed that n exponents of 1/3 and 1/4 are

the true values, then new values of c_α are obtained which are slightly different from the values found previously. The new values of c_α for exponent n equal to 1/3 and 1/4 are presented in Table 7-2. From knowledge of c_α and n, the convective coefficients c_0 and c^* can be computed from Eqns (14) and (10), and the relations between Nu and Ra or between Nu and Gr^* obtained. These relations are presented in Table 7-3.

TABLE 7-2. Coefficients c_α obtained for exponent n equal to 1/3 (turbulent flow) and 1/4 (laminar flow)

	c_α	n
Inner surface of roof	2.97±0.29	1/3
Upper surface of screen	3.09±0.27	1/3
Lower surface of screen	2.09±0.14	1/3
Heating pipes 1	3.42±0.12	1/4
Heating pipes 2	2.90±0.19	1/4
Heating pipes 3	2.98±0.18	1/4

TABLE 7-3. Free convective heat transfer correlations

	$Nu= c_0 Ra^n$		$Nu=c^*(Gr^*Pr)^b$	
	c_0	n	c^*	b
Inner surface of roof	0.270±0.026	1/3	0.374±0.036	1/4
Upper surface of screen	0.281±0.024	1/3	0.386±0.033	1/4
Lower surface of screen	0.191±0.013	1/3	0.289±0.020	1/4
Heating pipes 1	0.299±0.011	1/4	0.404±0.015	1/5
Heating pipes 2	0.254±0.017	1/4	0.358±0.024	1/5
Heating pipes 3	0.261±0.015	1/4	0.365±0.021	1/5

The convective heat transfer coefficients c_α and n shown in Tables 7-2 and 7-3 were compared with the equivalent convective heat transfer coefficients c_{0j} and n_j found by other authors through

$$(Nu_j/Nu)=(c_{0j}/c_0)Ra^{(n_j-n)} \quad (15)$$

where j refers to the author j in the literature reviewed. The results of (c_{0j}/c_0) and (n_j-n) are shown in Table 7-4.

TABLE 7-4. Comparison of convective heat transfer correlations found in this study with correlations found in literature reviewed [Eqn.(15)]

	(c_{0j}/c_0)	(n_j-n)	(c_{0j}/c_0)	(n_j-n)	(c_{0j}/c_0)	(n_j-n)	(c_{0j}/c_0)	(n_j-n)
	j=Stoffers [6]		j=GEC [12]		j=Holman [7]		j=Vliet and Ross [9]	
Inner surface of roof	-	-	-	-	-	-	0.77	-0.03
Upper surface of screen	1.09	0.00	0.61	0.00	0.57	0.00	-	-
Lower surface of screen	1.01	0.00	0.90	0.00	0.73	0.00	0.80	0.00
Heating pipes 1	0.88	0.00	-	-	0.82	0.00	-	-
Heating pipes 2	1.03	0.00	-	-	0.96	0.00	-	-
Heating pipes 3	1.01	0.00	-	-	0.94	0.00	-	-

7.6 Discussion

For the screen surfaces the exponent n is in agreement with the values found in the literature for turbulent flow which is the range covered in the experiments ($5.6x10^8 < Ra < 8.4x10^{10}$). According to Table 7-4, the coefficients c_0 found by Stoffers [6] for horizontal screens with roughness are less than 1% greater for the lower surface and 9% higher for the upper surface than the coefficients found in this work. This is within the margin of error of our experiments. Compared with coefficients found experimentally on smooth plates, our values are approximately 34

and 75% higher than the coefficient c_0 referred to by Holman [7]. GEC [12] presents coefficients c_0 which are 10 and 39% lower than the coefficients for the screen surfaces obtained in this study. The coefficients obtained by GEC [12] were found on a horizontal plate of size 3.66 m x 3.66 m with application in the range $5x10^9 < Ra < 1x10^{12}$.

The differences between convective heat transfer coefficients c_0 obtained in this study and the coefficients presented by Holman [7], Vliet and Ross [9] and GEC [12] may partly be owing to the fact that the screen is not a smooth plate but is rough. Rough plates transfer more heat than smooth surfaces because roughness induces extra local convection currents.

For the inner surface of the glass the power coefficient n is in agreement with the values found in the literature for turbulent flow, which is the range covered in the experiments. According to Table 7-4, the coefficient c_0 found in this work is 30% greater than the value presented by Vliet and Ross [9] on a plate with an inclination of 22° and with application in the range $10^4 < Ra < 10^6$. The coefficients c_0 presented by Papadakis et al. [5] (roof with span angle 15°) and by Stoffers [6] (roof with span angle 26°) cannot be compared directly with our results (roof with span angle 22°) because the convective heat transfer coefficient depends on the angle of inclination between the surface and the horizontal [13].

The exponent n for the heating pipes is in agreement with the values found in the literature for laminar flow, the range considered in the experiments. According to Table 7-4, for the heating pipes in compartments 2 and 3 (without artificial crop) the coefficient c_0 found in this work is approximately 2% lower than the coefficient found by Stoffers [6] and 5% higher than the coefficient referred to by Holman [7], but both fall within our interval of uncertainty. On the other hand, the coefficient c_0 found by us for heating pipes in compartment 1 (with artificial crop) is 22% higher than the underlying coefficient referred to by Holman [7] and 14% higher than that referred to by Stoffers [6].

In the literature reviewed, the convective heat coefficients for pipes are obtained with one or two cylinders in an "infinite space", that is, where air movement induced by other surfaces can be disregarded. In the case of compartment 1, extra air movement, induced by the presence of an artificial crop, influences the convective heat transfer at pipe surfaces. This effect explains the higher values obtained in compartment 1 compared with remaining compartments, and the similarity between the values found in compartments 2 and 3 and the literature reviewed.

The data collected in this study cover a Rayleigh number range which is not commonly found in heat transfer literature [7], mainly for the inner surface of the roof and the screen surfaces. However the data obtained in these experiments is commonly relevant to greenhouses.

7.7 Conclusions

1. The height of heating pipes above the soil surface (0.20 m and 2.10 m) did not influence the convective heat transfer between the heating pipes and the air.

2. The distance of heating pipes from the downward facing screen surface (0.80 m and 2.70 m) did not influence the convective heat transfer between the heating pipes and the air and between the lower surface of the screen and the air.

3. The presence of an artificial crop (LAI≈1.9) increased the convective heat transfer coefficient by approximately 16% between the heating pipes and the air.

4. The equations coefficient obtained in this study agree well with those presented by Stoffers [6] for similar conditions.

5. The equation coefficients obtained in this work are between 2% and 75% greater than the equivalent equation coefficients presented in heat transfer literature for experiments performed on smooth plates and cylinders.

6. The differences between screen equation coefficients obtained in this study and the equivalent equations presented by other authors can partly be attributed to the fact that

the screen is not a smooth plate but is rough.

7.8 References

[1] **Bailey B. J.** 1981. The evaluation of thermal screens in glasshouse commercial nurseries. Acta Horticulturae, **115**, 663-670

[2] **Bot G. P. A.** 1983. Greenhouse climate: from physical process to a dynamic model. Ph.D. Dissertation. Agricultural University of Wageningen, The Netherlands

[3] **Silva A. M.** 1988. A contribution to the study of the greenhouse climate: the analysis of some processes of energy transfer (Contribuição para o estudo do clima de uma estufa: estudo de alguns processos físicos de transferência). Ph.D. Dissertation. University of Évora, Portugal (In Portuguese)

[4] **Balemans L.** 1989. Assessment of criteria for energetic effectiveness of greenhouse screens Ph.D. Dissertation. University of Ghent, Belgium

[5] **Papadakis G., Frangoudakis A. and Kyritsis S.** 1992. Mixed, forced and free convection heat transfer at the greenhouse cover. Journal of Agricultural Engineering Research, **51**, 191-205

[6] **Stoffers J. A.** 1984.Energy fluxes in screened greenhouses. Ag Eng 84 Cambridge, United Kingdom

[7] **Holman J. P.** 1990. Heat transfer. Seventh edition. Singapore, MacGraw-Hill, New York, USA

[8] **Fishenden M. and Saunders O. A.** 1957. An introduction to heat transfer. London, Clarendon Press, United Kingdom

[9] **Vliet G. C. and Ross D. C.** 1974. Turbulent natural convection on upward and downward facing inclined constant heat flux surfaces. ASME Paper 74-WA/HT-32

[10] **Hollands K. G. T., Raithby G. D. and Konicek L.** 1975. Correlation equations for free convection heat transfer in horizontal layers of air and water. International Journal of Heat and Mass Transfer, **18**, 879-884

[11] **Silva A. M., Miguel A. F. and Rosa R.** 1991. Thermal radiation inside a single

span greenhouse with a thermal screen. Journal of Agricultural Engineering Research, **49**, 285-298

[12] GEC Heat transfer data book, 1982. Kaminsky, D. A. ed.. New York, General Electric Company, Sect. 504.2, 1-15, USA

[13] **Fujii T. and Imura H.** 1972. Natural convection heat transfer from a plate with arbitrary inclination. International Journal of Heat and Mass Transfer, **15**, 755-765

7.9 NOMENCLATURE

b, c_0, c_α, c^*, n	convective coefficients
g	gravitational acceleration [ms^{-2}]
Gr	Grashof number
Gr^*	modified Grashof number
l	characteristic length [m]
Nu	Nusselt number
Pr	Prandtl number
Q	heat flux density [Wm^{-2}]
Ra	Rayleigh number
T	temperature [K]
Greek symbols	
α	convective heat transfer coefficient across fluid layer [$Wm^{-2}K^{-1}$]
β	volumetric coefficient of expansion [K^{-1}]
Λ	thermal diffusivity [m^2s^{-1}]
λ	thermal conductivity [$Wm^{-1}k^{-1}$]
ν	kinematic viscosity [m^2s^{-1}]
Subscripts	
$c\alpha$	convective

e	electrical heaters
j	author in literature reviewed
rn	radiation
∞	free stream fluid.

8. FINAL DISCUSSION AND CONCLUSION

8.1 AIR INFILTRATION IN ENCLOSURES WITH PORES AND OPENINGS

In this thesis, a motion equation for porous media and openings is derived within the principles of fluid mechanics and thermodynamics. This validity is based on several simplifications, mainly on the assumption that the medium under study is homogeneous on a macroscopic scale, and that deformation and loss of mass by the solid matrix do not occur. In general terms, this description is valid to describe flow through porous media and through non-porous media (gaps, cracks, doors, windows) with permeability as the quantity which connects both extremes (pores and openings). Specifically, the equilibrium state of the fluid within the porous medium, as well as the importance of inertia effects and viscous effects on the fluid transport through the medium, are stated and quantified.

For a porous medium at low velocities ($Re<1$), viscous effects (viscous resistance force due to the momentum transfer at the matrix-fluid interface and viscous resistance of fluid flow) are dominant. Instead, for higher velocities ($Re>1$) fluid flow is strong dependent of the pore' inertial effects. For an opening, convective inertia effects are dominant.

The motion equation, together with the mass conservation and the state equation of gases, are used to describe air infiltration in enclosures. Airflow and internal pressures were related to characteristics of the openings, which connect the enclosure zones, and also to the characteristics of the enclosure and objects within the enclosure (volume, flexibility).

For an enclosure with a large free area opening, the internal pressure response to external pressure is oscillatory and exhibits damping. When the opening area decreases, the damping increases. If the use of porous screen in the opening is adopted, the internal is strongly damped and the equilibrium is reached immediately.

The flexibility of enclosure envelope also affects the internal pressure response. The increase of flexibility decreases the internal pressure amplitude and equilibrium pressure is reached more quickly.

The essence of the present research is to provide a theory which can be applied to practical situations. The developed approaches are therefore applied to a practical problem, the study of screened greenhouses. Three objectives are in view:

- to provide extra information for a better characterisation of the driving potential of the process (wind velocity, air temperature),
- to obtain easily measurable parameters which are required for the developed approaches,
- to test the approaches proposed against real data.

A complication in the evaluation of driving potentials is the fluctuate character of wind velocity. Most of works on fluid flow through openings and porous materials consider only the static flow. In the present study the effect of fluctuations is included.

To clarify and to characterize the structure of fluctuations of wind velocity, a power-spectrum analysis was performed. The frequencies of the main energetic eddies responsible for the air exchange were obtained, being located at frequencies of around 0.1-0.2 Hz. The turbulence contribution of wind velocity to the wind pressure was also obtained, and can reach 55% of the total pressure. These values were obtained for mean wind velocities between 0.5 ms^{-1} and 5.5 ms^{-1} and both results are supported by the studies of others authors.

The airflow characteristics of porous screens were input requirements of the proposed approaches. These characteristics were identified as being permeability and porosity, and they were obtained through relatively simple experimental procedures (DC-pressurisation method). From the experimental data obtained, it is possible to conclude that the screens used as thermal screens have permeabilities close to $10^{-11}m^2$ and insect screens smaller than $10^{-8}m^2$. Some thermal screens, mainly woven sheet screens, can be damaged by opening and closing the screen, and

due to this permeability can increase up to 3.5 times the original value. For a damaged screen, airflow predicted based on permeability of a new material underestimate the flow up to about 30%.

The approaches were tested with real data obtained in both small-scale measurements and full-scale measurements. The predictions made agree reasonably well with the experimental data. In general, differences between them were less than 20%.

8.2 FREE CONVECTIVE HEAT TRANSFER INSIDE A SCREENED GREENHOUSE

An experimental study on free convection heat transfer was performed in small greenhouses with a horizontal screen. The analysis of the data obtained emphasises the following conclusions

- the convective heat transfer coefficients between the air and the downward and upward surface of the screen were $Nu=0.191\ Ra^{0.33}$ and $Nu=0.281\ Ra^{0.33}$, respectively;
- the convective heat transfer coefficients between the air and the inner side of the roof was $Nu=0.270\ Ra^{0.33}$ (roof angle 22 °);
- the position of the heating pipes in relation to the screen (0.80 m and 2.70 m) does not seem to influence the convective heat transfer between the downward facing surface of the screen and the air, nor between the heating pipes and the air;
- the presence of an artificial crop seems to have an influence on the convective heat transfer between the heating pipes and the air, for the range of Rayleigh numbers considered in this study ($9.0x10^4<Ra<9.9x10^5$). The presence of an artificial crop ($LAI\approx1.9$) increases the convective heat transfer coefficient by approximately 16%.

The equation coefficients obtained in this study are between 2% and 75% greater than the equivalent equation coefficients found for smooth plates and cylinders by

other authors. This may partly be owing to the fact that the screen is rough and roughness induces extra local convective currents. Also, the presence of crop seems to induce extra convective currents, which explain the higher convective heat transfer between the heating pipes and the air in the compartment with crop.

Notice that, the data obtained in these experiments is not commonly found in heat transfer literature, but is relevant to greenhouses.

8.3 Final remarks

The description presented in this study contributes to clarify some important aspects of transport phenomena in multi-zone enclosures with permeable walls and has a wide application.

Nowadays, the interest in predicting the behaviour of physical systems through simulation programs is very important. These techniques are much less expensive than small scale or full-scale experiments, allowing the simulation of a very large number of situations in a short period of time. In order to enable an accurate simulation, advances in transport phenomena as a base for this modelling are fundamental.

The study presented in this thesis describes the main aspects concerning the transport phenomena in porous media and openings, which can be implemented in simulation programs with this topic. The formulation presented was incorporated in an existing dynamic climate model called KASPRO, developed by Zwart [1]. At present, model predictions are compared with experimental data obtained in screened greenhouses situated at Research Station PBG in Naaldwijk (west of the Zuid Holland province in the Netherlands) with very promising results [2,3]. In the future, the simulation study of greenhouse control strategies will support the climate control management. Particularly, it will allow establishment of rules for optimal air humidity control and energy saving strategies, combining the screen characteristics and the percentage of screen and window aperture.

8.4 References

[1] **Zwart H. F. de** 1996. Analysing energy-saving options in greenhouse cultivation using a simulation model. Ph.D. Dissertation, Agricultural University of Wageningen, the Netherlands

[2] **Braak N. J. van de, Swinkels G. L. A. M., Knies P. and Breuer J. J. G.** 1997. Verhoging energie-efficiëntie door verbeterde schermregeling (Higher energy efficiency by an improved screen control). Report note P97-XX, IMAG-DLO Wageningen, the Netherlands. [in Dutch]

[3] **Braak N. J. van de, Kempkes F. L. K., Bakker J. C. and Breuer J. J. G.** 1997. Application of simulation models to optimize the control of thermal screens. ISHS 97 Conference, August of 1997, Wageningen, the Netherlands.

SAMENVATTING

Warmte- en stoftransport zijn verschijnselen van groot belang in diverse natuurlijke en industriële processen, zoals klimaatbeheersing in ruimten met poreuze wanden of wanden met openingen (gebouwen, tuinbouwkassen, enz.). In dit proefschrift worden twee aspecten beschouwd: massatransport door poreuze materialen en openingen, en warmteoverdracht van en naar de wand. Deze verschijnselen zijn theoretisch onderzocht en vervolgens zijn de resultaten toegepast om een geschermde tuinbouwkas te bestuderen. Een gedetailleerde beschrijving van het doel van het onderzoek staat in Hoofdstuk 1.

In Hoofdstuk 2 wordt geforceerde convectie door poreuze materialen en openingen besproken. Er wordt een benadering gepresenteerd die is gebaseerd op de impulsbehoudswet met toepassing van volumemiddeling. De resulterende benadering is geldig voor zowel poreus als voor niet-poreus materiaal, en kan worden gebruikt in "computational fluid dynamics" om de snelheids- en drukverdeling over het stromingsveld te voorspellen. Er is vervolgens een nauwkeurige vereenvoudigde vorm ontwikkeld met een klein aantal parameters en eenvoudige mathematische bewerkingen.

In Hoofdstuk 3, wordt de benadering die is ontwikkeld in Hoofdstuk 2 samen met de massabehoudswet en de toestandsvergelijking van gassen, gebruikt om luchtuitwisseling geïnduceerd door fluctuerende uitwendige drukken te bestuderen. De stromingsvergelijkingen voor luchtuitwisseling in een uit meerdere compartimenten bestaande ruimte en vergelijkingen voor de druk binnen elke compartiment met samendrukbare lucht worden gepresenteerd.

Massatransport door permeabele materialen kan ook optreden als gevolg van temperatuur- en concentratiegradiënten, of als resultaat van gecombineerde effecten (gradiënten van temperatuur en concentratie samen met druk gegenereerd door wind of mechanische middelen). Een beschrijving van gecombineerde vrije en geforceerde convectie door poreuze media ondersteund door de basiswetten van de thermodynamica en vloeistofmechanica, wordt gepresenteerd in Hoofdstuk 4. Met het resultaat kan de

massaverandering van een poreus medium als gevolg van adsorptie en de interactie tussen de matrix van vaste stof en de lucht of vloeistof binnen het medium worden bestudeerd.

Hoofdstuk 5 is gewijd aan de meting van luchtstromingskarakteristieken van poreuze schermen. Negen verschillende thermische, schaduw- en insecten- schermen zijn getest door middel van een drukverschilmethode. Hun permeabiliteit en poreuze inertiefactor zijn bepaald overeenkomstig de Forchheimervergelijking De porositeit van het schermmateriaal is bepaald met behulp van microscoopmetingen. Er is speciaal aandacht geschonken aan de variatie van de luchtstromingskarakteristieken (permeabiliteit en porositeit) als gevolg van beschadiging en door "handling".

In Hoofdstuk 6 zijn de benaderingen gepresenteerd in Hoofdstuk 2 tot 4 toegepast op de studie van luchtuitwisseling in een geschermde tuinbouwkas. Deze studie is aangevuld met een vermogensspectrumanalyse van de windsnelheid, om de structuur van drukfluctuaties (turbulentie) te karakteriseren, en om de frequenties van de belangrijkste wervels in het windveld te identificeren. De fluctuaties in de windsnelheid zijn gerelateerd aan de gemiddelde windsnelheid, Ook de winddruk is geïnterpreteerd in termen van de gemiddelde windsnelheid.

Hoofdstuk 7 is gewijd aan warmteoverdracht door vrije convectie in geschermde kassen. De warmteoverdrachtscoëfficiënt aan verschillende oppervlakken is uitgedrukt als een relatie tussen het dimensieloze Nusseltgetal en het Rayleighgetal. Vervolgens is een experimentele studie uitgevoerd om de vrije convectie warmteoverdrachtscoëfficiënten te bepalen (tussen lucht en verwarmingspijpen, lucht en horizontaal scherm, en lucht en binnenste dakoppervlak) in een kas met karakteristieke lengten dicht bij die van echte kassen. Andere praktische aspecten, zoals de invloed van de positie van de verwarmingpijpen in relatie tot het scherm, en de aanwezigheid van een gewas, op de convectieve warmteoverdracht tussen de verschillende oppervlakken en de lucht, wordt besproken.

Tenslotte worden in Hoofdstuk 8 de belangrijkste conclusies van dit onderzoek gepresenteerd en aanbevelingen gedaan voor toekomstig onderzoek.

De implementatie van de gepresenteerde formulering in dynamische kasklimaatmodellen biedt verschillende mogelijkheden om het management van het kasklimaat te ondersteunen.

SUMÁRIO

A transferencia de massa e calor é um assunto de grande importância em diversos processos naturais e industriais como seja no controlo climático de cavidades com paredes permeáveis (edifícios residenciais, estufas, etc.). Nesta tese dois aspectos foram estudados: o transporte de fluidos através de poros e aberturas, e a transferência de calor entre as paredes interior da cavidade e o ar. Estes fenómenos foram estudados do ponto de vista teórico, e posteriormente aplicados ao estudo de estufas com écrans. A descrição detalhada do objectivo deste trabalho foi feito no primeiro Capitulo desta tese.

O segundo Capitulo foi dedicado ao estudo da convecção forçada através de poros e aberturas. O método denominado de "volume averaging" é aplicado à tradicional equação de balanço de momento, resultando numa equação valida para materiais porosos e para aberturas. A equação resolvida numericamente permite a obtenção da variação temporal e espacial dos campos da velocidade e da pressão. A resolução numérica desta equação não é fácil, e em problemas mais práticos o detalhe da solução obtida nem sempre é necessário. Uma forma simplificada mas precisa da equação foi também apresentada, para ser usada em casos em que apenas são requeridos o valor media dos campos da velocidade e da pressão.

A equação apresentada no Capitulo 2 conjuntamente com a equação de conservação da massa e a equação de estado dos gases, foi usada para estudar trocas de ar induzidas devido à flutuação na pressão (Capitulo 3). Baseado nestas equações foi apresentado um modelo para quantificar as trocar de ar e a pressão numa cavidade com varias zonas.

O transporte de fluido através de materiais permeáveis pode ocorrer devido a gradientes de pressão originados pela velocidade do vento ou por meios mecânicos, mas também devido a gradientes de temperatura ou de concentração, ou através do efeito combinado (gradientes de pressão, concentração, pressão gerada pelo vento ou meios mecânicos). O estudo da convecção mista através de meios porosos, baseado nas leis da termodinâmica e da mecânica de fluídos, foi o tema do Capitulo 4. Como aplicação do modelo

apresentado, foi estudada a variação da massa de meios porosos sujeitos a diferentes condições exteriores, bem como a interacção matriz-fluido.

No Capitulo 5 foram obtidas experimentalmente as características do diversos écrans porosos ao transporte de fluido. Nove amostras de diferentes tipos de écrans foram testados usando uma metodologia denominada de ''DC-pressurization method''. As suas permeabilidade ao transporte de fluido bem como o factor de inércia dos poros foram obtidos com base na equação de Forchheimer (a porosidade foi obtida com a ajuda de um microscópio). O efeito da degradação do écran, devido ao seu uso, na variação da permeabilidade ao fluido e na porosidade, foi também estudada.

No Capitulo 6 os modelos apresentados no capitulo 2 a 4 foram aplicados ao estudo das trocas de ar em estufas com écrans. O estudo contem também a analise espectral da velocidade do vento, com o objectivo de caracterizar as flutuações de pressão (turbulência), e a identificação da frequência dos principais vórtices presentes nos campos de pressão originados pelo vento.

O Capitulo 7 foi dedicado ás transferencias convectivas de calor (convecção natural) no interior de estufas com écrans. Os coeficientes de transferencia de calor para diferentes superfícies foi definido como a relação entre os números adimensionais de Nusselt e de Rayleigh. Posteriormente foi feito, um estudo experimental com o objectivo de determinar os coeficientes de transferencia de calor entre o ar e o sistema de aquecimento, o ar e o écran, e o ar e a face interior da cobertura da estufa. O écran usado neste estudo apresentava alguma rugosidade tal como acontece nos écrans usados em estufas. O efeito da posição do sistema de aquecimento em relação ao écran, bem como a presença de vegetação, no coeficiente de transferência convectiva de calor entre as diferentes superfícies e o ar, foi também estudado.

Finalmente, no Capitulo 8, foram apresentadas as principais conclusões deste estudo, e incluídas também algumas possíveis linhas de investigação futura.

A futura implementação da formulação apresentada neste estudo em modelos dinâmicos, constituirá uma ferramenta importante no estudo do clima interior de cavidades com varias zonas.

SUMMARY

Exchange of mass and heat is a topic of great importance in diverse natural and industrial processes as, for instance, in indoor climate control in enclosures with permeable boundaries (residential buildings, greenhouses, etc.). In this thesis two aspects were considered: fluid transport through pores and openings, and heat transfer between the enclosure surfaces and the inside air. Firstly, these phenomena are examined theoretically and subsequently they are applied to the study of screened greenhouses. A detailed description of the aims of this research can be found in Chapter 1.

In Chapter 2, forced convection through pores and openings is discussed. An approach based on the momentum equation, developed in terms of the method of volume averaging, is presented. The resulting approach is valid for porous material and non-porous material, and can be used in computational fluid dynamics to predict the velocity and pressure throughout the flow field. An accurate simplified form has also been developed, with a small number of parameters and simple mathematical operations.

In Chapter 3, the approach developed in Chapter 2 together with the mass conservation equation and the state equation of gases is used to study the air exchange induced by fluctuating pressures. The flow equations for air exchange in a multi-zone enclosure and equations for the pressure within each zone with compressible air are presented.

Fluid transport through permeable materials can also occur due to gradients of temperature and concentration, or as a result of combined effects (gradients of temperature, concentration and pressure generated by wind or mechanical means). A description of mixed convection through porous media, supported by thermodynamics and fluid mechanics basic laws, is presented in Chapter 4. As a result, the mass variation of the medium and the interaction between the matrix and the fluid within the medium can be studied.

Chapter 5 is devoted to the measurement of the airflow characteristics across porous screens. Nine different thermal, shading and insect screens were tested by

means of a DC-pressurisation method. Their permeability and porous inertia factor were determined according to Forchheimer equation (porosity measured with a microscope). Special attention is given to the airflow characteristics variation (permeability and porosity) due to screen damage by handling.

In Chapter 6, the approaches presented in Chapters 2 to 4 are applied to the study of air exchange in a screened greenhouse. This study is complemented with a power-spectrum analysis of wind velocity, in order to clarify and characterise the structure of pressure fluctuations (turbulence), and to identify the frequencies of the main eddies present in the wind field. The fluctuations in the wind velocity are related to the mean velocity, and the wind pressure is interpreted in terms of the mean wind velocity.

Chapter 7 is devoted to free convective heat transfer inside screened greenhouses. The heat transfer coefficient at various surfaces is expressed as a relation between the dimensionless Nusselt number and the Rayleigh number. Subsequently, an experimental study is performed to determine free convection heat transfer coefficients (between air and heating pipes, air and horizontal screen, and air and inner roof surface) in a greenhouse with characteristic lengths, close to those of real greenhouses. The screen surfaces presented some roughness, as the screens used in greenhouses. Other practical aspects are discussed, such as the influence of the position of the heating pipes in relation to the screen, and the presence of a crop, on the convective heat transfer between the various surfaces and the air.

Finally, Chapter 8 presents the most important conclusions of the present study and includes a recommendation on possible future research.

The formulation presented in this thesis can be implemented in dynamical climate models offering several possibilities of sustainable climate control management.

摘 要

在各种自然和工业化活动中，物质和热能交换是非常重要的问题，比如用可渗透材料覆盖的室内气候控制（住宅、温室等等）。本书包含两方面内容：液体通过孔和开口流动，热力在覆盖界面和内部空气间流动。首先从理论上研究这些现象，然后应用到有遮屏的温室中。在第一章可以找到详细描述本研究的目的。

第二章讨论了通过孔和开口进行的对流活动。根据瞬间平衡公式，提出了动力平均数的技术。本技术对多孔质材和非多孔质材均有效，也可通过计算流体动力学来预测速度和压力。同时也有简化的公式，少刃的参数和简单的数学运算公式。

在文章的第三章，根据第二章的技术及触刃守恒定律，静止气体公式，研究了由于压力波动而引起的气体缩环，提出了覆盖物界面的气体交换公式及每个界面压力的公式。由于温度和浓度的梯度或两者相互影响，液体通过可渗透材料而流动。在第四章，根据动力学和流体动力学理论，描述了通过多孔介质而进行的对流活动，因此可以研究媒界的物质变异及媒界中基质和液体的相互作用。

第五章研究了多孔屏蔽的气体流动特性，通过DC-压力技术，试验了9种不同的防热、遮阴、防虫的屏蔽材料。根据Forchhei公式计算了渗透性及多孔的惰性因子（用显微镜测定多孔率），同时特别关注了由于操作过程中被环境所造成的气体流动特性的变化（渗透性和多孔率）。

在第六章，根据第二章和第四章的技术研究了温室气体交换状况。为说明压力波动的结构（湍流），研究者析了风速的动力学参数，阐明了风速中主要的旋涡频率。风速的波动与平均风速有关，用平均风速来描述了风的压力情况。

第七章阐述了温室内自由热能的对流。不同界面中热能交换参数表示为无维数的Nusselt和Rayleigh的关系值。因此根据试验确定了热能对流参数（室气加热管之间，室气和水平屏蔽间，室气和内部屏蔽间）。讨论了应用性方面的情况，如加热管的位置对不同界面与室气间热能对流的影响。

最后第八章，总结了目前研究的重要结论，指出了未来研究的可能领域。本书提供的公式可用于气候的动力学模型研究，提供了持续气候管理的几种可能性。

LIST OF AUTHOR REFEREED PUBLICATIONS

Publications included in this dissertation:

Forced fluid motion through openings and pores 1998. A. F. Miguel, N. J. van de Braak, A. M. Silva and G. P. A. Bot. Building and Environment (in press) *(chapter 2)*

Analysis of air exchange and internal pressure in enclosures induced by fluctuating outside pressures 1998. A. F. Miguel, N. J. van de Braak, A. M. Silva and G. Bot. Building and Environment (in press) *(chapter 3)*

Modelling mixed fluid motion through porous media: description of interaction matrix-fluid 1998. A. F. Miguel, N. J. van de Braak, A. M. Silva and G. P. A. Bot. To be submitted to Transport in porous media *(chapter 4)*

Analysis of airflow characteristics of greenhouse screens 1997. A. F. Miguel, N. J. van de Braak, A. M. Silva and G. P. A. Bot. Journal Agr.. Engng. Research **67**, 105-112 *(chapter 5)*

Physical modelling of natural ventilation through screens and windows in greenhouses 1998. A. F. Miguel, N. J. van de Braak, A. M. Silva and G. P. A. Bot. Journal Agr.. Engng. Research (in press) *(chapter 6)*

Free convection heat transfer in screened greenhouses 1998. A. F. Miguel, N. J. van de Braak, A. M. Silva and G. P. A. Bot. Journal Agr.. Engng. Research (in press) *(chapter 7)*

Others publications:

Solar irradiation inside a single span greenhouse 1989. R. Rosa, A. M. Silva and A. F. Miguel. Journal Agr.. Engng. Research, **43**, 221-229

Thermal radiation inside a single span greenhouse with a thermal screen 1991. A. M. Silva, A. F. Miguel and R. Rosa. Journal Agr. Engng. Research, **49**, 285-298

Experimental determination of the thermal conductivity of a solid body

1992. A. F. Miguel and A. M. Silva, Gazette of Physics, **15** (2), 67-70

Solar irradiation inside a single span greenhouse with shading screens 1994. A. F. Miguel, A. M. Silva and R. Rosa. Journal Agr.. Engng. Research, **59**, 61-72.

Modelling of transport phenomena near greenhouse screens 1998. A. F. Miguel, A. M. Silva, N. J. van de Braak and G. P. A. Bot. Acta Hortic. (in press)

Airflow through porous materials: from theory to practical considerations 1998. A. F. Miguel. Energy and Buildings (in press)

The influence of porous screens on climate behaviour of greenhouses 1998. A. F. Miguel and A. M. Silva. Agr. and For. Meteorology (submitted)